AFRL-AFOSR-JP-TR-2016-0065

Ultrafast Optics - Vector Cavity Lasers: Physics and Technology

Dingyuan Tang
NANYANG TECHNOLOGICAL UNIVERSITY

06/14/2016
Final Report

Air Force Research Laboratory
AF Office Of Scientific Research (AFOSR)/ IOA
Arlington, Virginia 22203
Air Force Materiel Command

REPORT DOCUMENTATION PAGE

Form Approved
OMB No. 0704-0188

1. REPORT DATE *(DD-MM-YYYY)*	2. REPORT TYPE	3. DATES COVERED *(From - To)*
14-06-2016	Final	28 Mar 2013 to 27 Mar 2016

4. TITLE AND SUBTITLE
Ultrafast Optics - Vector Cavity Lasers: Physics and Technology

5a. CONTRACT NUMBER

5b. GRANT NUMBER
FA2386-13-1-4096

5c. PROGRAM ELEMENT NUMBER
61102F

6. AUTHOR(S)
Dingyuan Tang

5d. PROJECT NUMBER

5e. TASK NUMBER

5f. WORK UNIT NUMBER

7. PERFORMING ORGANIZATION NAME(S) AND ADDRESS(ES)
NANYANG TECHNOLOGICAL UNIVERSITY
50 NANYANG AVENUE
SINGAPORE, 639798 SG

8. PERFORMING ORGANIZATION REPORT NUMBER

9. SPONSORING/MONITORING AGENCY NAME(S) AND ADDRESS(ES)
AOARD
UNIT 45002
APO AP 96338-5002

10. SPONSOR/MONITOR'S ACRONYM(S)
AFRL/AFOSR IOA

11. SPONSOR/MONITOR'S REPORT NUMBER(S)
AFRL-AFOSR-JP-TR-2016-0065

12. DISTRIBUTION/AVAILABILITY STATEMENT
A DISTRIBUTION UNLIMITED: PB Public Release

13. SUPPLEMENTARY NOTES

14. ABSTRACT
High power fiber lasers are currently a hot research topic. Conventional studies on the fiber lasers have mainly focused on the scalar field operation of the lasers, for the lack of simplicity. However, light propagation in a real high power fiber laser cavity could also involve in the nonlinear coupling between the two orthogonal polarization components of the light, which could result in a number of interesting features. In the project we have both experimentally and numerically investigated the operation of fiber lasers where the vector nature of the light propagation in the laser cavity has to be considered. We have called such a fiber laser as the vector cavity fiber laser. Experimental studies on the operation of the fiber lasers have revealed a great number of interesting phenomena, such as the phase or the group velocity locked vector solitons, induced solitons, bright-dark pulse pairs, induced dark solitons in the anomalous dispersion cavity fiber lasers etc. Numerical simulations have also well confirmed the experimental observations and shown that the formation of the observed phenomena could be well explained by the nonlinear coupling between the two orthogonal polarization components of the light in the vector fiber cavity. Other effects have also been observed and theoretically studied.

15. SUBJECT TERMS
Fiber Laser, Laser Dynamics, Nonlinear Optical Materials, Vector Cavity Fiber Laser

16. SECURITY CLASSIFICATION OF:			17. LIMITATION OF ABSTRACT	18. NUMBER OF PAGES	19a. NAME OF RESPONSIBLE PERSON
a. REPORT	b. ABSTRACT	c. THIS PAGE			ROBERTSON, SCOTT
Unclassified	Unclassified	Unclassified	SAR	91	19b. TELEPHONE NUMBER *(Include area code)* +81-042-511-7008

Final Report for AOARD Grant FA2386-13-1-4096

"Ultrafast Optics: Vector Cavity Fiber Lasers - Physics and Technology"

Name of Principal Investigator: A/Prof. Tang Dingyuan

Email: edytang@ntu.edu.sg

School of Electrical and Electronic Engineering

Nanyang Technological University, Singapore 639798

50 Nanyang Avenue, Singapore 639798

Phone: 65-67904337

Period of Performance: 03/28/2013 – 03/28/2016

Abstract: High power fiber lasers are currently a hot research topic. Conventional studies on the fiber lasers have mainly focused on the scalar field operation of the lasers, for the lack of simplicity. However, light propagation in a real high power fiber laser cavity could also involve in the nonlinear coupling between the two orthogonal polarization components of the light, which could result in a number of interesting features. In the project we have both experimentally and numerically investigated the operation of fiber lasers where the vector nature of the light propagation in the laser cavity has to be considered. We have called such a fiber laser as the vector cavity fiber laser. Experimental studies on the operation of the fiber lasers have revealed a great number of interesting phenomena, such as the phase or the group velocity locked vector solitons, induced solitons, bright-dark pulse pairs, induced dark solitons in the anomalous dispersion cavity fiber lasers etc. Numerical simulations have also well confirmed the experimental observations and shown that the formation of the observed phenomena could be well explained by the nonlinear coupling between the two orthogonal polarization components of the light in the vector fiber cavity. Other effects of the fiber lasers, such as the cavity induced modulation instability, temporal cavity soliton formation, polarization domain formation have also been experimentally observed and theoretically studied.

Introduction

Fiber lasers due to their advantages of easy maintenance, excellent stability, compact size and low cost have found widespread applications in industrial material processing, scientific research and military systems. Researches on the various types of fiber lasers, specialty fiber designs, and novel fiber components fabrication have attracted great attention worldwide currently. A characteristic of fiber lasers, compared to other types of lasers, is that strong light is confined to propagate long distance in the fiber core that has a very small area of cross section. This has the consequence that the nonlinear light interaction with the matter has a very long length, which results in that the strength of all the nonlinear optical processes is strongly amplified. A conventionally very weak nonlinear optical effect can even become significant. Therefore, apart from the practical applications, fiber lasers also constitute an ideal platform for the exploration of the various complex nonlinear dynamics.

Previous studies on the operation of fiber lasers have already revealed many interesting nonlinear optical phenomena. Studying on these nonlinear optical effects not only has led to a better understanding on the operation of fiber lasers, but also has driven the performance of the fiber lasers to the extreme through exploiting features of the nonlinear optical effects for better laser operation. However, previous studies on the fiber lasers have mainly focused on the simple scalar cavity lasers, which ignore the vector nature of light propagation in fibers. For many practical cases e.g. a fiber laser with a polarization sensitive component in the cavity, this is justified as the existence of the polarization sensitive component fixes the polarization of light in the laser cavity. However, for the comprehensive understanding on features of fiber lasers the vector nature of light propagation in the cavity fibers has to be considered. Theoretical studies have shown that the vector light propagation in single mode fibers involves in the nonlinear coupling between the two

orthogonal polarization components of light, which could introduce a number of new nonlinear dynamics, such as various types of vector soliton formation, polarization domains and domain walls, black-white vector solitons. The aim of the research project is to investigate the operation of fiber lasers with a quasi-vector cavity both numerically and experimentally. It is expected that through the study a deep and comprehensive understanding on the operation of the fiber lasers could be gained, and fiber lasers with novel features could be further developed.

We have mainly focused on studies of two types of quasi-vector cavity fiber lasers. One is with a saturable absorber in the cavity where due to the effect of the saturable absorber, the laser will be automatically mode locked. Mode locking generates a high peak power optical pulse in the laser cavity. Depending on the concrete laser operation conditions, the mode locked pulse would then be shaped into various forms of dissipative solitons through the nonlinear propagation in the laser cavity. Our experimental studies based on the atomic layer graphene mode locked fiber lasers have revealed a number of interesting dissipative soliton operation features. Another type is the case of the vector cavity fiber lasers without any saturable absorber in the cavity. For such type of fiber lasers we show that due to the cavity detuning strong CW emission is intrinsically unstable as a result of the cavity induced modulation instability. It automatically becomes a periodic pulse train. Under strong pumping the peak power of the pulses could become sufficiently strong so that the nonlinear pulse shaping drives the pulses into dissipative solitons. As there is no saturable absorber in the cavity, the dynamics and features of the dissipative solitons are different from those with a saturable absorber in the cavity. Following the literature we have called the dissipative solitons the “temporal cavity solitons”.

Part 1: Vector temporal cavity solitons in fiber lasers

1. Theoretical Background

To have a better understanding on the experimental results reported later in the report, here we give a brief review on the features of light propagation in single mode fibers (SMFs). It is well known that the light propagation in SMFs is governed by the nonlinear Schrodinger Equation (NLSE). If light is propagating in an active fiber or a fiber laser cavity, then the effects of the gain medium have to be considered. In this case the light propagation is described by the extend Ginzburg-Landau Equation (GLE). A fiber laser is essentially a dissipative nonlinear dynamic system. Although under steady state operation of a laser the laser gain is always balanced by the cavity losses, and the light propagation exhibits similarities to those of light propagation in a single mode fiber, they are different dynamic al systems.

1.1 Light propagation in single mode fibers and the soliton solutions

The light propagation in SMFs is described by the nonlinear Schrodinger Equation (NLSE) [1]

$$\frac{\partial E}{\partial z}+i\frac{\beta_2}{2}\frac{\partial^2 E}{\partial t^2}-i\gamma\left|E\right|^2E+\frac{\alpha}{2}E=0 \qquad (1.1)$$

where E is the slow amplitude of the optical field in optical fiber, α is fiber loss, β2 is the second-order group velocity dispersion coefficient (for SMF, β_2<0) and γ is the nonlinear coefficient of fiber. The loss in optical fiber is usually very small, so the last term of Eq. (1.1) usually can be neglected and it becomes a conservative system. The second term of Eq. (1.1) represents the influence of GVD and the third term represents the effect of nonlinearity, which is realized through self-phase modulation (SPM) here. It usually uses normalization to turn Eq. (1.1) into a dimensionless form

$$i\frac{\partial u}{\partial \xi}+\frac{1}{2}\frac{\partial^2 u}{\partial \tau^2}+|u|^2 u=0 \tag{1.2}$$

where $L_{NL}=1/\gamma P_0$, $L_d=T_0^2/|\beta_2|$, $u\sqrt{P_0}=E$, $\eta=\mathrm{sgn}(\beta_2)$, $\xi=z/L_d$ and $N^2=L_d/L_{NL}=1$,

where P_0 and T_0 are the peak power and pulse width of a reference pulse.

When the fiber dispersion is anomalous, $\eta=\mathrm{sgn}(\beta_2)=-1$, Eq. (1. 2) has a special solution as

$$u(\xi,\tau)=\mathrm{sech}(\tau)\exp(i\xi/2) \tag{1.3}$$

Eq. (1.3) describes a sech^2-shape wave whose shape is only the function of time. Physically, it describes a sech2-shape light pulse which propagate freely in the optical fiber without broadening and maintaining its shape unchanged. This particle-like light pulse is called optical soliton. The optical soliton was first experimentally observed in 1980 by Mollenauer et al. [2].

In a NLSE system in the form of Eq. (1.2), strong CW light is intrinsically unstable due to the modulation instability (MI) [1]. Mathematically, it means that a steady-state solution of Eq. (1.2) will become unstable under small perturbation. As a result of the MI a continuous wave will break up into a periodic pulse train due to weak perturbations, such as background noise, which is inevitable in real fibers. Akhmediev et al. firstly found an analytical MI solution of the NLSE, which has a breather-like structure, and it was called the "Akhmediev Breather (AB)" [3]. The AB solution of Eq. (1.2) is written in the form

$$u(\xi,\tau)=\left[\frac{(1-4a)\cosh(b\xi)+ib\sinh(b\xi)+\sqrt{2a}\cos(\Omega\tau)}{\sqrt{2a}\cos(\Omega\tau)-\cosh(b\xi)}\right]e^{i\xi} \tag{1.4}$$

Here Ω is the dimensionless modulation frequency, $a=\frac{1}{2}\left(1-\frac{\Omega^2}{4}\right)$, where 0 < a < 1/2 determines the frequencies that experience the instability gain and $b=\left[8a(1-2a)\right]^{1/2}$ determines the instability gain growth. When the modulation frequency is very small, the limiting solution for a → 0.5 has a particular

fractional form that has led this class of solution to be described as a 'rational soliton', as firstly derived by D. H. Peregrine and also known as 'Peregrine Soliton' [4]. The solution is in the form of

$$u(\xi,\tau)=\left[1-\frac{4(1+2i\xi)}{1+4\tau^2+4\xi^2}\right] \tag{1.5}$$

Fig. 1.1 plotted the Akhmediev Breather based on Eq. (1.4) under difference modulation frequency parameter a and the ideal Peregrine soliton based on Eq. (2.5)

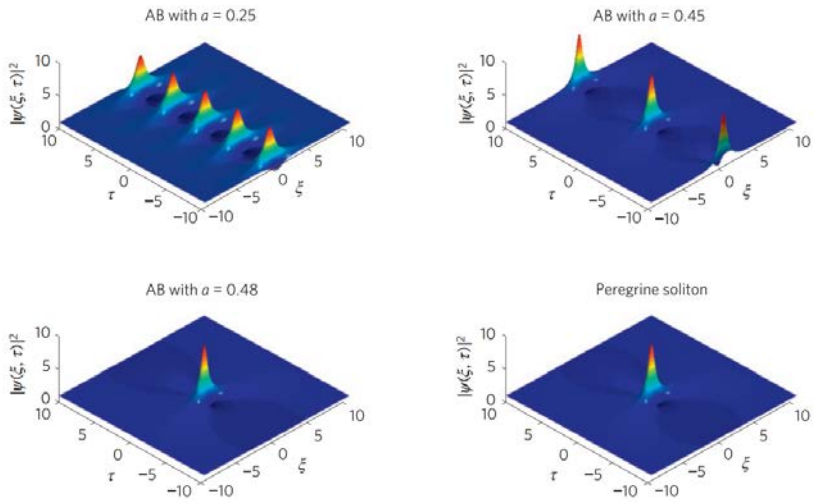

Figure 1.1. Plotted Akhmediev breather of modulation parameter ***a***=0.25, ***a***=0.45, a= 0.48 and the Peregrine solution when ***a***→0.5. (After Ref. [5]; © 2010 Nature Physics.)

From Fig. 1.1 it is clearly to see that with the increasing of ***a***, thus the decreasing of modulation frequency, the temporal separation between the adjacent peaks increases, at the same time the compressed temporal width of each individual peak decreases. When ***a*** approaches 0.5, the pulse becomes Peregrine soliton which is extremely localized in both temporal and spatial domain.

The phenomena described above are the cases of linearly polarized light propagation in optical fibers. However, the real optical fibers support two orthogonally polarized modes. The light propagation in real fibers also involves in the coupling between the two polarization modes. Taking the vector property of light propagation in the single mode fibers, the dynamics of light propagation is then described by the coupled NLSEs of the form

$$\begin{aligned}\frac{\partial u}{\partial z}&=i\beta u-\delta\frac{\partial u}{\partial t}-\frac{ik''}{2}\frac{\partial^2 u}{\partial t^2}+i\gamma\left(|u|^2+\frac{2}{3}|v|^2\right)u+\frac{i\gamma}{3}v^2u^*+\frac{g}{2}u+\frac{g}{2\Omega_g^2}\frac{\partial^2 u}{\partial t^2}\\ \frac{\partial v}{\partial z}&=-i\beta v+\delta\frac{\partial v}{\partial t}-\frac{ik''}{2}\frac{\partial^2 v}{\partial t^2}+i\gamma\left(|v|^2+\frac{2}{3}|u|^2\right)v+\frac{i\gamma}{3}u^2v^*+\frac{g}{2}v+\frac{g}{2\Omega_g^2}\frac{\partial^2 v}{\partial t^2}\end{aligned} \tag{1.6}$$

where ***u*** and ***v*** represent the normalized amplitude of the optical field on the two orthogonal polarization components, $2\beta = 2\pi\Delta n / \lambda = 2\pi / L_b$ is the wave number difference between these two polarization modes, Lb is the beat length of optical fiber which describes the strength of birefringence. $2\delta = 2\beta\lambda / 2\pi c$ is the group velocity difference, k'' is the second-order dispersion coefficient, γ represents the nonlinearity of the fiber. The last two terms on the right hand side of Eq. (1.6) represent the SPM, cross-phase modulation (XPM) and four-wave-mixing (FWM) effect, respectively. The coupled-NLSEs support vector solitons [6] and bright-dark soliton pair [7, 8] in optical fiber.

1.2 Theoretical description of light propagation in fiber lasers

In addition of some necessary discrete components, like the output coupler and wavelength-division-multiplexer (WDM), a fiber laser cavity is mainly made of single mode fibers. Hence light propagation in a fiber cavity resembles essentially the light propagation in the fibers. However, different from the light propagation in fibers, in a laser cavity there are also gain and loss, and in the steady state laser operation the light must also satisfy the cavity resonant condition. Therefore, the real situation is much more complicated than that of light propagation in single mode fibers. First, we consider the light propagation in one cavity roundtrip. Without loss of generality we assume that the laser gain is filled up the whole cavity, considering the gain effects, the NLSE is changed to the following form

$$i\frac{\partial E^n}{\partial z_n} - \frac{\beta_2}{2}\frac{\partial^2 E^n}{\partial t^2} + \gamma\left|E^n\right|^2 E^n - i\frac{g}{2}E^n - i\frac{g}{2\Omega_g}\frac{\partial^2 E^n}{\partial t^2} = 0 \qquad (1.7)$$

where $E^n = E^n(z_n, t)$ are the complex envelopes of the optical field, ***n*** denotes the *n* th passage through the fiber laser cavity, $\boldsymbol{\beta_2}$ is the group velocity dispersion (GVD) coefficient, $\boldsymbol{\gamma}$ is the nonlinear coefficient, ***g*** is the gain coefficient and $\boldsymbol{\Omega_g}$ is the effective gain bandwidth of fiber laser. $\boldsymbol{z_n}$ is the light propagation distance parameter and ***t*** is the retarded time in a reference frame traveling with the group velocity of light. When light is circulating in the cavity, it should also fulfill the cavity boundary condition:

$$E^{n+1}(z_n = 0, t) = \rho\exp(-i\phi)E^n(z_n = L, t) \qquad (1.8)$$

where ***L*** is the cavity length, ρ and θ are the amplitude reflection and transmission coefficient between each cavity cycle, $\rho^2 = 1-\theta^2$. ϕ is the linear phase delay generated when light propagates one round trip in the cavity.

For a good cavity operating near the resonance and having a cavity length (***L***) far shorter than the dispersion length ($\boldsymbol{L_d}$) in the cavity, we have the following approximation:

$$\begin{aligned} \rho &\approx 1-\theta^2/2 \equiv 1-\varepsilon\theta'^2/2 \\ (2m\pi-\phi)/\pi &= \delta/\pi \approx \varepsilon \\ L/L_d &\approx \varepsilon \end{aligned} \qquad (1.9)$$

where ε is an arbitrary small parameter ($\varepsilon<<1$), m is the order of the cavity mode closest to the cavity resonance and δ is the cavity detuning parameter, therefore the boundary condition Eq (2.8) can be simplified as

$$E^{n+1}(z_n = 0,t) = (1 - i\varepsilon\pi - \varepsilon\theta'^2/2)E^n(z_n = L,t) + O(\varepsilon^2) \qquad (1.10)$$

and Eq. (1.7) can be rewrite in one cavity cycle as

$$E^n(z_n = \varepsilon L_d,t) - E^n(z_n = 0,t) = -i\varepsilon L_d \frac{\beta_2}{2}\frac{\partial^2 E^n}{\partial t^2} + i\varepsilon L_d \gamma \left|E^n\right|^2 E^n + \frac{\varepsilon L_d g}{2}E^n + \frac{\varepsilon L_d g}{2\Omega_g}\frac{\partial^2 E^n}{\partial t^2}$$

(1.11)

Combining Eq. (2.10) and (2.11), one has

$$E^{n+1}(z_n = 0,t) = E^n(z_n = 0,t) - i\varepsilon L_d \frac{\beta_2}{2}\frac{\partial^2 E^n}{\partial t^2} + i\varepsilon L_d \gamma \left|E^n\right|^2 E^n + \frac{\varepsilon L_d g}{2}E^n + \frac{\varepsilon L_d g}{2\Omega_g}\frac{\partial^2 E^n}{\partial t^2} - (i\varepsilon\pi E^n + \varepsilon\theta^2/2)E^n(z_n = 0,t) + O(\varepsilon^2) \qquad (1.12)$$

Under good cavity condition, the variation of the optical field over one cavity cycle is very small, so we can approximate the spatial differential as

$$\left.\frac{\partial E(z,t)}{\partial z}\right|_{z=n\varepsilon L_d} = \frac{E(z=(n+1)\varepsilon L_d, t) - E(z=n\varepsilon L_d, t)}{\varepsilon L_d} \qquad (1.13)$$

Substituting Eq. (1.12) into Eq. (1.13) we get

$$i\frac{\partial E}{\partial z} - \frac{\beta_2}{2}\frac{\partial^2 E}{\partial t^2} + \gamma\left|E\right|^2 E + i\frac{\theta^2}{2L}E - i\frac{g}{2}E - i\frac{g}{2\Omega_g}\frac{\partial^2 E^n}{\partial t^2} - \frac{\delta}{L}E = 0 \qquad (1.14)$$

Normalize Eq. (1.14) by $L_{NL} = 1/\gamma P_0$, $L_d = T_0^2/|\beta_2|$, $u\sqrt{P_0} = E$, $\eta = \mathrm{sgn}(\beta_2)$, $\xi = z/L_d$, $N^2 = L_d/L_{NL} = 1$, where P_0 and T_0 are the peak power and pulse width of a reference pulse. For simplicity, the normalized cavity detuning is set as $\Delta = L_d\delta/L$ and $a = \theta L_d^2/L$ is the normalized loss coefficient of the cavity. $G = gL_d$ is the normalized gain coefficient and $\Omega = \Omega_g T_0$ is the normalized gain bandwidth, then Eq. (2.14) can be rewritten as

$$i\frac{\partial u}{\partial \xi} - \frac{\eta}{2}\frac{\partial^2 u}{\partial \tau^2} + \left|u\right|^2 u - i\frac{(G-a)}{2}u - i\frac{G}{2\Omega^2}\frac{\partial^2 u}{\partial \tau^2} - \Delta u = 0 \qquad (1.15)$$

Eq. (1.15) describes the average dynamics of light circulation in an active fiber ring cavity. It has the same form of the Ginzburg-Laudau Equation (GLE), which admits the dissipative soliton solutions. However, the parameters now are the averaged value over the cavity length. It is the averaged values that control the dynamics of a laser. We note that equation (1.15) is physically equivalent to the Hermann Haus's master equation [9] without the saturable absorber term. The gain in the fiber laser is described as

$$g = \frac{g_0}{1 + \int |u|^2 dt / Es} \qquad (1.16)$$

where $\mathbf{g_0}$ is the small gain coefficient and $\boldsymbol{E_s}$ is the saturation energy of the gain medium. Eq. (1.16) represents the gain saturation in laser cavity, which is an intrinsic feature of all lasers. When a laser is in the steady operation state, the gain is always balanced by the cavity losses. Therefore, the fourth term of Eq. (1.15) can be neglected. However, the light power in steady operation state is directly related with $\boldsymbol{E_s}$ and $\mathbf{g_0}$, which vary with the pumping strength of fiber laser.

We note that for some fiber lasers the effective cavity gain bandwidth could be far broader than the laser emission bandwidth, if the optical field is in resonance with the cavity, then the last two terms of Eq. (1.15) could be ignored. In that case the Eq. (1.15) can be simplified to the form of NLSE, as Eq. (1.2). It means that the averaged dynamics of light propagation in fiber laser cavity is analog to those of the NLSE, despite the fact that the fiber laser is naturally a dissipative system. Therefore, those phenomenon theoretically supported by the NLSE can also be observed in a fiber laser. Therefore, under the effect of MI, the CW output of fiber laser will turn into a periodic pulse train. Moreover, under suitable conditions these periodic pulses could further evolve to Akhmediev breathers and Peregrine soliton.

When a strong CW beam circulates in a fiber ring cavity, in addition to the conventional modulation instability it is also prone to the cavity induced modulation instability (CIMI) [10, 11]. The CIMI not only has lower threshold than the conventional modulation instability, but also has linear cavity detuning dependent modulation frequency. Through appropriately selecting the linear cavity detuning the cavity induced modulation instability lasing could also generate periodic pulses with GHz to tens of GHz repetition rate [11]. Therefore, in fiber laser, there are two kinds of modulation instability effect that can lead to the breaking-up of a CW and forming of periodic pulse trains. We note that the modulation frequency of conventional MI has usually hundreds of GHz, which is unobservable with an electronic detection system like an oscilloscope, except using the autocorrelator. The repetition rate of periodical pulse train that can be distinguished in oscilloscope trace is usually no more than tens of GHz, which is initiated by the CIMI.

However, for the majority of fiber lasers, considering the passing bandwidth of the intra-cavity components and the gain bandwidth of doped fiber, there is effective gain bandwidth limitation in the cavity. Hence, the fifth term in Eq. (1.15) cannot be ignored. In this case the dynamics of a fiber laser deviate from those of the NLSE. In particular, when the effective gain bandwidth plays a role, Eq. (1.15) admits the dissipative soliton solutions [12]. The properties of dissipative solitons are determined by fiber laser cavity parameters, such as gain and loss, gain saturation and bandwidth. Therefore, initiated by MI or CIMI, the CW light beam in fiber laser may break up into pulse train, and the pulses could be further shaped into dissipative solitons. These solitons are quite different

from the solitons generated in the mode-locked fiber lasers. As the solitons have a similar formation mechanism as the temporal cavity solitons reported, we have named them the temporal cavity solitons in fiber lasers.

If there are no polarization dependent components in cavity, and the fibers have weak birefringence, one must also consider the coupling between the two polarization components of light in the fiber cavity. In this case light propagation in the cavity is described by the coupled extended GLEs

$$\begin{aligned}\frac{\partial u}{\partial z} &= i\beta u - \delta\frac{\partial u}{\partial t} - \frac{ik''}{2}\frac{\partial^2 u}{\partial t^2} + i\gamma\left(|u|^2 + \frac{2}{3}|v|^2\right)u + \frac{i\gamma}{3}v^2u^* + \frac{g}{2}u + \frac{g}{2\Omega_g^2}\frac{\partial^2 u}{\partial t^2} \\ \frac{\partial v}{\partial z} &= -i\beta v + \delta\frac{\partial v}{\partial t} - \frac{ik''}{2}\frac{\partial^2 v}{\partial t^2} + i\gamma\left(|v|^2 + \frac{2}{3}|u|^2\right)v + \frac{i\gamma}{3}u^2v^* + \frac{g}{2}v + \frac{g}{2\Omega_g^2}\frac{\partial^2 v}{\partial t^2}\end{aligned} \quad (1.17)$$

where the fifth term on the right hand side shows the combination of SPM and XPM effect, the sixth term on the right hand is the FWM term. There is no doubt that according to Eq. (1.17), vector dissipative solitons should also exist in a quasi-vector cavity fiber laser.

2. Scalar temporal cavity solitons

For the completeness of the research we also investigated the scalar cavity soliton formation in fiber lasers. As shown above, the propagation of light in fiber laser is described by the Ginzburg-Laudau Equation (GLE), which can be numerically solved by the Split-Step Fourier (SSF) method [1]. Therefore, we have numerically simulated the scalar cavity soliton formation in a fiber laser. The numerical simulation verified the possibility of the spontaneous generation of temporal cavity solitons in fiber laser. Guided by the simulation results, we further conducted experimental study on the operation of an anomalous fiber laser, and confirmed the spontaneous temporal cavity soliton formation.

2.1 Numerical study

Our numerical method is based on the Split-Step Fourier (SSF) method, which is widely used in solving the nonlinear partial differential equations like the NLSE and GLE. We have used a model fiber laser cavity that has the same cavity parameters as the fiber lasers we used in the experiment. Specifically, it has a 13 m fiber ring cavity consisting of 3 m Erbium-doped fiber (EDF) with GVD parameter of -48 ps/nm/km and 10 m SMF with GVD parameter of 18 ps /nm/km. The net dispersion of the cavity is in the anomalous dispersion regime and has a value of 2.78 ps/nm/km. We use the fiber nonlinear coefficient γ =3 $km^{-1}W^{-1}$, cavity effective gain bandwidth Ω_g =20nm and 10% cavity output loss. Considering a CW fiber laser operation destabilized by the cavity-induced modulation instability (CIMI), we artificially introduced a weak field $U(0,\tau) = U_0\cos(2\pi f_c\tau)$ as an initial periodic modulation on the CW laser field, where f_c is the modulation frequency. Fig. 2.1 shows the evolution of the laser emission under existence of the effective gain bandwidth limiting. When the gain bandwidth is appropriately selected, a stable periodic pulse train is always formed under the MI effect.

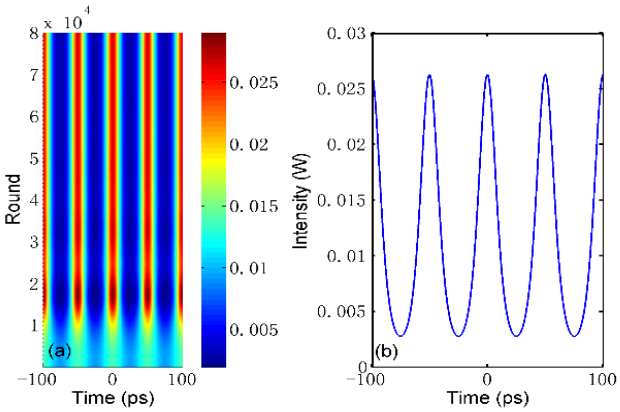

Figure 2.1. (a) Formation of stable periodic pulse pattern in a fiber laser under the effect of modulation instability and effective gain bandwidth limiting. E_s =0.3pJ, Ω_g =20nm and fc = 20GHz. (b) A steady state laser emission.

Without the effective gain bandwidth limitation, the laser emission would display the Akhmediev breathers, as shown in Fig. 2.2. This simulation result is the same as reported in Ref. [3], which verifies that the light propagating in fiber laser cavity without gain bandwidth limitation has the same properties as the light propagation in optical fibers described by NLSE.

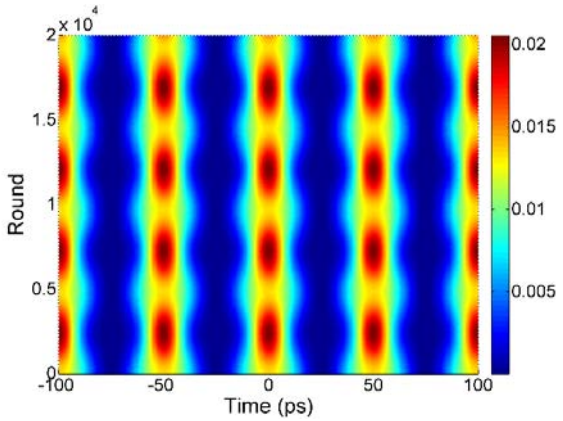

Figure 2.2. Formation of Akhmediev Breather structure in fiber laser cavity where ignoring the gain bandwidth limitation as the condition of Fig. 2.1.

Carefully checking the periodic pulse train in Fig. 2.1, it is identified that there is a CW background on the pulse train. However, as the saturation energy is gradually increased, the pulse width narrows down and the CW level decreases. Eventually all the pulses in the pulse train effectively become dissipative solitons and the soliton is highly localized with each other, as shown in Fig. 2.3.

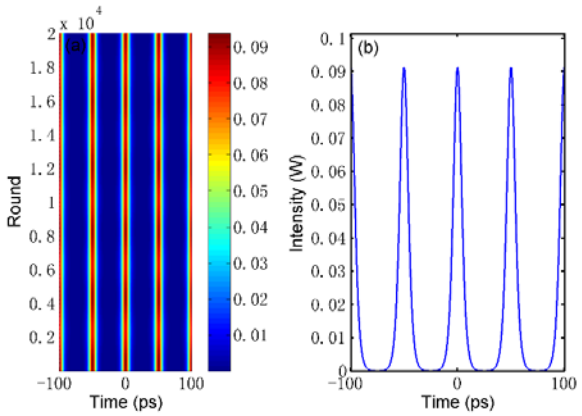

Figure 2.3. (a) Formation of stable dissipative soliton pulse train in a fiber laser under the effect of modulation instability and effective gain bandwidth limiting. E_s =0.5pJ, Ω_g=20nm and f_c=20GHz. (b) A steady state of the laser emission.

To confirm that each pulse in the periodic pulse train is eventually shaped into a dissipative soliton, whose parameters are determined by the laser operation condition, we have further compared the steady-state pulse amplitude and phase profiles with those of the theoretically predicted fundamental dissipative soliton [13]. A dissipative soliton has a chirped-sech profile in the form of

$$u(\tau) = N_s \operatorname{sech} h(p\tau) \exp[-iq \ln(\cosh p\tau)] \qquad (2.1)$$

where N_s, p, q are constants related to the pulse height, width, and frequency chirp, respectively. Taking N_s, p, q as the fitting parameters we found that the numerically calculated pulse profile and phase profile well match those of the dissipative solitons, as shown in Fig. 2.4.

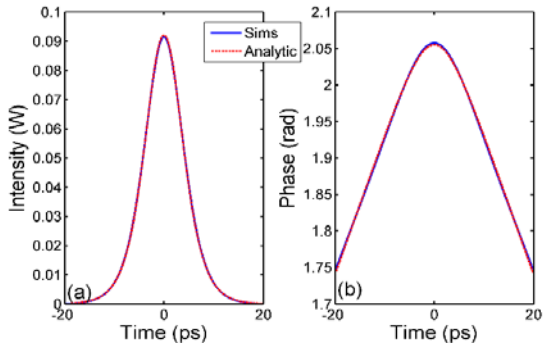

Figure 2.4. Comparison of (Right) amplitude and (Left) phase profile of the steady state pulse with those of the analytic fundamental dissipative soliton.

The steady-state pulses under different effective laser gain bandwidths have been calculated and the pulse width varied with the effective gain bandwidth. However, no matter how the pulse width varies, the steady-state pulse profiles always have the characteristics of a fundamental dissipative soliton. When keeping increasing the saturation energy, like the operation of the conventional dissipative soliton fiber lasers [14], the solitons will break up and form a new pulse train with non-uniform soliton separation, as shown in Fig. 2.5.

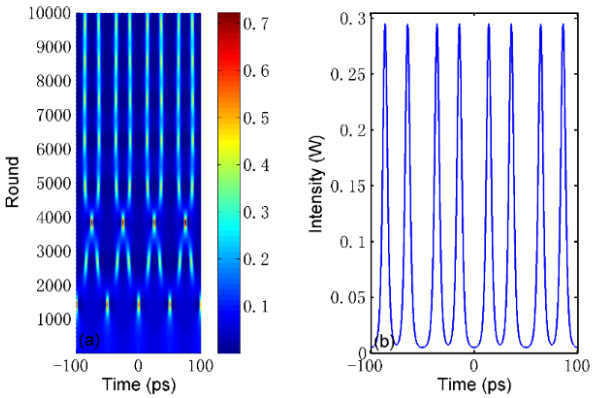

Figure 2.5. (Right) Dissipative soliton breaking when the beam intensity is strong. E_s =2pJ, Ω_g=20nm and f_c=20GHz. (Left) A state of the laser emission.

In the simulations laser emission under various modulation frequencies, gain bandwidth, and saturation energy were also checked. The above features were found independent of the concrete laser parameter selections, suggesting that they are general properties of the fiber lasers. We note that mathematically the state shown in Fig. (2.1) can be considered as a stable periodic solution of Eq. (2.15). Periodic solutions known as cnoidal waves were found for the NLSE [15]. It is known that as the periods approach infinity, the limiting case of the cnoidal waves is a soliton. Since Eq. (2.15) could be simplified to the NLSE, it is expected that a similar feature would also occur on the periodic solutions of Eq. (2.15). Increasing the pumping power, the intensity of the periodic waves could also increase. Therefore, it would be plausible that under sufficient high energy, a train of dissipative solitons could be formed as a result of the nonlinear shaping of its periodic waves.

In summary, our numerical simulations have shown that for a fiber ring laser with anomalous cavity dispersion, as far as the laser power is strong, the MI always destabilizes its CW operation. If there is no effective gain bandwidth limitation, the system is described by NLSE. The MI or CIMI will only lead to the formation of the Akhmediev breathers or the formation of Peregrine soliton as the limiting case. However, under existence of the effective gain bandwidth limiting, the system is described by the extend-GLE. The MI will lead to the formation of a stable train of periodic pulses or temporal cavity solitons (or dissipative solitons). Nevertheless, the periodic soliton trains could be easily destroyed by the system noises, especially in the case of low pulse repetition rate. Consequently, multiple mutually independent dissipative solitons would be formed in the laser cavity.

2.2 Experimental setup and results

Numerical simulations confirmed the spontaneous generation of temporal cavity solitons from a periodic pulse train in the net anomalous dispersion fiber lasers. Guided by the numerical simulations, we further conducted experimental studies on the spontaneous dissipative soliton formation in anomalous dispersion cavity fiber lasers. We set up a fiber ring laser with a cavity configuration as shown in Fig. 2.6. The fiber laser had the same parameters as used for the numerical simulation: the cavity length was 13 m long, consisting

of 3 m EDF and 10 m SMF. A polarization independent isolator was employed in the cavity to force the unidirectional operation of the cavity, and an intra-cavity polarization controller (PC) was used to tune the linear cavity birefringence. A wavelength division multiplexer (WDM) was used to couple the pump beam into the cavity. The laser was pumped by a 1480 nm high power Raman fiber laser source whose maximum output pump can be as high as 5 W. About 80% of the pump power could be coupled into the fiber cavity. A fiber output coupler with 10% output coupling was used to output the laser emission.

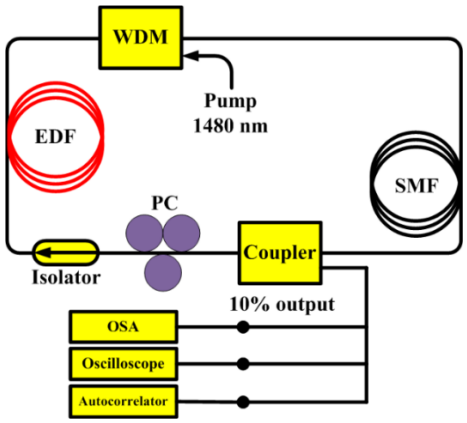

Figure 2.6. A schematic of the Erbium-doped fiber laser. EDF: Erbium-doped fiber. SMF: Single mode fiber. WDM: Wavelength division multiplexer. PC: Polarization controller

The fiber laser has a very simple cavity configuration. Different from the conventional soliton fiber lasers that need either an active or passive mode locker inserted in the cavity to initiate the pulse operation, there is no mode locker in our experiment. Therefore, no mode locking will occur. Under low power pumping the laser is always in a CW emission state. Depending on the linear cavity birefringence, which is controlled by changing the orientations of the paddles of the intra-cavity PC, the CW laser emission either consists of two different wavelengths and the emission at each wavelength is linearly polarized along one of the two orthogonal polarization directions of the cavity, or has a single wavelength with an elliptical (or linear) polarization.

We first investigated the case that the laser cavity has very weak linear birefringence. It was found that under strong pumping power (pump power >500 mW), linearly polarized CW laser emission could always be obtained. We attributed the linearly polarized laser operation to the polarization instability of light propagation in weakly birefringent fibers [16]. Operating in such a linearly polarized state, as the pump power is further increased, it is experimentally observed that the CW laser emission could be suddenly changed to a train of optical pulses, as shown in Fig. 2.7.

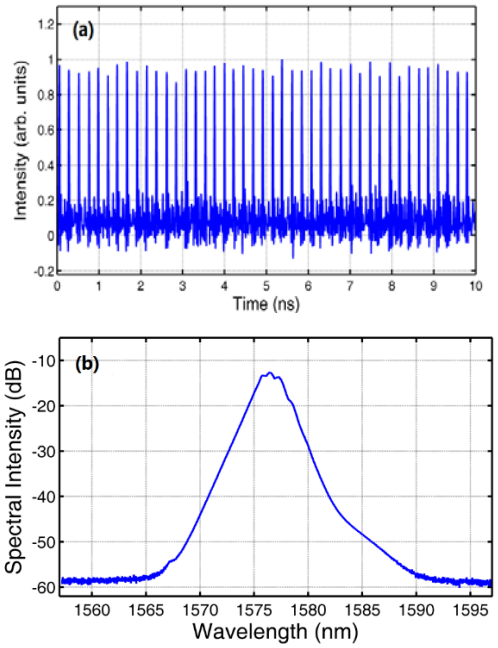

Figure 2.7: A typical case of the suddenly formed periodic pulse train emission of the fiber laser. (a) Oscilloscope trace of the laser emission. (b) the corresponding optical spectrum.

The repetition rate of the pulse train is tunable by carefully changing the orientation of the intra-cavity PC, which means it is initialed by the cavity induced MI (CIMI) [10, 11]. The pulses are very stable in the cavity. Carefully checking the pulse train, it can be identified that the pulse train is on a CW background, as shown in Fig. 2.7(a).

Once the periodic pulse train with a CW background is obtained, further increasing the pump power, the pulse intensity will increase and the CW background level will decrease. It's just the same as the previous numerical simulation results. Eventually the pulses start to move freely in the cavity, and the pulse distribution in the cavity becomes random, as shown in Fig. 2.8(a). Fig 2.8(b) is the corresponding optical spectrum. We can see that the optical spectrum of the laser emission becomes significantly broader. In particular, there are some obvious Kelly sidebands on the spectrum, which is the signature of the formation of solitons in the fiber ring laser. Once solitons are formed in the cavity, it was found that the dynamics of the solitons are similar to those observed on the conventional mode-locked soliton fiber lasers [16].

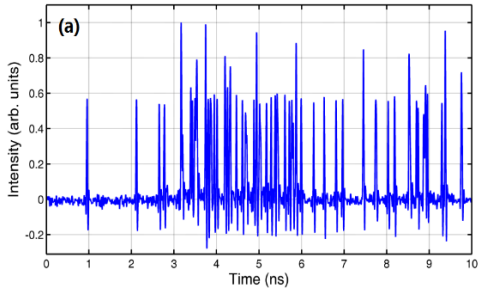

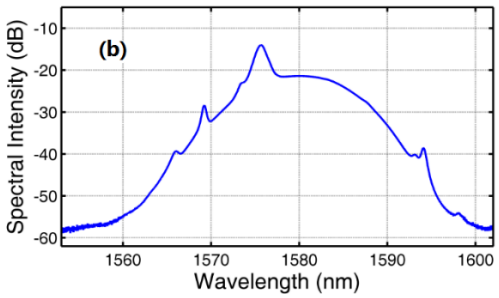

Figure 2.8. A typical case of the suddenly formed dissipative soliton emission state of the fiber laser. (a) A snapshot of the oscilloscope trace. (b) The corresponding optical spectrum.

Fig. (2.9) and Fig. (2.10) further show the operation of the fiber laser under relatively large linear cavity birefringence. In this case the laser emissions along the two orthogonal cavity birefringence axes have different wavelengths. Hence, the two orthogonally polarized laser beams are incoherently coupled. It was shown that the incoherent coupling results in the formation of the polarization domains, displaying that the laser emission alternates between the two coupled orthogonal polarization directions, as shown in Fig. (2.9).

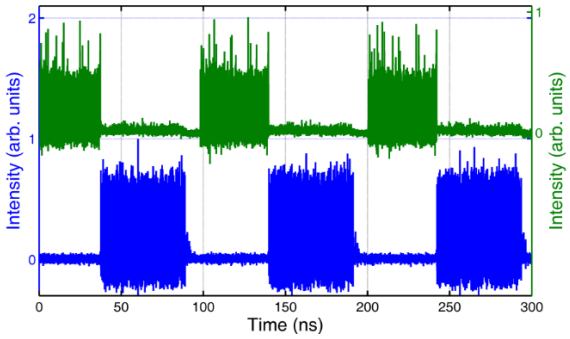

Figure 2.9. Dissipative soliton formation in each polarization domain. The two oscilloscope traces show the laser emission along each of the two orthogonal polarizations of the cavity. Zoom-in the trace the dissipative soliton distribution looks like that shown in Fig. 2.7(a).

Under relatively low pumping intensity, the laser emission in each domain is CW. However, as the intensity of the laser beam in a domain becomes sufficiently strong, a periodic pulse train could automatically form in the domains. The formation of the periodic pulse train is attributed to the effect of the CIMI. Initially the pulses are uniform and static in a domain. As the beam intensity is increased, the pulse distribution then becomes non-uniform, as shown in Fig. 2.9; in the meantime, the Kelly spectral sidebands also appear on the optical spectrum. Note that some pulses in Fig. 2.9 have high intensity, this can be explained by the fact that two pulses were too close to each other.

Normally, the formed pulses are confined within a domain, like the case shown in Fig. 2.9. However, under strong beam intensity it was also experimentally observed that the pulses could even constantly move out of a domain. Fig. 2.10 shows a case where the intensities along the two polarizations are asymmetric. Along one polarization direction, as the intensity is weak, no MI occurred. The

emission of the laser is in CW, while in the other polarization direction pulses are formed and the pulses have very high repetition rate. Because of the high pulse density, some of the pulses "diffused" out of the domain. On the real-time oscilloscope one could clearly monitor the pulse movement. The situation is similar to the so-called "soliton rain" observed in the mode-locked fiber lasers [17]. Again, the experimental result suggests strongly that the formed pulses are dissipative solitons.

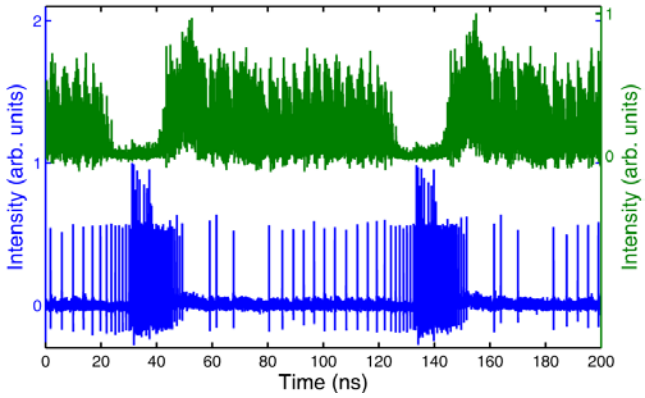

Figure 2.10. Dissipative soliton formation in one of the asymmetrical polarization domains. The two oscilloscope traces show the laser emission along ach of the two orthogonal polarizations of the cavity.

2.3 Conclusions

The numerical simulations have shown that under even a very weak periodic perturbation the strong CW emission of a fiber laser can become a periodic pulse train. Moreover, when the pump strength is increased, the periodic pulse train can become a train of periodic dissipative solitons. In the simulations the periodic perturbation was phenomenologically aided. However, we note that a strong CW beam in a detuned laser cavity is prone to the cavity induced modulation instability, and the effect of the modulation instability is to introduce a periodic modulation on a strong CW beam. Hence, based on the numerical result one could easily understand why a periodic pulse train could automatically form in a fiber laser. The experimental results have clearly confirmed the numerical simulations.

It is to point out that because the initial condition of the current soliton formation is different from that of the soliton formation in a mode locked laser, in the current case a periodic pulse train is always initially formed in the fiber laser cavity. This state is very different from the initial state of a mode locked fiber laser, where initially only several solitons are formed in the cavity and they could have an arbitrary soliton distribution in cavity.

3. Vector Temporal Cavity Solitons

As discussed above, in a near-isotropic fiber laser cavity the vector nature of light has to be considered. In the case of nonlinear light propagation the cross coupling between the two orthogonal polarization components of the light has to be considered. We have both theoretically and experimentally investigated the fiber laser operation. It was found that the temporal vector cavity soliton could also be formed in the fiber lasers. Depending on the laser operation

conditions, different forms of temporal cavity solitons have been experimentally observed. The formation mechanisms of the vector solitons can be traced back either to the coherent or incoherent cross polarization coupling.

3.1. Experimental setup and results

Fig. 3.1 shows a typical fiber laser configuration experimentally used. It has a similar configuration as that reported above for the scalar soliton formation, except that the length of the SMF is changed from 10 m to 9 m. The net average cavity dispersion is about 1.5 ps/nm/km. To experimentally resolve the two orthogonal polarization components of the laser emission, an external cavity polarization beam splitter (PBS) is used to separate the two orthogonal polarization components of the light field. A polarization controller is inserted before the external polarization beam splitter to balance the linear polarization change caused by the lead-fibers. The two orthogonal polarization components are simultaneously monitored with a high-speed detection system.

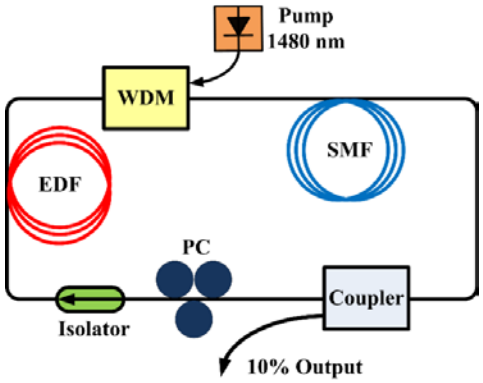

Figure 3.1. A schematic of the Erbium-doped fiber laser. EDF: Erbium-doped fiber. SMF: Single mode fiber. WDM: Wavelength division multiplexer. PC: Polarization controller.

No saturable absorber (SA) or polarization dependent components are inserted in the laser cavity, so no mode locking could happen. Experimentally, as the pump power was increased beyond the lasing threshold, CW emission was always established in the fiber laser, and depending on the net cavity birefringence, it was found that the CW laser emission could have different operation states. When the net cavity birefringence was weak, the laser emissions along the two orthogonal polarization directions of the cavity would have almost the same frequency. In this case when the pump power became sufficiently strong, coherent coupling between the two polarization components occurred. If the net cavity birefringence was strong, the laser emissions along the two orthogonal polarization directions of the cavity had obviously different frequencies. In this case the coupling between the two polarization components is incoherent.

We started from a laser operation state of coherent polarization coupling. In this situation the CW emission of the laser was elliptically polarized, and depending on the concrete laser operation condition, the ellipticity of the beam varied. Fig. 3.2 shows a case of the laser operation where the two polarization components had comparable intensity. It was experimentally observed that as the pump power was increased to about 600 mW, the CW emission along both polarizations simultaneously changed to periodic pulsing. The pulses along the two polarization directions were synchronized and had the same repetition rate. Carefully tuning the intra-cavity PC, the repetition

rate of the periodic pulses could be continuously altered, which suggests that the periodic pulsing was caused by the cavity induced modulation instability (CIMI) [10, 11]. However, different from the experimental results reported above, which is a scalar pulse train, we had now a vector periodic pulse train. With fixed laser operation conditions, the periodic vector pulse train state was very stable. Contrary to the periodic pulse trains caused by modulation instability effect in the light propagation case, no breathing of the pulses was observed [3].

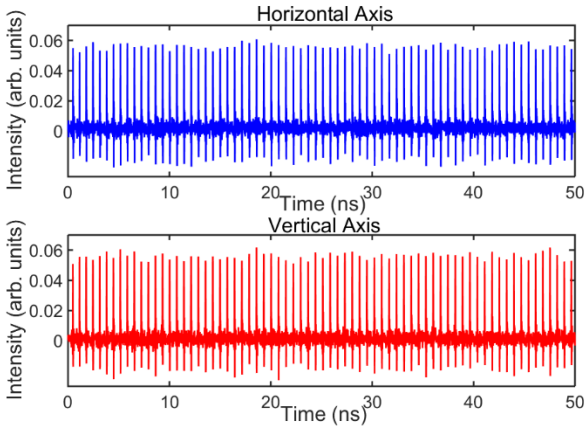

Figure 3.2. Laser emission state of the vector periodic pulses

Keeping increasing the pump power or decreasing the pulse repetition rate by tuning the intra-cavity PC, the peak power of each individual pulse increased. Eventually, the pulse distribution in the cavity became aperiodic. Especially the pulses started to move independently in the cavity, as shown in Fig. 3.3(a). Fig. 3.3(b) shows the corresponding polarization-resolved spectra. From the spectra one can clearly identify the appearance of two spectral sidebands, which are symmetric with respect to the central wavelength. The appearance of the spectral sidebands indicates that the pulses are solitons [18]. According to the theory of temporal cavity solitons, these solitons are dissipative solitons. We note that the sideband locations and the soliton center wavelengths of the two polarization components are almost the same, which suggests that the solitons along each of the two orthogonal polarizations had the same parameters and properties. Despite of the fact that there was a strong CW field along the two polarization directions, the solitons along each of the polarizations moved synchronously in the cavity. Once the vector solitons were formed, slightly changing the linear cavity birefringence couldn't destroy them. Carefully reducing the pump power, first the CW beam power was reduced. Eventually, on the optical spectra no CW components were visible, associated with the pump power decreasing the number of soliton in the cavity could also be reduced one by one. The similar features have also been observed on the solitons formed in the mode locked fiber lasers. Fig. 3.3(c) further shows the measured autocorrelation trace of the solitons. It has a FWHM width of about 1.37 ps, suggesting that the width of the solitons at the laser output is about 880fs if a $Sech^2$-shape pulse profile is assumed.

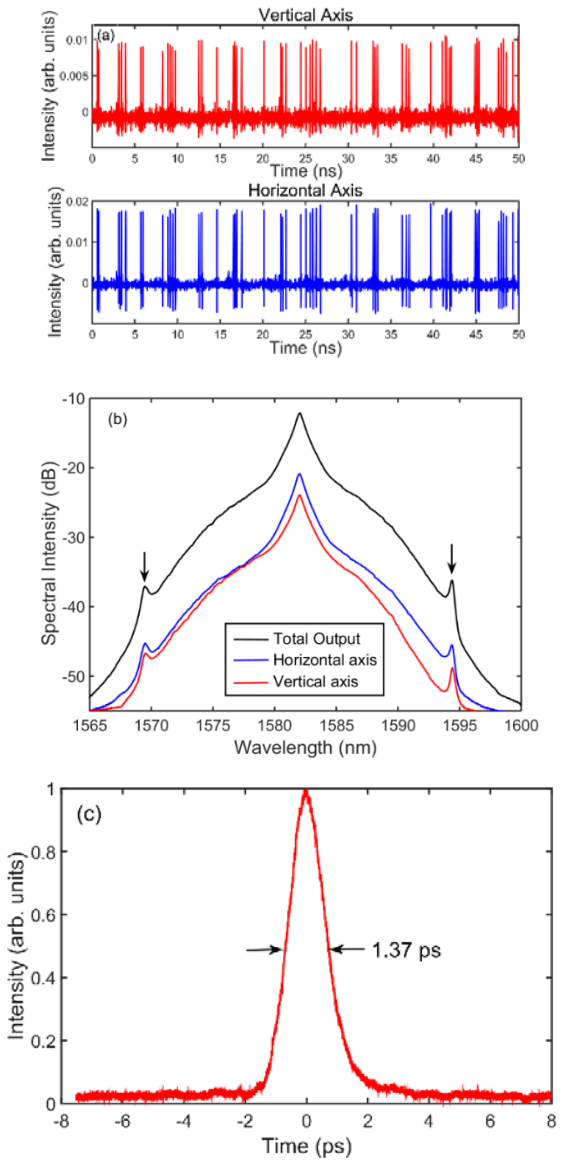

Figure 3.3. A state of the vector cavity soliton emission of the laser. (a) Oscilloscope traces of the two orthogonal polarization components; (b) Polarization-resolved spectra; (c) the autocorrelation trace

Depending on the laser operation conditions, the relative strength of the two coherently coupled polarization components could be very different. Fig. 3.4 shows a case where the laser was almost linearly polarized along the horizontal polarization direction. Based on the intensity trace of the laser emission, the soliton pulses along the vertical polarization direction were hardly to be measured. However, from the polarization-resolved spectra it is to see that there were also solitons formed along the vertical polarization direction as suggested by the broad spectrum with some clear spectral sidebands. Carefully comparing the spectral sidebands with those of the solitons polarized along the orthogonal polarization direction, they located at the same spectral positions and exhibited the peak-dip relation, suggesting that they were formed due to the coherent coupling between the two orthogonal polarization components [19]. We note that there is also a big spectral dip near the center part of the spectrum of the vertical polarization component. We postulate that it was also formed due to the coherent coupling of the two polarization components. The spectral intensity difference of the two orthogonal polarization components is larger than 25 dB. Obviously the

beam intensity along the vertical polarization direction alone couldn't support the spontaneous soliton formation. Therefore, the formed soliton should be induced by the cavity solitons formed in the horizontal polarization direction. Zhang *et al.* reported a similar phenomenon of induced solitons in a mode locked fiber laser previously [20]. Our experimental result once again confirmed the formation of the type of induced solitons between the coherently coupled light beams.

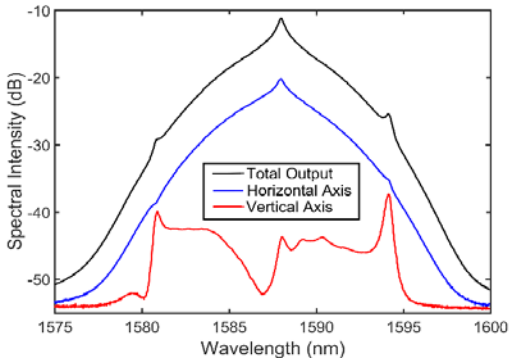

Figure 3.4. Polarization-resolved spectra of the laser emission that shows the induced cavity soliton formation under weak net cavity birefringence.

In our experiment induced temporal cavity solitons were also observed even when the net linear cavity birefringence was relatively large, as shown in Fig. 3.5. Different from the case shown in Fig. 4.4, the induced solitons shown in Fig. 3.5 have obviously different central wavelength from that of the inducing solitons. Moreover, the Kelly sidebands of the induced solitons also locate at different positions from those of the inducing solitons. We note that similar phenomenon was also reported in Ref. [20], which was explained as a result of the incoherent coupling between the two polarization components. Our experimental result supports the explanation again, as shown in Fig. 3.5, on the polarization-resolved spectra of the solitons no energy exchange sidebands are visible.

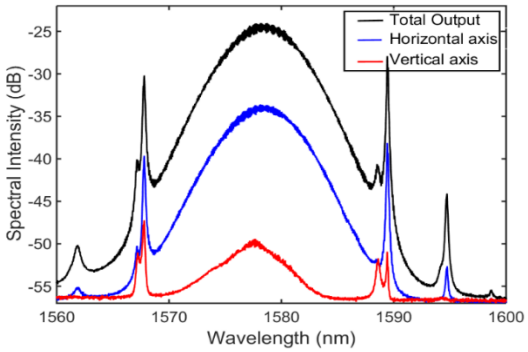

Figure 3.5. Polarization-resolved spectra of the laser emission showing the induced soliton formation under relatively large net cavity birefringence.

In addition to the results shown in Fig. 3.4 and Fig. 3.5, another situation of the induced cavity soliton formation as shown in Fig. 4.6 and Fig. 3.7 was also experimentally observed. Fig. 3.6 shows the case of the incoherent coupling between the two orthogonal polarization components, while Fig. 3.6 shows that of the coherent coupling. Different from the results shown in Fig. 3.3 and Fig. 3.4 where due to the

cavity induced MI the strong CW beam itself was first destabilized, and then the temporal cavity solitons were formed from the destabilized CW beam, Fig. 3.5 and Fig. 3.6 show that a strong CW beam along one polarization direction could induce the formation of periodic pulsation along the orthogonal polarization direction where initially either a weak CW or no light exists, and further lead to the formation of the temporal cavity solitons along that polarization direction. Once the cavity solitons are formed, they further induce soliton formation on the CW side. However, in the case of incoherent coupling the induced solitons are too weak to be seen on the oscilloscope trace, while in the case of coherent coupling clear induced solitons are visible on the strong CW background, as shown in Fig. 3.6(a). Associated with the induced solitons broad intensity depths were also formed on the CW beam, whose formation is a manifestation of the polarization domains as reported previously in [21].

The results shown in Fig. 3.5 and Fig. 3.6 can be attributed to the modulation polarization instability (MPI) effect [22, 23]. As first theoretically predicted by Wabnis *et al.*, through cross polarization coupling a strong CW beam in a linearly birefringent single mode fiber polarized along one eigen-polarization direction could induce the MI of light polarized along the orthogonal polarization direction. Different research groups have previously experimentally observed the MPI effect [24-27]. However, to the best of our knowledge there is no experimental observation of the effect occurred in a laser cavity. Comparing to the previous experimental observations of the phenomenon, obviously in an active cavity the threshold of the MPI could be significantly reduced. Bearing in mind that the MPI could destabilize the light polarized along the orthogonal polarization, under the same mechanism of the temporal cavity soliton formation shown in Fig. 3.3 and Fig. 3.4, the appearance of the temporal cavity solitons on the weak CW side as shown in Fig. 3.5 and Fig. 3.6 could be easily understood.

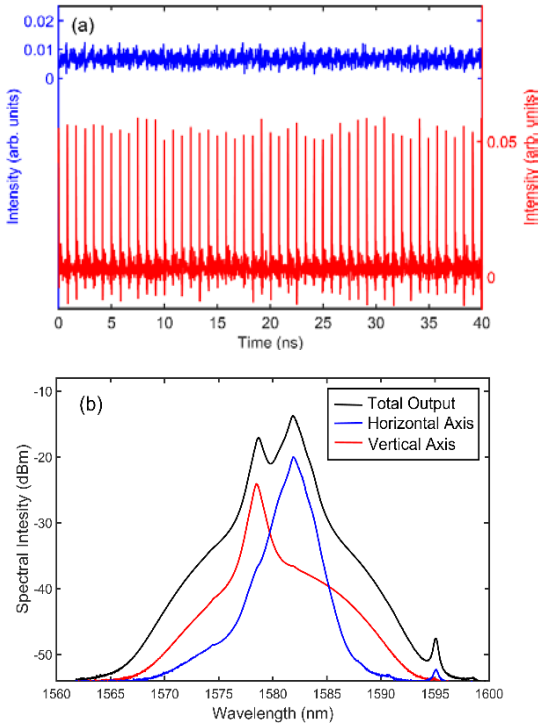

Figure 3.6. Temporal cavity soliton formation caused by the MPI effect in the laser under large net cavity birefringence. (a) The

polarization-resolved oscilloscope traces, (b) the corresponding optical spectra.

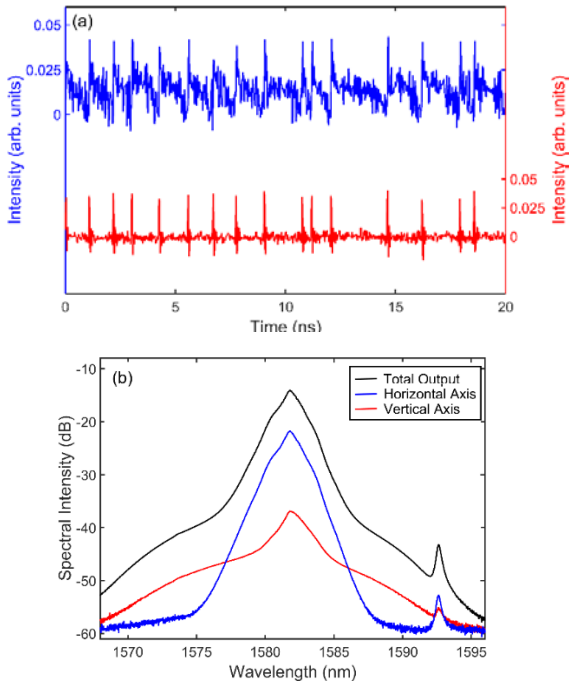

Figure 3.7. Temporal cavity soliton formation caused by the MPI effect in the laser under small net cavity birefringence. (a) The polarization-resolved oscilloscope traces, (b) the corresponding optical spectra.

3.2. Numerical studies

To verify the temporal vector cavity soliton formation in fiber lasers, we have also conducted numerical simulation on the operation of the fiber lasers. Our emphasis is to show that in a quasi-vector cavity fiber laser, as a result of the combined effect of the cavity induced modulation instability, the coherent coupling between the orthogonal polarization components and the effective gain bandwidth limitation, a stable periodic vector pulse train could be automatically formed. As a fiber laser is intrinsically a dissipative system, when the pump of the laser is increased, and/or the repetition rate of the pulses is decreased, the intensity of the formed pulses would increase. Eventually the pulses could be shaped into temporal vector cavity solitons, just like the case of the scalar temporal cavity soliton formation reported previously [28]. Once a temporal vector cavity soliton is formed, it is stable in the cavity.

Our simulation is based on the coupled Ginzburg-Landau equations (GLEs), which describe the light propagation in a weakly birefringent gain fiber

$$\begin{aligned}\frac{\partial u}{\partial z} &= i\beta u - \delta\frac{\partial u}{\partial t} - \frac{ik''}{2}\frac{\partial^2 u}{\partial t^2} + i\gamma\left(|u|^2 + \frac{2}{3}|v|^2\right)u + \frac{i\gamma}{3}v^2u^* + \frac{g}{2}u + \frac{g}{2\Omega_g^2}\frac{\partial^2 u}{\partial t^2} \\ \frac{\partial v}{\partial z} &= -i\beta v + \delta\frac{\partial v}{\partial t} - \frac{ik''}{2}\frac{\partial^2 v}{\partial t^2} + i\gamma\left(|v|^2 + \frac{2}{3}|u|^2\right)v + \frac{i\gamma}{3}u^2v^* + \frac{g}{2}v + \frac{g}{2\Omega_g^2}\frac{\partial^2 v}{\partial t^2}\end{aligned} \tag{3.1}$$

where u and v describe the optical fields of the two orthogonal polarization components in the fiber, $2\beta = 2\pi\Delta n/\lambda = 2\pi/L_b$ is the wave number difference between these two polarization modes, $2\delta = 2\beta\lambda/2\pi c$ is the group velocity difference, ***k''*** is

the second-order dispersion coefficient, γ represents the nonlinearity of the fiber cavity, g is the gain coefficient of the gain fiber and Ω_g is the effective gain bandwidth. The gain saturation is defined as

$$g = G\exp\left[-\frac{\int\left(|u|^2+|v|^2\right)dt}{E_0}\right] \qquad (3.2)$$

where G is the small signal gain coefficient and E_0 is the gain saturation energy, which is related to the pumping power in the experiment. In our simulations we have possibly used the real experimental parameters such as the actual cavity length, the dispersion-managed cavity, and the fiber dispersion etc. At a certain CW laser operation state we start the simulation by adding a weak periodic modulation on the optical field, and then let the light circulate in the fiber cavity until a stable state is reached. We consider each such obtained stable state as a possible laser emission state experimentally observed.

We first considered the case of a fiber laser that has a weak cavity birefringence. To the end we have set the beat length (L_b) as 100 m in the simulation. It represents the averaged birefringence strength of the fiber cavity. When the lasing condition is fulfilled, CW emission is established in the cavity, whose intensity increases with the pump power. In the case the optical field along the two orthogonal polarization directions of the cavity is coherently coupled. To simulate the cavity induced modulation instability effect, we artificially introduced an initial field $u(0,t)=U_0\cos(2\pi\Delta\nu t)\sin(\theta)$ and $v(0,t)=U_0\cos(2\pi\Delta\nu t)\cos(\theta)$, where $\Delta\nu$ is the modulation frequency and θ is the polarization angle. Numerically it is found that if the effective gain bandwidth limitation term Ω_g in the simulation is ignored, the CW beam on each polarization components always turns into the Akhmediev breather structures, which is a typical modulation instability phenomenon supported by the NLSE [3]. However, with an appropriate effective gain bandwidth selection, the modulated CW will become a periodic pulse train embedded on a CW background. Keeping increasing the saturation energy, the pulses will narrow down and the CW level will decrease. Eventually the periodic pulse train turns into cavity solitons, as shown in Fig. 3.7. The cavity soliton nature of the pulses is confirmed by their pulse profile, which is uniquely determined by the laser parameters such as the effective gain bandwidth and the balance between the gain and losses [28].

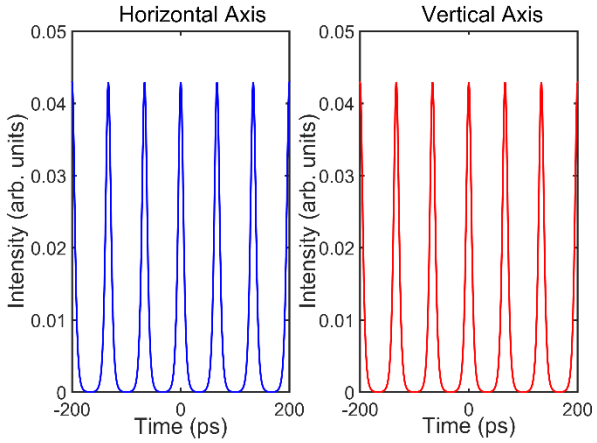

Fig. 3.7: Formation of vector cavity solitons in a fiber laser. The parameters used are: E_0=25 pJ, Ωg =10 nm, G=640/km and $\Delta\nu$ =15 GHz.

We then numerically simulated the induced cavity soliton formation by the cross-phase modulation (XPM) effect in a weakly birefringent cavity. To simulate the experimental observation, the initial input state is set as $u(0,t) = U_0 \cos(2\pi\Delta\nu t)$ and $v(0,\mathrm{t}) = V_0$, where $U_0 \geq V_0$. By appropriately choosing the effective gain bandwidth and saturation energy, we observe that not only a stable train of cavity soliton can be formed on the strong CW side, like the case of the scalar cavity soliton formation reported previously in Ref. [28], but also a stable train of cavity soliton are formed on the weak CW side in the orthogonal polarization direction due to the XPM effect, as shown in Fig. 3.8. The induced solitons have very low peak power and are embedded in the weak CW beam. The solitons on both polarization components are synchronized and have nearly the same pulse width, which is the same as the experimental observations.

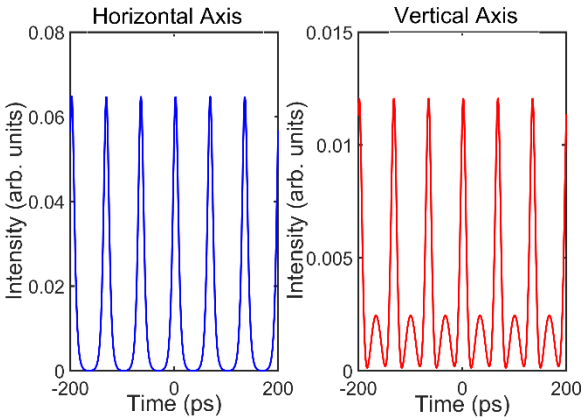

Figure 3.8. The XPM induced temporal cavity solitons. The parameters used are: $\boldsymbol{E_0}$=75 pJ, $\boldsymbol{\Omega g}$=10 nm, $\boldsymbol{G}$=640/km, $\boldsymbol{Lb}$= 100m and $\Delta\nu$ =15 GHz.

At last we simulated the MPI induced temporal cavity soliton formation. To this end we have set the input as $u(0,t) = U_0$ and $v(0,\mathrm{t}) = V_0 \cos(2\pi\Delta\nu t)$, where $U_0 \geq V_0$. The modulation in the vertical polarization direction is set as 15 GHz, which is induced by the cavity induced MPI effect. Again the beat length of the fiber cavity is set as 100 m to represent the weakly birefringence cavity. Under appropriate effective gain bandwidth and saturation energy, we can again get a stable pulse train in the vertical axis, as shown in Fig. 3.9. From the simulation result it is to see that the formed temporal cavity solitons further induce cavity solitons on the horizontal direction and the induced solitons are embedded in the strong CW beam.

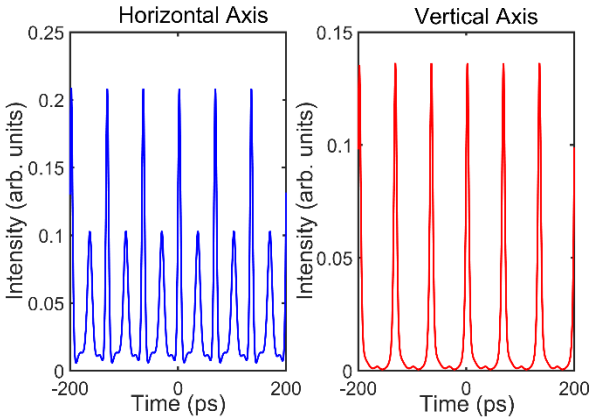

Figure 3.9. The MPI induced temporal cavity soliton formation. Parameters used are E_0=25 pJ, Ωg=10 nm, G=640/km, Lb= 100m and $\Delta\nu$ =15 GHz.

3.3.Temporal vector cavity solitons in normal dispersion regime

3.3.1 Experimental setup and results

Our fiber laser is schematically shown in Fig. 3.10. It has a dispersion-managed fiber ring cavity that consists of a piece of 4 m Erbium doped fiber (EDF) with a dispersion parameter of -48 ps/nm/km, 10.7 m single mode fiber (SMF) with a dispersion parameter of 18 ps/nm/km and 15.6 m dispersion compensation fiber (DCF) with a dispersion parameter of -4 ps/nm/km. The total cavity length is ~30.3 m with a net normal average dispersion parameter of -2.04 ps/nm/km. A polarization independent isolator is inserted in the cavity to force the uni-directional circulation of light in the cavity. Besides, an intra-cavity polarization controller (PC) is used to fine-tune the linear cavity birefringence. The fiber laser is pumped by a 1480 nm high power Raman single-mode fiber laser source whose maximum output power can be as high as 5 W. A wavelength division multiplexer (WDM) is used to couple the pumping light into the cavity, and a 10% fiber output coupler is used to output the light. The pumping coupling efficiency from the pump source to the cavity is about 60%. An external cavity polarization beam splitter (PBS) is used to experimentally resolve the two orthogonal polarization components of the laser emission. And a polarization controller is inserted before the external polarization beam splitter to balance the linear polarization change caused by the lead-fibers. The two orthogonal polarization components are simultaneously monitored with a high-speed electronic detection system made of two 40 GHz photo-detectors and a 33 GHz bandwidth real-time oscilloscope. There are no saturable absorber (SA) or polarization dependent components in the laser cavity, so no mode locking could happen in the laser. Meanwhile, the components used in our experiment have very low polarization dependent loss (PDL) (WDM: 0.01 dB, Isolator: 0.04 dB, Coupler: 0.01 dB). Therefore, the PDL induced mode locking is also unlikely to occur in our experiment [46].

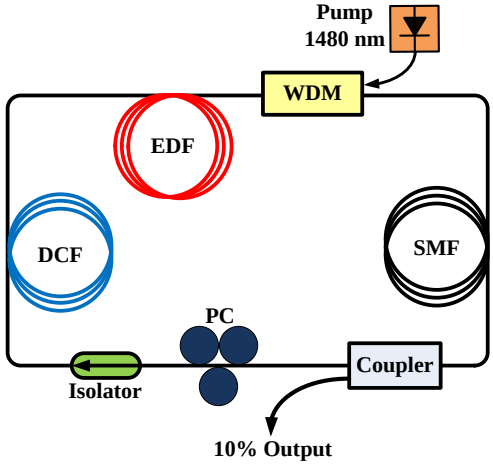

Figure 3.10. A schematic of the Erbium-doped fiber laser. EDF: Erbium-doped fiber. SMF: Single mode fiber. DCF: Dispersion compensation fiber. WDM: Wavelength division multiplexer. PC: Polarization controller.

The fiber laser starts lasing when the pump power is ~100 mW. When the pump power is increased to about 1W, by carefully tuning the intra-cavity PC, a stable quasi-periodic vector pulse train emission state, as shown in Fig. 3.11(a), could be obtained. Fig. 3.11(b) is the corresponding polarization-resolved optical spectra of the laser emission. The sharp edges are typical for the dissipative solitons obtained in the normal dispersion cavity fiber lasers [29]. This confirms that the vector pulses are vector dissipative solitons. As there is no saturable absorber in the cavity, these dissipative solitons can be regarded as the temporal cavity solitons, which are in principal dissipative solitons. The 3-dB spectral bandwidth of the solitons is about 13.5 nm. Moreover, on the polarization resolved spectra spectral sidebands with clear peak-dip intensity relation are visible at 1593 nm. According to studies on the phase locked vector solitons formed in the anomalous dispersion cavity fiber lasers, such a peak-dip spectral sidebands are formed as a result of the coherent coupling between the two orthogonal polarized soliton components. It is an indication of the energy exchange between them [19]. To the best of our knowledge, this is the first experimental observation of such energy exchange between the components of vector dissipative solitons formed in the normal dispersion cavity fiber lasers. We note that different from the coherent energy exchange sidebands observed on the solitons formed in the anomalous dispersion cavity fiber lasers, where they appear almost symmetrically with respect to the soliton central wavelength, here only one peak-dip structure is observed. We believe it could be due to the large frequency chirp of the dissipative solitons formed in the normal dispersion regime. Fig. 3.11(c) is the corresponding autocorrelation trace of the dissipative solitons. It has a FWHM width of about 18.6 ps, suggesting that the width of the solitons is about 12.1 ps if a Sech-shape pulse profile is assumed. The time-bandwidth product is about 19.5, indicating the solitons are strongly chirped. We measured that the intra-cavity power is about 175 mW and the repetition rate is about 400 MHz, so we can calculate the single pulse energy is about 437.5 pJ.

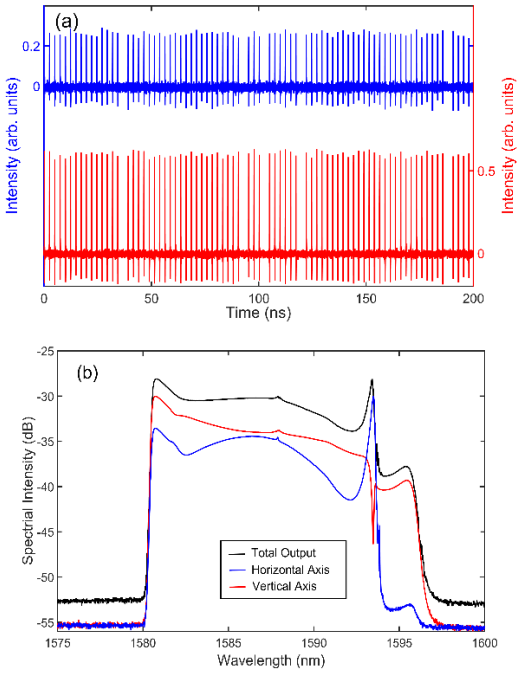

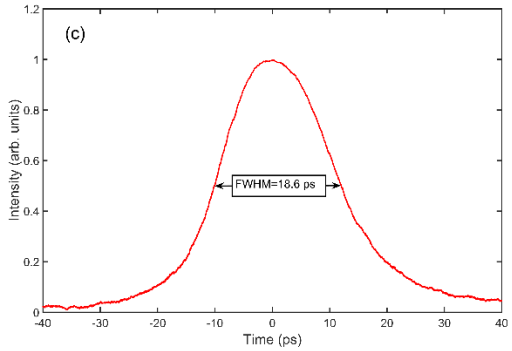

Figure 3.11. A typical vector temporal cavity soliton emission state (a) Polarization resolved oscilloscope traces. (b) Polarization-resolved optical spectra. (c) The autocorrelation trace.

In our experiment once the near periodic vector temporal cavity soliton train is obtained, further changing the intra-cavity PC or the pumping power, the soliton pulse train will break up and the soliton distribution in the cavity will become inhomogeneous, as shown in Fig. 3.12(a). With less number of soliton in the cavity, the energy of each individual soliton also becomes larger. Consequently, the edges of the soliton spectrum stretch out and become no longer sharp. As the spectrum of the solitons extends out, different from the Fig. 3.11(b) with only one energy exchange structure, more energy exchange spectral sidebands appear on the two stretched edges of the polarization resolved spectra, as shown in Fig. 3. 12(b).

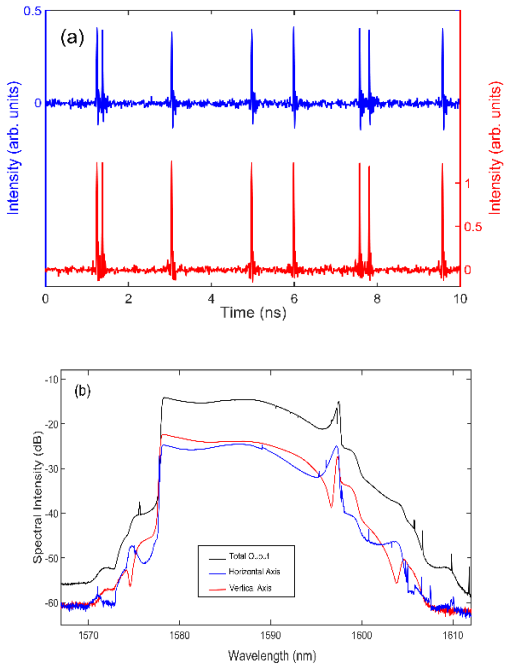

Figure 3.12. Vector temporal cavity soliton operation of the fiber laser with random soliton distribution in cavity. (a) Polarization resolved oscilloscope traces. (b) Polarization-resolved optical spectra.

As there are no saturable absorber (SA) or polarization dependent components in the laser cavity, no self-started mode locking could occur in the laser, therefore, the formation of the vector dissipative solitons can't be attributed to the soliton shaping of the mode locked pulse. A plausible explanation is that they are induced by the cavity

induced modulation instability (CIMI), which also exists in the normal dispersion regime. CIMI will break the CW emission and under effect of the effective gain bandwidth limitation, the CW changes into a periodic pulse train. In case that the formed pulse intensity is sufficiently strong the pulses are further shaped into dissipative solitons under the mutual interaction of the average normal cavity dispersion, the nonlinear Kerr effect, laser gain and loss [17, 29]. We emphasize that the pulse formation in our laser is not through the mode locking process. In addition, the formed solitons are not subject to the influence of the saturable absorber or a mode locker as in a mode locked laser case. To distinguish the dissipative solitons from those generated in the mode-locked fiber lasers and to emphasis the role played by the effective gain bandwidth limitation on the soliton formation, this dissipative soliton can be also regarded as the temporal cavity solitons.

From the state shown in Fig. 3.12 if the intra-cavity PC is further tuned so that the soliton spectrum further extends out, the solitons in the cavity could come together to form a giant energy pulse, as shown in Fig. 3.13(a). Zooming in the pulse shown in Fig. 3.13(a) with a larger time scale, random varying fine structures are visible within the pulse. Experimentally, the pulse width and energy increases with the pump power. At a pump power of ~ 2 W, where intra-cavity power is about 400 mW, so the energy of the whole "Big Pulse" can be calculated as 60 nJ. Such a pulse is known as the noise-like pulse [30, 31]. The noise like pulse emission is one of the typical operation states of the soliton fiber laser in the normal dispersion cavity regime. Previous study of the laser emission was speculated that the noise like pulses could be caused by the saturable absorber in the cavity. However, there is no any mode-locker our fiber laser but the same state of laser emission could still be formed. Hence, the formation of noise-like pulse can't only be attributed to the effect of saturable absorber. In Fig. 3.13(b) we have compared the optical spectra of the above three laser operation states. In our experiment by simply tuning the intra-cavity PC the laser emission could move from one state to the other.

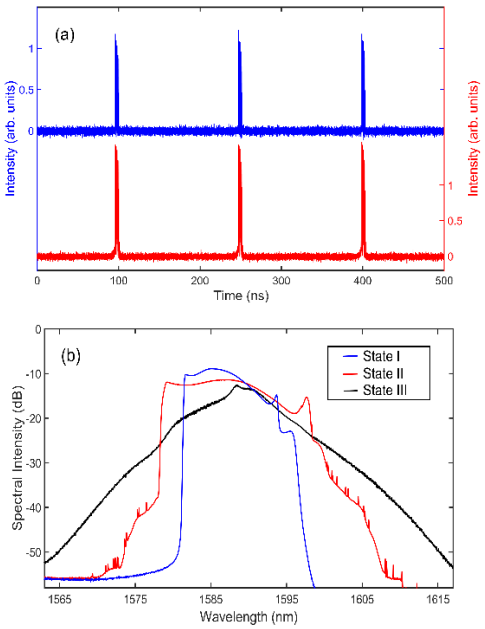

Figure 3.13. (a) Polarization resolved oscilloscope traces of a vector noise-like pulse emission state of temporal cavity soliton. (b) Optical

spectra of the laser emission in I: a near-periodic soliton train state; II: a state with random soliton distribution; III: a noise-like pulse state.

Occasionally, before the noise like pulse state is reached, experimentally another state of the laser operation as shown in Fig. 3.14 could also be observed. In the state the solitons don't come together to form a noise-like pulse, but form a so-called "soliton rain" state [32, 33]. In the current soliton rain state the solitons continuously move away from the soliton condensate. Based on the experimental result we suspect that a noise like pulse could be actually an ensemble of many solitons that have come very close to each other in the cavity.

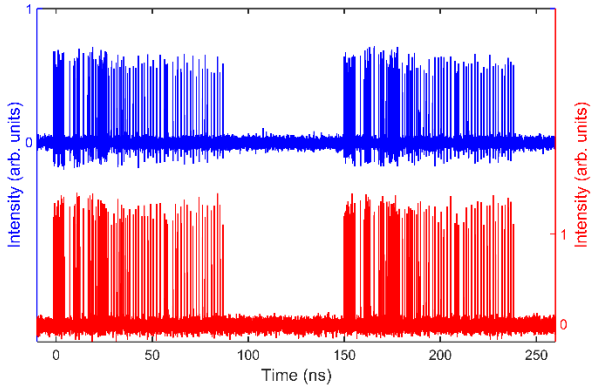

Figure 3.14. The vector soliton rain formed in the fiber laser cavity.

3.3.2 Conclusions

In conclusion, the formation of temporal vector cavity solitons in either anomalous or normal dispersion cavity fiber lasers has been experimentally observed. In both cases the formation of temporal vector solitons is induced by the cavity induced modulation instability. In the anomalous dispersion regime, vector solitons formed either through the coherent or incoherent coupling between the two orthogonal polarization components are obtained. Numerical simulations have well reproduced the experimental results and confirmed their formation mechanisms. Besides, in the normal cavity dispersion regime, vector temporal cavity solitons were also first experimentally revealed. The vector cavity solitons possess all the characters of the dissipative solitons. Moreover, our experimental results have shown that the noise-like and soliton rain states are two special case of the multiple solitons operation of the fiber lasers.

4. Other features of the vector cavity fiber lasers

When two or more intense optical fields with different wavelengths co-propagate in an optical fiber, they will couple with each other through the fiber nonlinearity. The cross-phase modulation (XPM) is the most common way of coupling. While the XPM process always occurs and doesn't cause energy transfer between the lights, therefore, referred to as an incoherent coupling, the four-wave-mixing (FWM) type of coupling occurs when the phase matching condition is fulfilled. FWM involves in the energy transfer between the lights. Coupling of lights in a single mode fiber can result in a variety of interesting nonlinear optical phenomena, e.g. it is theoretically predicted by B. Malomed *et*

al. that the incoherent coupling between two travelling plane waves could lead to the formation of optical domains [34, 35]. It is well known that due to the fiber bending and/or technical imperfection of fiber drawing, a single mode fiber always exhibits birefringence and hence supports two orthogonal polarization modes. The light propagation in a practical SMF also involves in the coupling between the two orthogonal polarization modes. It has been shown both theoretically and experimentally that the cross polarization coupling of light in a SMF could result in various effects, such as the polarization switching [36], polarization modulation instability [24], group velocity locked or phase locked vector solitons [37]. A fiber cavity is an interesting nonlinear system that possesses both the features of light propagation in SMFs and a nonlinear cavity. The conventional soliton formation in the mode locked anomalous dispersion cavity fiber lasers is an effect that could be traced back to the nonlinear light propagation in the SMFs, which has been extensively investigated previously. Soliton period-doubling route to chaos [38], soliton quasi-periodicity [39] were also observed in fiber lasers, which could be well understood based on the nonlinear cavity theory. Recently, Zhang *et al.* reported the induced soliton formation in a birefringence cavity fiber laser [20]. Tang *et al.* demonstrated the polarization domain formation in a quasi-isotropic cavity fiber laser [21]. Formation of these effects could be well explained based on the coherent or incoherent polarization coupling between the lights in the fiber cavity.

4.1. Soliton-dark pulse pair formation

In this section we will focus on some special features of the quasi-vector cavity fiber lasers. As described above, when light propagates in a quasi-vector cavity fiber laser the vector nature of light has to be considered. In the nonlinear case the two orthogonal polarization components are either coherently or incoherently coupled. Theoretical studies on the light propagation in weakly birefringent fibers have shown that as a result of the cross coupling between the orthogonal polarization components many novel effects could be formed. Light propagation in a fiber laser cavity mimics the light propagation in single mode fibers. It is to expect that similar phenomena could also be observed in the quasi-vector cavity fiber lasers. Here we will report the experimental observation of some of the phenomena.

4.1.1 Experimental setup and results

The fiber ring laser we used has a cavity configuration as shown in Fig. 4.1. The fiber ring has a total length of 13.5 m, consisting of a piece of 3 m Erbium doped fiber (EDF) with a group velocity dispersion (GVD) parameter of -48 ps/nm/km, 9.7 m single mode fiber (SMF-28) with a GVD parameter of 18 ps/nm/km and 0.8 m of dispersion compensation fiber (DCF) with a GVD parameter of -4 ps/nm/km. The fiber laser is pumped by a 1480 nm single mode Raman fiber laser whose maximum output power is 5 W. A polarization independent isolator is inserted in the cavity to force the unidirectional circulation of light in the cavity. In addition, an intra-cavity polarization controller (PC) is used to fine-tune the linear cavity birefringence. A wavelength division multiplexer (WDM) is used to couple the pumping light into the cavity, and a 10% fiber output coupler is used to output the light. The components used in our experiment have very low polarization dependent loss (PDL) (WDM: 0.01 dB, Isolator: 0.04 dB, Coupler: 0.01 dB). Therefore, the PDL induced mode locking is

unlikely to occur in our experiment [46]. The fiber ring cavity is estimated to have an average net anomalous GVD parameter of 2.03 ps/nm/km. An external cavity polarization beam splitter (PBS) is used to experimentally resolve the two orthogonal polarization components of the laser emission. To the end a polarization controller is inserted before the external polarization beam splitter to balance the linear polarization change caused by the lead-fibers. To appropriately set the PC orientation experimentally we first operate the laser in a stable polarization domain emission state. Based on the polarization switching between the domains we then carefully adjust the external PC position so that the two orthogonally polarized laser emissions can be well separated. The polarization resolved laser emissions are simultaneously monitored with a high-speed electronic detection system made of two 40 GHz photo-detectors and a 33 GHz bandwidth real-time oscilloscope.

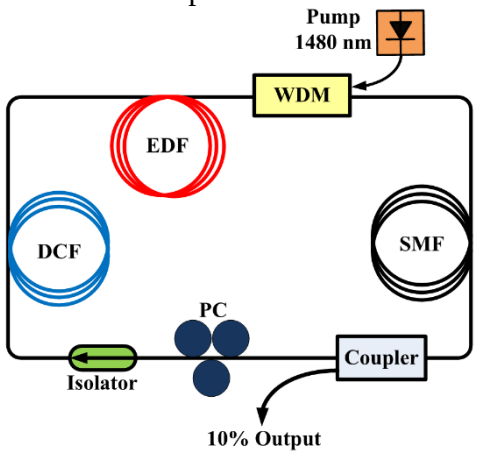

Figure 4.1. A schematic of the Erbium-doped fiber laser. EDF: Erbium-doped fiber. SMF: Single mode fiber. DCF: Dispersion compensation fiber. WDM: Wavelength division multiplexer. PC: Polarization controller.

Under low pump power the laser always emits continuous wave (CW). However, depending on the net cavity birefringence, the laser emission could exhibit different polarization features. In the special case of very weak net cavity birefringence, the laser could emit an elliptically polarized beam. However, the most frequent situation is that the laser emits simultaneously CW along the two orthogonal polarization directions of the cavity. Carefully tuning the orientation of the intra-cavity polarization controller, which alters the net linear cavity birefringence, the oscillation wavelength difference between the CWs could be tuned. The experimental result suggests that the laser emission wavelength difference is related to the linear cavity birefringence. In our experiment we used the wavelength separation as an indication on the strength of the net cavity birefringence. Operating the laser under different pump strength and net cavity birefringence, we could experimentally observe various interesting features of the laser emission. At first, we operated the laser at very small net cavity birefringence and under a pump power of about 2 W, where the intra-cavity light intensity is about 630 mW. By carefully setting the orientation of the intra-cavity PC, it is experimentally observed that the CW emission along one polarization direction could suddenly break up into a periodic bright pulse train, and associated with each of the bright pulses there is a dark pulse formed on the CW background along the orthogonal polarization direction, as shown in Fig. 4.2(a).

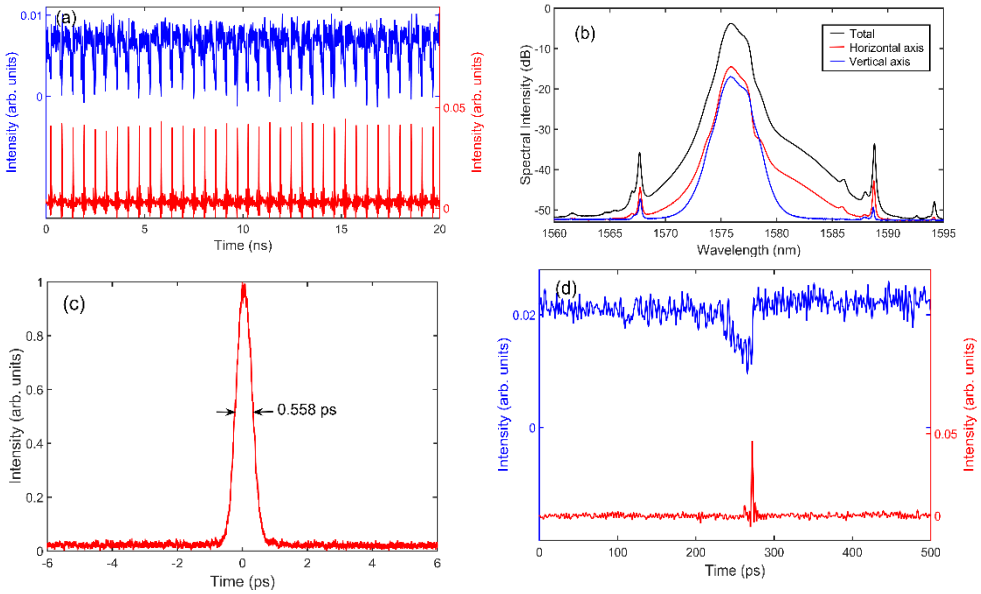

Figuer 4.2. Experimental results of soliton-dark pulse pair formation in a fiber laser. (a) The polarization resolved oscilloscope traces of the laser emission. (b) Polarization-resolved spectra. (c) Autocorrelation trace of the bright solitons. (d) The zoom-in oscilloscope traces of a soliton-dark pulse pair.

The automatic formation of a periodic bright pulse train in the fiber laser could be understood as a result of the CIMI described above. In our experiment we have investigated the features of the formed bright and dark pulses. Fig. 4.2(b) shows the polarization-resolved spectra of the laser emission. The spectrum of the light polarized along the horizontal polarization is significantly broadened. Its 3-dB bandwidth is estimated ~ 8 nm. Moreover, clear Kelly spectral sidebands are formed on the spectrum. Formation of the Kelly sidebands is a typical characteristic of the soliton operation of a laser [18]. The appearance of Kelly sidebands on the pulse spectrum unambiguously shows that the formed bright pulses are solitons. The central wavelength of the solitons is at 1578.76 nm, which is different from that of the CW laser emission of the same polarization direction. So far we have not understood why the central soliton wavelength is far away from that of the CW. We suspect it could be due to that the soliton and the CW beam have different loss dispersion in the cavity. Due to the weak net cavity birefringence, the CW wavelengths of the laser along the two orthogonal polarization directions are almost the same, which is at ~1575.7 nm. The spectra of the CW lights are also slightly broadened. From the traces shown in Fig. 4.2(a), one can observe that the CW background is very noisy. This is due to the modulation instability of the beam, which occurs when the CW intensity is high and has a high modulation frequency. This also explains why the spectra of the CW components are broad. Experimentally we measured the average output power of the laser emission along the two orthogonal polarizations. It has a ratio of about 1:6 (bright soliton side: dark pulse side).

Fig. 4.2(c) shows the autocorrelation trace of the bright solitons. It has a FWHM width of about 0.558 ps, suggesting that the width of the solitons at the laser output is about 362 fs if a Sech-shape pulse profile is assumed. Thus the

time-bandwidth product (TBP) of the pulses is 0.348, which means that the solitons are slightly chirped. Fig. 4.2(d) shows the zoom-in of a dark pulse. Different from the bright solitons, the dark pulses are broad intensity 'holes' embedded in the CW background. In our experiment if the total laser emission is measured, the oscilloscope trace then shows a dark-bright pulse pair on the CW background. A similar dark-bright pulse pair emission was also observed on a figure-of-eight fiber laser, and it was found that the dark and bright pulse belongs to different wavelength bands of the laser emission, respectively [40]. Experimentally we found that the dark pulse width decreased with the increase of the CW power and the coupling strength between the two polarizations. Under our experimentally accessible pump strength, dark pulses as narrow as several tens of picosecond could be obtained. However, the dark pulses are significantly broader than the bright pulses. Slightly tuning the intra-cavity PC or carefully reducing the pump power, the number of solitons in the cavity could be changed and the periodic pulse train could also become inhomogeneous. Nevertheless, no matter how the bright solitons are distributed in the cavity, corresponding to each bright soliton there is always a dark pulse appeared on the CW background. Here we note that if one observes the oscilloscope trace under a large time scale or using a low-speed detection system, this kind of soliton-dark pulse pair would look like a 'bright-dark soliton pair' [7, 41].

We then operated the laser under relatively large net cavity birefringence. In this case the wavelength separation between the two orthogonally polarized CW emissions has a large value. Fig. 4.3 shows the case experimentally observed. Fig. 4.3(a) shows the oscilloscope traces of the laser emission along the two orthogonal polarizations. Fig. 4.3(b) is the polarization resolved optical spectra. As a result of the incoherent cross coupling between the two orthogonally polarized CW components, polarization domains are formed, characterized as the intensity alternation of the CW laser emissions between the two orthogonal polarization directions. We have shown previously that the appearance of the polarization domains is an intrinsic feature of the fiber laser emission under the incoherent coupling of the two orthogonal polarization modes [21]. However, in the current state as a result of the strong pumping, simultaneously a periodic bright soliton train is also formed on one polarization direction. The bright soliton train fills up the whole cavity. Again the formed bright solitons have different central wavelength than the CW component. When the oscilloscope is triggered by the edge of the polarization domain shown in the upper trace, the bright solitons move with respect to the polarization domain. It is to point out that in the polarization domain where there is coupling between the bright solitons and a CW beam polarized along the orthogonal polarization direction, the bright solitons induce dark pulse formation on the CW background, as shown in Fig. 4.3(a). Zooming in the region of the coupled soliton-dark pulse pairs, again corresponding to each bright soliton there is a dark pulse. Moreover, the dark pulses have a much broader pulse width than the bright solitons.

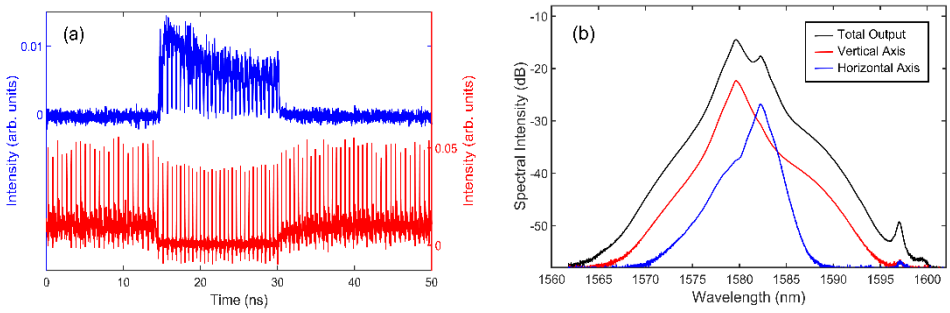

Figure 4.3. The soliton-dark pulse pairs formed in a polarization domain where there is incoherent coupling between solitons and a CW beam. (a) Laser emissions along the two orthogonal polarization directions. (b) The corresponding polarization resolved spectra.

The "soliton rain" is an interesting feature of the soliton fiber laser operation whose formation mechanism is not yet clearly explained [42]. Under the same pumping power, by appropriately setting the orientation of the intra-cavity PC, the soliton rain feature is also observed on the formed bright solitons in our fiber laser, as shown in Fig. 4.4. Because of the incoherent coupling of the orthogonally polarized CW components, polarization domains are formed. On one polarization bright solitons are formed. In particular, the formed bright solitons exhibit the soliton rain feature where the solitons move with accelerated speed away from the soliton condensate. Again, each bright soliton induces a dark pulse on the orthogonally polarized CW. Consequently the dark pulses also exhibit the similar pulse evolution.

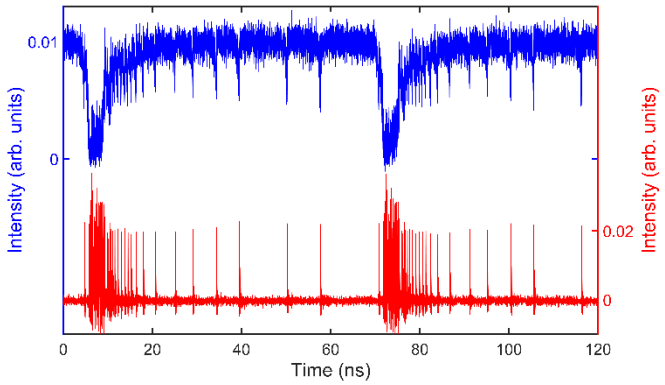

Figure 4.4. The soliton rain effect of the soliton-dark pulse pairs. The two oscilloscope traces are the polarization resolved emissions of the fiber laser.

4.1.2 Experimental results analysis

Our experimental results clearly demonstrated that as a result of the cross polarization coupling, a bright soliton could induce the formation of a dark pulse. To understand the dark pulse formation in our laser we note that the polarization domain formation is an intrinsic feature of the quasi-vector cavity fiber lasers under the cross polarization coupling. Required by the system minimum energy condition, within one polarization domain the laser would only emit in one polarization state. A soliton-dark pulse pair could be considered as a special case of the polarization domains, where the appearance

of a soliton in one polarization will demand a temporal no lasing, or an intensity hole, on the orthogonal polarization direction. Hence, a dark pulse will always be formed in association of a bright soliton. We note that D. N. Christodoulides had once theoretically predicted the formation of a kind of black-white soliton pair in weakly birefringent SMF under coherent polarization coupling [7]. Although the bright soliton and the dark pulse observed in our experiment are coupled, their coupling is incoherent. Moreover, the formed dark pulses have an asymmetric pulse form and a much broader pulse width than the bright solitons. It is unlikely that the observed dark pulses are dark solitons.

In our fiber laser as there is no any mode-locking element in the cavity, so no mode locking could occur. We explain that the bright soliton formation is initialed by the cavity induced modulation instability (CIMI). This also explains why initially a stable soliton pulse train is always formed in our laser. It is also a unique feature of the fiber laser that differs from the soliton operation of the mode locked fiber laser. Finally, we point out that the observed bright soliton-dark pulse pair formation is independent on the concert laser cavity parameters. Actually under different cavity conditions (different cavity length, net anomalous dispersion) we have observed the phenomenon, which shows that it is a general effect of the fiber lasers.

4.2 Induced dark soliton

4.2.1 Experimental setup and results

Our fiber ring laser setup is schematically shown in Fig. 4.5. The fiber ring has a total length of 22.6 m, consisting of a piece of 3 m Erbium doped fiber (EDF) with a group velocity dispersion (GVD) parameter of -48 ps/nm/km, 13.5 m single mode fiber (SMF-28) with a GVD parameter of 18 ps/nm/km and 6.1 m dispersion compensation fiber (DCF) with a GVD parameter of -4 ps/nm/km. The fiber ring cavity is estimated to have an average net anomalous GVD parameter of 3.3 ps/nm/km. The fiber laser is pumped by a 1480 nm single mode Raman fiber laser whose maximum output power is 5 W. A polarization independent isolator is inserted in the cavity to force the unidirectional circulation of light in the cavity. Besides, an intra-cavity polarization controller (PC) is used to fine-tune the linear cavity birefringence. A wavelength division multiplexer (WDM) is used to couple the pumping light into the cavity, and a 10% fiber output coupler is used to output the light. The pumping coupling efficiency from the pump source to the cavity is about 60%. All the components used in our experiment have very low polarization dependent loss (PDL) (WDM: 0.01 dB, Isolator: 0.04 dB, Coupler: 0.01 dB). An external cavity polarization beam splitter (PBS) is used to experimentally resolve the two orthogonal polarization components of the laser emission. To this end a polarization controller is inserted before the external polarization beam splitter to balance the linear polarization change caused by the lead-fibers. The two orthogonal polarization components are simultaneously monitored with a high-speed electronic detection system made of two 40 GHz photo-detectors and a 33 GHz bandwidth real-time oscilloscope.

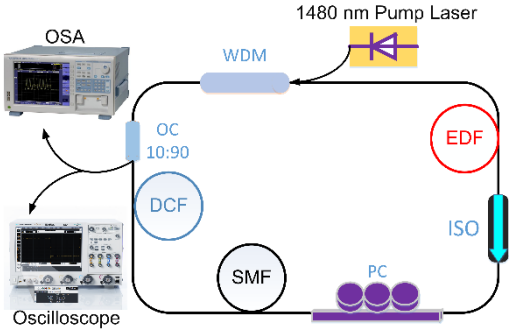

Figure 4.5: A schematic of the Erbium-doped fiber ring laser. EDF: Erbium-doped fiber. SMF: Single mode fiber. DCF: Dispersion compensation fiber. WDM: Wavelength division multiplexer. PC: Polarization controller. ISO: Isolator. OC: Output coupler. OSA: Optical spectrum analyzer.

Under low pump power the laser always emits continuous wave (CW). However, depending on the net cavity birefringence, which can be altered experimentally by changing the orientation of the intracavity polarization controller, the laser emission could be in different polarization states. In the case of very weak net cavity birefringence, the laser could emit either an elliptically polarized beam where the two polarization modes have the same oscillation wavelength, or a linearly polarized beam which can be attributed to the effect of polarization instability [43]. However, the most common state is that the laser emits CW along the two orthogonal polarization modes simultaneously, and each CW has different oscillation wavelengths. Experimentally it is identified that the wavelength difference of them varies with the net cavity birefringence. Specifically, strong birefringence leads to big wavelength difference. Hence experimentally we used the wavelength difference as an indicator on the strength of the net cavity birefringence and operated the laser under different pump strength and net cavity birefringence.

Increasing the pumping power to about 1.0 W (30 dBm), by tuning the intra-cavity PC, a kind of soliton-dark pulse pair emission similar to that shown in Fig. 4.6 (a) is obtained. In a previous paper, we have reported the phenomenon and explained its formation mechanism [44]. Briefly, because the bright solitons and the CW in the opposite polarization direction have different central wavelengths, there is incoherent polarization coupling between them. Consequently, an effect similar to the polarization domain formation takes place, leading to that corresponding to each bright soliton a broad dark pulse is generated on the CW background. We note that the formed dark pulse is much broader than the bright soliton, and the stronger the pump power the narrower the dark pulses. When we keep increasing the pumping power to about 3.2 W (35 dBm), in the meantime also slightly tuning the intra-cavity PC to make the net cavity birefringence very weak, a special phenomenon as shown in Fig. 4.6 is further observed. Fig. 4.6(a) shows the oscilloscope traces of the polarization resolved laser emission. It shows that the laser emits stable bright soliton-dark pulse pairs, as the phenomenon reported in Ref. [44]. However, different from that, associated with each of the bright solitons there is a narrow dark pulse formed on the bottom of each of the broad dark pulses. Fig. 4.6(b) shows the zoom-in of one bright-dark pulse pair. The broad dark pulse is about 250 ps

wide. On the bottom of the dark pulse there is an additional narrower dark pulse of about 30 ps wide, which is the bandwidth limitation of our oscilloscope. The narrow dark pulse synchronizes with the bright soliton in the orthogonal polarization direction. Fig. 4.6(c) is the autocorrelation trace of the bright soliton, whose FWHM width is 1.46 ps, suggesting that the width of the bright soliton is about 944 fs if a Sech-shape pulse profile is assumed.

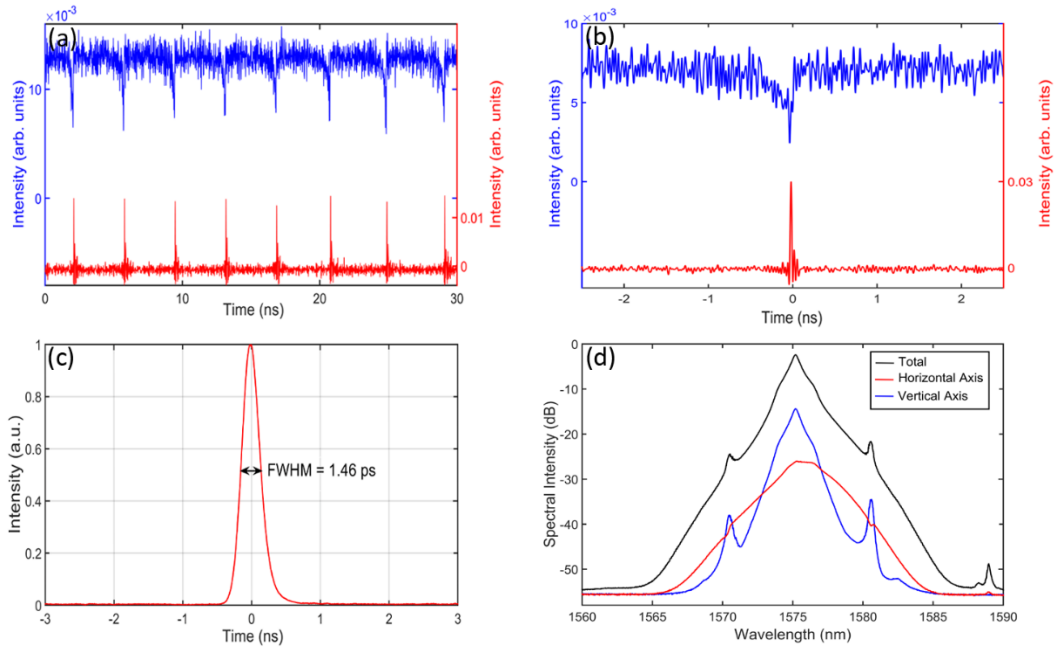

Figure 4.6. Experimental results of induced dark solitary pulse formation in a fiber laser. (a) The polarization resolved oscilloscope traces of the laser emission. (b) The zoom-in oscilloscope traces of a soliton-dark pulse pair. (c) Autocorrelation trace of the bright solitons. (d) The Polarization-resolved spectra.

Fig. 4.6(d) shows the polarization-resolved optical spectra of the laser emission. The central wavelength of CW light (in vertical axis) is 1575.2 nm. The central wavelength of the bright soliton (the broadened spectrum in horizontal axis) is about 1575.5 nm, which can be estimated by fitting the spectrum profile. A Kelly sideband locates at 1588.95 nm, which indicates that the bright pulses in the horizontal axis have fully evolved into solitons [18]. Besides, we can clearly see two peak-dip spectral structures locating at 1570.45 nm and 1580.6 nm, which stands for the energy exchange between the two polarization components and is the symbol of coherent coupling between the bright solitons and the dark pulses [19]. To confirm that the narrow dark pulse is induced by the coherent polarization coupling of the bright soliton, we have experimentally deliberately changed the cavity birefringence so that the two polarization components are in the incoherent coupling. In this case the broad dark pulse still exists, while the narrow dark pulse become not measurable. In the meantime, no coherent energy exchange spectral sidebands appear on the optical spectra. The experimental result clearly suggests that the weak dark pulse could be an induced dark soliton by the bright soliton through the coherent polarization coupling. We note that there is also some spectral broadening of the CW beam. It is due to the

modulation instability effect. This is also reflected by the noise background of the oscilloscope trace of the CW beam.

In addition to the induced dark solitons, under the coherent polarization coupling, experimentally we have also observed the induced bright soliton formation inside the wide dark pulse, as shown in Fig. 4.7. Fig. 4.7(a) shows again the polarization resolved oscilloscope traces of the laser emission. Note that in the cavity multiple bright solitons are formed. Associated with each of the bright solitons a weak bright soliton is induced in the orthogonal polarization. Fig. 4.7(b) is the polarization resolved optical spectra. Note that the soliton wavelength and the CW wavelength are not the same. Hence, there is incoherent polarization coupling between them. This explains why each bright soliton also induces a broad dark pulse on the CW beam. The polarization-resolved spectra further show that the induced bright solitons have the same central wavelength as that of the inducing bright solitons. This could be identified by drawing the spectral profiles of the pulses and comparing their Kelly sideband positions. The Kelly sidebands on both polarization directions are clearly visible and they have the same locations. Moreover, the energy exchange spectral sidebands are also visible on the optical spectra, suggesting that the weak bright solitons are coherently induced. We point out that formation of induced bright solitons in mode locked fiber lasers were reported before [38]. We found that the induced bright solitons have very similar features to those reported previously.

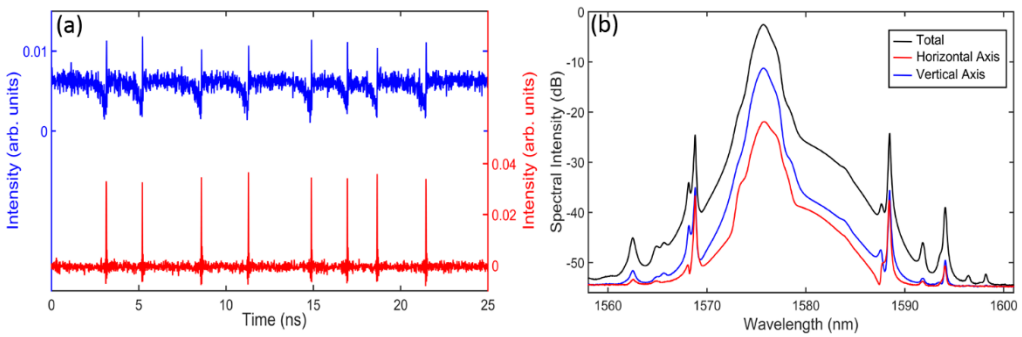

Figure 4.7. The induced bright soliton formation inside the wide dark pulse of bright-dark pulse emission state. (a) Laser emissions along the two orthogonal polarization directions. (b) The corresponding polarization resolved spectra.

For the formation mechanism of the narrow dark solitary pulse inside the dark pulse, we notice that D. N. Christodoulides theoretically proved the existence of bright-dark soliton pair by the coherent coupling between polarization modes in Ref. [7]. Therefore, we conjecture that in our experiment, the formation of the narrow dark solitary pulse in the wide dark pulse is induced by the bright soliton in its orthogonal polarization mode through coherent coupling. Besides, this is a special phenomenon because in SMF environment, only bright soliton can propagate steady in the anomalous dispersion regime and dark soliton in normal dispersion regime. In our experiment, we find the dark solitary wave also can exist in anomalous dispersion regime. We suggest it's due to the coherent coupling between two polarization modes and dissipative properties of fiber laser.

4.2.2 Numerical simulations and discussion

We had investigated both experimentally and theoretically the polarization domain formation in quasi-vector cavity fiber laser and shown that it is an intrinsic feature of the incoherent polarization coupling in the fiber lasers [21, 45]. The bright soliton-dark pulse pair formation of the laser under relatively low pump power or even high pump power but incoherent polarization coupling could be considered as a special case of the polarization domain formation [44]. Here due to the influence of the strong nonlinear self-phase modulation the domains are represented in a different form. What is interesting here is that once the polarization coupling becomes coherent, in addition to the broad dark pulse formation, a weak dark or bright soliton is further induced. The formation of induced dark soliton under the polarization coupling was theoretically predicted before [46, 47], and formation of induced bright solitons in a mode locked fiber laser was also experimentally reported [20]. However, to the best of our knowledge, no induced dark solitons in the anomalous dispersion regime are experimentally observed. In order to understand how the dark soliton is formed, we numerically simulated the operation of the fiber ring laser. Our simulation is based on the coupled complex Ginzburg-Landau equations (CGLE), which describe the light propagation in a weakly birefringent fiber cavity,

$$\begin{aligned}\frac{\partial u}{\partial z} &= i\beta u - \delta\frac{\partial u}{\partial t} - \frac{ik''}{2}\frac{\partial^2 u}{\partial t^2} + i\gamma\left(|u|^2 + \frac{2}{3}|v|^2\right)u + \frac{i\gamma}{3}v^2u^* + \frac{g}{2}u + \frac{g}{2\Omega_g^2}\frac{\partial^2 u}{\partial t^2} \\ \frac{\partial v}{\partial z} &= -i\beta v + \delta\frac{\partial v}{\partial t} - \frac{ik''}{2}\frac{\partial^2 v}{\partial t^2} + i\gamma\left(|v|^2 + \frac{2}{3}|u|^2\right)v + \frac{i\gamma}{3}u^2v^* + \frac{g}{2}v + \frac{g}{2\Omega_g^2}\frac{\partial^2 v}{\partial t^2}\end{aligned} \qquad (4.1)$$

where ***u*** and ***v*** describe the optical fields of the two orthogonal polarization components in the fiber cavity. $2\beta = 2\pi\Delta n/\lambda = 2\pi/L_b$ is the wave number difference between these two polarization modes. $2\delta = 2\beta\lambda/2\pi c$ is the group velocity difference, which are related with the value of beat length L_b and stand for the cavity birefringence. ***k"*** is the second-order dispersion coefficient, γ represents the nonlinearity of the fiber cavity, ***g*** is the gain coefficient of the gain fiber and Ω_g is the effective gain bandwidth. The gain saturation is defined as

$$g = G\exp\left[-\frac{\int\left(|u|^2 + |v|^2\right)dt}{E_0}\right] \qquad (4.2)$$

where ***G*** is the small signal gain coefficient and E_0 is the gain saturation energy, which is related to the pumping power in the experiment.

We have numerically solved the Eq. 4.1 and 4.2 using the split-step method and details on the numerical techniques used were reported previously [6]. To model the induced dark or bright soliton formation in the laser, we have set the initial state as a soliton-dark pulse pair, which is similar to the experimental situation. The initial bright soliton has the form of $u = A\cdot\mathrm{sech}(B\cdot t)$, while for the initial dark pulse we have either the form of $v = C\cdot\tanh(D\cdot t)$, where there is a phase

jump in the center of the dark pulse; or $v = C \cdot \sqrt{\left(1 - \mathrm{sech}^2\left(D \cdot t\right)\right)}$, where there is no phase jump. Here ***A*** and ***C*** stand for the bright soliton intensity and dark pulse depth, usually ***A*** is set much bigger than ***C*** because the bright soliton peak power is much higher than the CW power in our experiment. ***B*** and ***D*** stand for the width of bright soliton and the dark pulse. ***B*** is set much smaller than ***D***, in accordance with the experimental results that the dark pulse is much wider than the bright solitons. In all our simulations we have possibly used the actual laser cavity parameters if possible, e.g. the cavity length ***L***=22.6 m and the average cavity dispersion is 3.3 ps/nm/km. In our experiment results, the coherent coupling between two orthogonal polarization components can only happen under very weak cavity birefringence. So we set L_b = 50 km, which means the cavity birefringence is very weak.

First, we numerically simulated the case of dark pulse with a phase jumping $v = C \cdot \tanh\left(D \cdot t\right)$. Under appropriate parameter selection, we can obtain a stable state laser emission as shown in Fig. 4.8. Like what was observed in the experiment, a narrow pulse width bright soliton polarized along one polarization eigenmode of the fiber laser could induce a weak dark soliton on the bottom of a broad dark pulse, and consequently form a coupled bright-dark soliton pair. Both the broad and narrow dark pulses are stable and they are trapped with the bright solitons and propagate together in the cavity. To confirm that the narrow dark soliton is induced by the coherent coupling, we also deliberately removed the four-wave-mixing (FWM) terms from the CGLEs and did the simulations with the same parameters. No induced dark soliton could be formed inside the broad dark pulse. Therefore, we conclude that the formation of the induced dark solitary pulse is a result of the coherent polarization coupling between the two polarization modes.

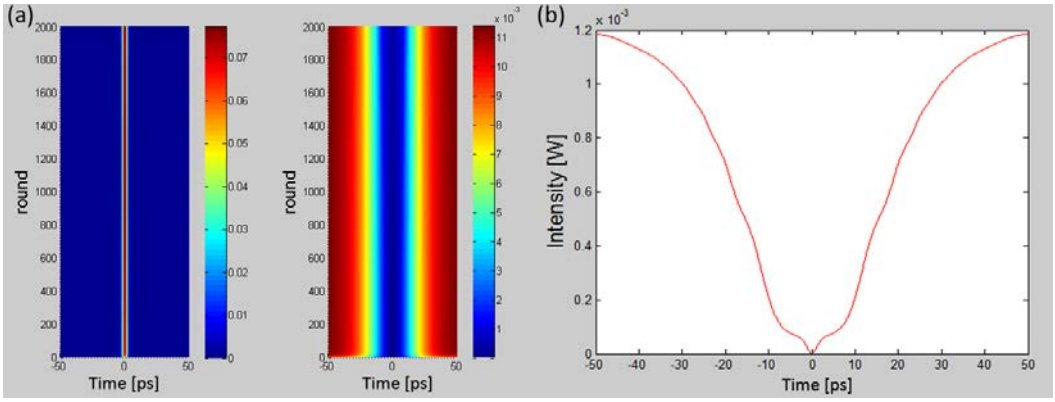

Figure 4.8. (a) Stable soliton-dark pulse emission of the laser when the input dark pulse has a phase jump. The saturation energy E_0=0.1 pJ and the small signal gain ***G***=640 m^{-1}. (b) Zoom-in of the dark pulse. The induced dark soliton is on the bottom of the broad dark pulse.

We then repeated the numerical simulations for the case of no phase jump dark pulse $v = C \cdot \sqrt{\left(1 - \mathrm{sech}^2\left(D \cdot t\right)\right)}$. We used exactly the same simulation parameters as the previous one. The results are shown in Fig. 4.9. In this case instead of that an induced dark solitary pulse is formed, a bright solitary pulse is formed inside

the broad dark pulse. The numerically simulated results are well in qualitative agreement with the experimental observations.

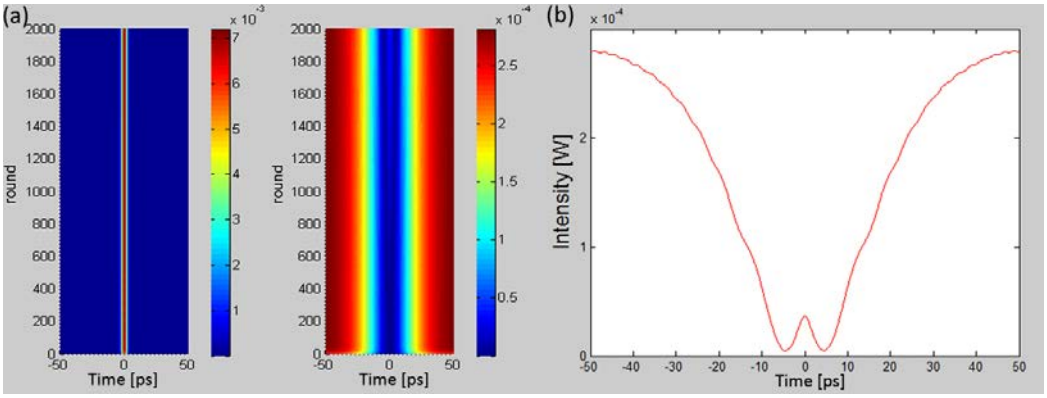

Figure 4.9. (a) Stable soliton-dark pulse emission of the fiber laser when the input dark pulse has no phase jump. The saturation energy E_0=0.1 pJ and small signal gain G=640 m^{-1}. (b) Zoom-in of the dark pulse. The induced bright soliton is on the bottom of the broad dark pulse.

Based on the numerical simulations it is to see that as a result of the coherent polarization coupling, a bright soliton in an anomalous dispersion cavity fiber laser could induce either an dark soliton or a bright soliton on the bottom of a broad dark pulse polarized along the orthogonal polarization, depending on if there is a phase jump in the broad dark pulse or not. Finally, we point out that strictly speaking all solitons formed in a fiber laser should be dissipative solitons as a laser is intrinsically a dissipative system due to the gain and losses balance [17, 29]. In view of that a bright dissipative soliton could either be formed in the normal or anomalous cavity dispersion regimes, it should also be possible that a dissipative dark soliton could be formed either in the normal or anomalous dispersion regime.

4.2.3. Conclusions

In conclusion, we have experimentally observed the formation of soliton-dark pulse pair and induced solitary in a birefringent cavity fiber laser. It is found that due to the incoherent coupling between the two orthogonal polarization modes of the fiber cavity, a bright soliton pulse always induces a dark pulse on the CW background polarized along the orthogonal polarization. In particular, the formed soliton-dark pulse pairs are stable in the cavity. The features of the formed bright solitons and dark pulses were experimentally investigated. Under our experimental accessible conditions it is found that the formed dark pulses always have a broader pulse width than the bright solitons. We pointed out that the mechanism of the dark pulse formation could be understood based on the polarization domain formation. Meanwhile, in a quasi-vectorial cavity fiber laser, under the coherent polarization coupling, a bright soliton polarized along one polarization eigenmode of the cavity could either induce the formation of a weak dark soliton or a bright soliton on the bottom of a broad dark pulse in the orthogonal polarization direction in a net anomalous dispersion cavity fiber laser. In particular, the induced solitons are stable in the cavity. Numerical simulations based on the coupled complex GLEs have well confirmed the

experimental observations. The numerical simulations have further revealed that whether a dark or bright soliton is induced depends on if there is a phase jump in the broad dark pulse.

Part 2: Vector soliton operation of graphene mode locked fiber lasers

Vector soliton formation in weakly birefringent single mode fibers (SMFs) was theoretically extensively investigated. C. R. Menyuk first theoretically studied optical pulse propagation in birefringent optical fibers [48]. He found that above a certain pulse intensity level two orthogonally polarized solitons with different centre wavelengths could couple together and propagate at the same group velocity. The entity of the coupled solitons was later known as a group velocity locked vector soliton. V. V. Afanasjev theoretically investigated the pulse propagation in weakly birefringent SMFs and found an approximate analytic solution for the polarization rotation vector soliton [49]. Christodoulides and Joseph [50], and Akhmediev *et al.* [51] also theoretically predicted different forms of polarization locked vector solitons in weakly birefringent optical fibers. In contrast to the theoretical studies, except that the group velocity locked vector soliton was experimentally confirmed [52], experimental observation of the other types of the theoretically predicted vector solitons were hampered by the stringent requirement on the birefringence property of the SMFs. To form these types of vector solitons the SMFs need to have stable weak birefringence over a long distance, while in practice it is difficult to make such SMFs. However, it was recently found that the requirement could be satisfied if the optical pulse is propagating in a fiber cavity, where as far as the average birefringence over one cavity roundtrip is close to zero, the phase locked vector solitons could be formed.

Nowadays, vector soliton fiber lasers have captured considerable attentions due to their potential applications in optics communications. To generate vector solitons, passively mode locked fiber laser without polarization sensitive components is an essential condition. Recently, soliton operation of fiber lasers mode-locked with atomic layer graphene was reported. Graphene has been shown to have not only extraordinary electronic properties but also novel optical properties. A novel optical property of graphene is its broadband saturable absorption, which has been exploited for passively mode locking lasers of different wavelengths [53-57]. The two dimensional structure of graphene determines that its saturable absorption is independent on the light polarization when the light is incident perpendicularly to its plane. Like a semiconductor saturable absorption mirror (SESAM), this polarization insensitive saturable absorption of graphene could be used to passively mode lock a laser and introduce no polarization discrimination. Moreover, as graphene saturable absorbers are easy to make, and have superbroad bandwidth and variable modulation depth when different number of graphene layers is used, it is superior for generating vector solitons in fiber lasers.

In this part, we focus on the study of vector soliton operation in graphene

mode-locked erbium-doped fiber lasers, which includes the vector soliton formation, properties of the formed vector solitons, multiple vector soliton interactions and other interesting relative phenomena. The part is organized as the following: In Section 1 we will show the experimental observation of the polarization locked and polarization rotation multiple vector solitons formed in an all-anomalous dispersion fiber laser mode locked with an atomic layer graphene saturable absorber. In Section 2, various operation states of multiple vector-solitons in a laser cavity and their mutual interactions are experimentally investigated. Section 3 discusses the bound states of vector solitons in fiber lasers. Section 4 reports the quasi-periodicity of the vector solitons in a graphene mode-locked fiber laser. Section 5 introduces the noise like pulses in graphene mode-locked fiber laser. Section 6 summarizes the results and concludes the part of the report.

1. Polarization Rotation and Locking of Multiple Vector Solitons

Vector soliton formation in passively mode locked fiber laser was first experimentally observed by S. T. Cundiff *et al.* In their experiment both the polarization rotation and the polarization locked vector solitons were obtained. Vector soliton formation in fiber lasers passively mode locked with SESAM were also experimentally confirmed by several other groups [58-61]. However, the formation of polarization rotation and polarization locked vector solitons in graphene mode locked fiber lasers has not been reported. We have experimentally investigated the features of vector solitons formed in graphene mode locked fiber lasers. It was found that both the polarization locked and polarization rotation vector solitons could be formed in the fiber lasers.

1.1 Experimental setup and results

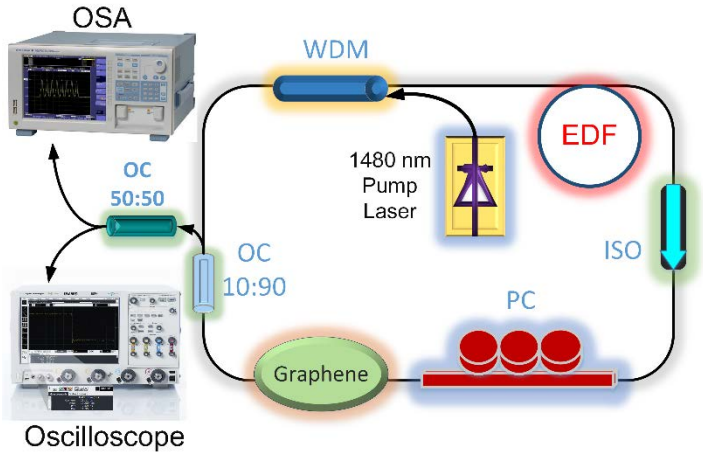

Figure 1.1 A schematic diagram of the fiber laser setup. SMF: Single-mode fiber, PC: Polarization controller, EDF: Erbium doped fiber, WDM: Wavelength-division multiplexer, OC: Optical coupler, ISO: Isolator, OSA: Optical spectrum analyser.

The graphene mode-locked fiber laser is schematically shown in Figure 1.1. The laser cavity is a fiber ring that consists of 0.7 m erbium-doped fiber (EDF Er80-8/125 from Liekki) with a GVD parameter of -22.9 ps^2/km and 22 m

standard SMF (SM28). In addition, a 10% fiber output coupler is used to output the signal, a polarization independent isolator is used to force the unidirectional operation of the ring cavity, and an intra-cavity polarization controller (PC) is used to fine tune the linear cavity birefringence. All the passive components are made of the SMF or pigtailed with SMFs. The laser is pumped by a high power Raman fiber laser (KPS-BT2-RFL-1480-60-FA) of a wavelength 1480 nm. The graphene was fabricated with the chemical vapour deposition (CVD) method [62]. The CVD graphene is a free standing atomic layer graphene film that can be readily lifted off from the deionized water and transferred onto a fiber pigtail. The number of graphene layers in a film can be identified from its Raman spectrum and the optical contrast spectroscopy. As more layers of graphene correspond to a high absorption, by simply measuring the saturable absorption strength of the graphene film we can also estimate the number of layers. It is estimated that the graphene used has 3~5 atomic layers with a saturable absorption modulation depth of ~23%. The soliton spectra of the laser are measured with an optical spectrum analyzer (ANDO AQ6317). The soliton pulse train emitted by the laser is monitored by a 1 GHz oscilloscope (Lecroy Waverunner 6100) together with three 1.2 GHz photo-detectors (Thorlab DET01CFC).

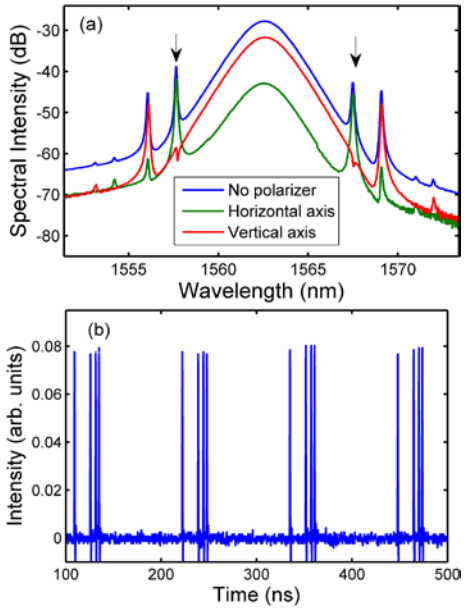

Figure 1.2 Vector soliton emission of the fiber laser. (a) Soliton spectra. Blue line: the total laser emission without passing through a polarizer; Red and Green lines: the two orthogonal polarization components resolved with an external cavity polarization beam splitter. (b) Oscilloscope trace of the solitons.

Self-started mode locking is always obtained in the laser when the pump power is increased to ~90 mW. Immediately after mode locking, multiple pulses are normally obtained in the laser cavity. Occasionally the pulses are observed moving randomly in the cavity. However, through carefully adjusting the intracavity polarization controller and/or changing the pump power, a stable state where the multiple pulses stay stationary with respect to each other in the cavity, could always be obtained. Such a state was shown in Figure 1.2 for example. Figure 1.2(a) shows the measured optical spectra. The Kelly

sidebands are obvious on the spectra [63,64], confirming that the pulses are optical solitons. The central wavelength of the solitons is at 1562.40 nm. Figure 1.2(b) is the measured oscilloscope trace of the soliton pulses. Several uniform soliton pulses trains can be clearly observed, indicating that the solitons possess the soliton energy quantization property. We note that different from the soliton spectra obtained from a nonlinear polarization rotation (NPR) mode locked fiber laser, apart from the Kelly sidebands, there are also another set of spectral sidebands (indicated by the arrows) on the soliton spectrum shown in Figure 1.2(a). At first sight one may confuse that all the sharp spectral peaks on the soliton spectra are the Kelly sidebands. However, as one carefully adjusts the intra cavity PC, it will be observed that one set of the spectral sidebands shift their positions remarkably on the soliton spectra, while the other set of spectral sidebands have almost no position change. The latter set of spectral sidebands is the Kelly sidebands. We point out that the appearance of the other set of spectral sidebands is a result of the vector soliton formation in the fiber laser. To clearly identify the difference of the spectral sidebands, it is better to measure the polarization resolved spectra of the vector solitons. As in our laser there is no any polarization discrimination component in the cavity, the net cavity birefringence could be tuned to a very small value. Consequently, the formed solitons are all vector soliton and consist of two orthogonal polarization components. To simultaneously measure the polarization resolved spectra of the vector solitons, experimentally we used a fiber pigtailed external cavity polarization beam splitter to separate the two orthogonal polarization components. In order to balance the fiber pigtail induced linear polarization rotation, we inserted a polarization controller between the laser output port and the polarization beam splitter. The polarization resolved spectra of the solitons measured are also shown in Figure 1.2(a). On the polarization resolved spectra while the Kelly sidebands always exhibit as spectral peaks, the other set of spectral sidebands displays either as a spectral peak or a spectral dip, between the two orthogonal polarization components there is always a peak-dip relationship, indicating the existence of coherent energy exchange between the two soliton components. In a previous work it has been shown that such a spectral sideband relationship is formed due to the coherent coupling between the two polarization components of the vector solitons in a laser [65]. It is worth noting that four-wave mixing between the two orthogonal polarization components of light in weakly birefringent SMFs were experimentally observed by Trillo *et al.* [66] and numerically investigated by Blow *et al.* [67]. It was shown that this effect could cause polarization instability. However, different from the case of light propagation in SMFs, which can be treated as a conservative system, light propagation in a laser cavity also experiences gain and losses. The formation of a stable soliton in a laser needs to fulfill the gain-loss balance. They are intrinsically dissipative solitons. Moreover, we note that a soliton circulating in a cavity also has to satisfy the cavity boundary condition. Haelterman *et al.* have theoretically shown that the cavity detuning could alter the phase matching condition of the coherent wave coupling in a dispersive cavity [68]. Indeed, in our experiments it was observed that the positions of the extra spectral sidebands vary remarkably with the adjustment of the paddles of the intra-cavity PC.

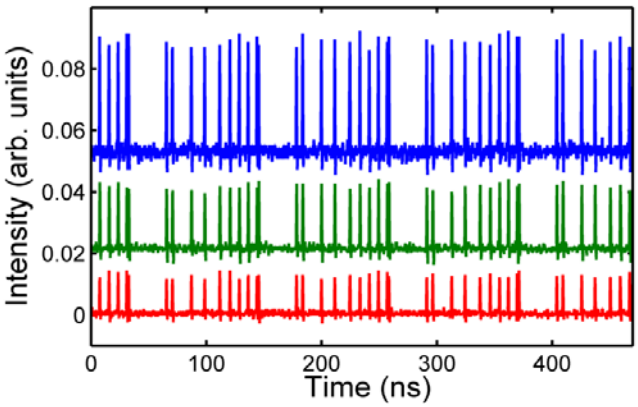

Figure 1.3 Oscilloscope traces of the pulse train in a phase locked vector soliton operation state. Blue line: the total laser emission without passing through a polarizer; Red and Green lines: the two orthogonal polarization components resolved with an external cavity polarization beam splitter.

Like that the appearance of Kelly sidebands is a characteristic of the soliton formation in a laser, we found that the appearance of the above extra spectral sidebands is a characteristic of the vector soliton formation in our fiber laser. Experimentally, we further noticed that depending on the laser operation conditions, two types of vector solitons could be formed: The polarization locked vector solitons and the polarization rotation vector solitons. Figure 1.3 shows the oscilloscope traces of a state with multiple polarization locked vector solitons in cavity. In this case all vector solitons in the cavity have exactly the same polarization and their polarization features remain unchanged as they propagate in the cavity. Therefore, when measured after an external cavity polarizer, after every cavity roundtrip all the solitons in the cavity remain the same pulse intensity. Optical spectra of all the polarization locked vector solitons are similar to those as shown in Figure 1.2(a), except that the positions of the extra spectral sidebands vary.

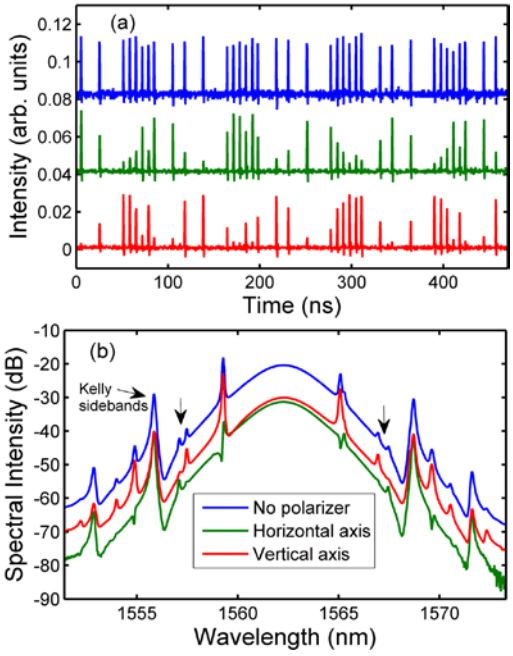

Figure 1.4 A polarization rotation vector soliton state of the laser. (a) The total and the polarization resolved soliton pulse trains with multiple solitons in cavity. (b) Optical spectra of the solitons. Blue line: the total laser emission without passing through a polarizer; Red and Green lines: the two orthogonal polarization components resolved with an external cavity polarization beam splitter.

Figure 1.4 shows the oscilloscope traces and spectra of a polarization rotation vector soliton state. Without passing through an external cavity polarizer, the oscilloscope trace shows no difference to that of a polarization locked state, as shown in Figure 1.3. However, from the polarization resolved traces, one can clearly identify the soliton pulse intensity variations. Carefully checking the pulse intensity variations, it can be identified that the polarization of the vector solitons shown in Figure 1.4 is rotating in the cavity. After every three cavity-roundtrips their polarization rotated back. We found experimentally that whenever the polarization of the vector solitons was rotating in the cavity, another two sets of weak spectral sidebands (indicated with arrows in Figure 1.4(b) further appeared on the soliton spectrum. Comparing Figure 1.4(b) with Figure 1.2(a) it is easy to see that apart from the Kelly sidebands, there are another three sets of spectral sidebands visible on the soliton spectrum now. Based on the polarization resolved spectra, one set of the sidebands is due to the coherent energy exchange between the two orthogonal polarization components, as described above. Each of the other two sets of the weak new sidebands (indicated with arrows in Figure 1.4(b)) appears only on spectrum of one of the two orthogonal polarization components, respectively. Moreover, no matter how the two orthogonal polarization components are split, the weak new sidebands always exhibit as spectral peaks while no spectral dip could be obtained. The feature of the weak new sidebands is similar to that of the Kelly sidebands.

1.2 Discussions

Obviously, the new sets of weak spectral sidebands are formed due to the polarization rotation of the vector solitons. The periodic polarization rotation of the vector solitons introduces an extra periodic soliton parameter variation, therefore, leading to the formation of another set of spectral sidebands. As the soliton polarization rotation has a different period than that of the soliton circulation in the cavity, the new spectral sidebands have different positions to those of the conventional Kelly sidebands. We point out that similar to the formation of the Kelly sidebands, the formation of the new weak spectral sidebands is a linear effect. They are caused by the constructive interference between the dispersive waves emitted by the solitons as their polarizations periodically rotate in the cavity. For a vector soliton it has two orthogonal polarization components, in a state of polarization rotation each soliton polarization component would have different phases. It could be due to the subtle difference between the two polarization components that each soliton component formed its own new spectral sidebands under polarization rotation of the vector solitons. Finally, we point out that although the polarization rotation spectral sidebands have the same formation mechanism as those of the Kelly sidebands, their positions varied remarkably with the laser operation conditions, because the rotation speed of the vector solitons varied with the

experimental conditions.

2. States of multiple vector soliton operation

Multiple soliton formation is a well-known phenomenon of the mode locked fiber lasers and has been extensively investigated in the past [69,70]. It has been shown that various mechanisms could lead to the formation of multiple solitons. These mechanisms include the wave-breaking effect, the effective spectral filter effect, the soliton peak clamping effect, and the soliton shaping of dispersive waves. Indeed, in previous experimental studies on the multiple solitons formed in the fiber lasers, people have observed various modes of multiple soliton operation, such as soliton bunches, soliton collisions [71], vibration of soliton pairs [72], restless solitons [73], bound state of solitons [74-78] and so on. Some of these effects can be traced back as a result of the direct soliton interaction of the dissipative solitons, or the dispersive waves mediated nonlinear Schrodinger equation (NLSE) type of soliton interaction. Therefore, based on the different features of the multiple soliton operation of a fiber laser one can get an insight into the properties of the formed solitons. Recently, a novel form of multiple soliton operation named as “soliton rain” was reported by S. Chouli *et al.* [79,80]. It was shown that the multiple soliton formation in a fiber laser could even manifest the process of the rain-drop formation in the nature, or in another word, the multiple soliton interaction in a fiber laser follows the universal statistics of the many body systems. However, most of the previous experimental studies on the multiple soliton operation of fiber lasers were focused on fiber lasers passively mode-locked with the nonlinear polarization rotation (NPR) technique, in which the scalar solitons are always formed.

To study the multiple vector soliton formation, the semiconductor saturable absorber mirror (SESAM) was initially employed in the fiber laser cavity [73,81]. In an experiment with a SESAM as the passive mode locker Zhao *et al.* have observed a state of so-called bunched restless vector solitons [73]. Vector soliton bunching controlled by SESAMs with different recovery times was also experimentally investigated by R. Gumenyuk *et al.* [81]. Recently, the mode locking of fiber lasers with atomic-layer graphene based saturable absorbers has attracted considerable attention of research [53,82,83]. Compared with the SESAMs, graphene has a number of novel characteristics, e.g. their saturable absorption have super broad bandwidth and ultrafast recovery time, which render that the formed multiple vector solitons could have many new dynamic features.

In this section we report on the experimental study of the multiple vector soliton operation of an erbium-doped fiber laser mode-locked with atomic-layer graphene. We show experimentally that depending on the laser cavity design and the concrete laser operation conditions, five different characteristic modes, namely bunches of multiple vector solitons, random static distribution of vector solitons, vector soliton rain, restless vector solitons and giant pulse of the multiple soliton operation were obtained in our vector soliton fiber lasers. Worth of mentioning is that vector soliton rains with either the polarization locked or the polarization rotating vector solitons were firstly experimentally

revealed.

The graphene mode-locked fiber laser used has the same cavity configuration as that shown in Figure 1.1. The same 0.7 m highly erbium doped fiber (Liekki Er80-8/125) with anomalous dispersion was used as the gain medium. Other fibers used are the standard single mode fiber (SMF28) with a GVD parameter of 18 (ps/nm)/km. The cavity length is slightly different, which is now about 22.6 m. The atomic layer graphene used is also synthesized with the CVD method [53]. The graphene sheets were carefully deposited on the end facet of an optical fiber, which was inserted in a FC/APC connector. It is to note that the graphene used here is the same as that reported in Section 3.1. The graphene has 3~5 atomic layers with a saturable absorption modulation depth of ~23%. In order to measure the details of the pulse train in the time domain, a 33 GHz high-speed oscilloscope (Agilent DSA-X 93204A) together with two 45 GHz photo-detectors (New focus 1014) was used.

a. Bunches of Multiple Vector Solitons

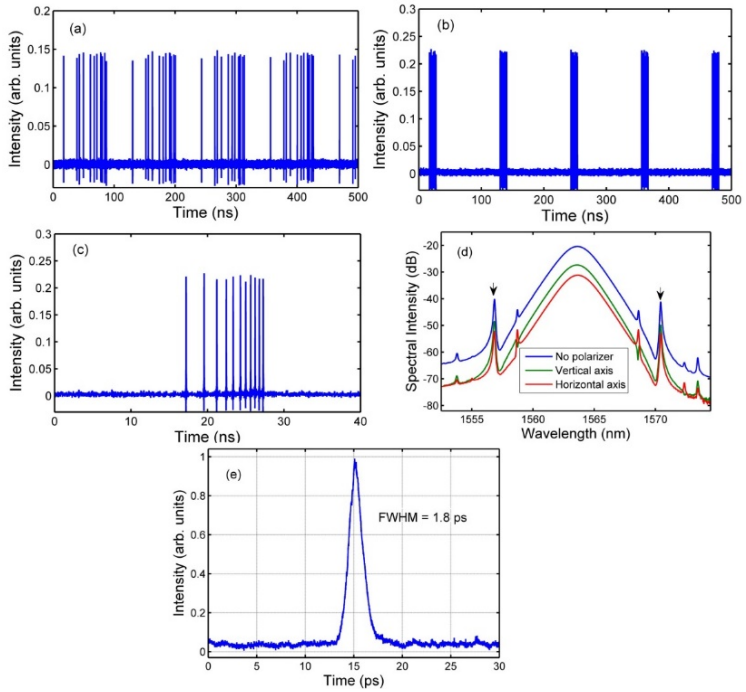

Figure 2.1 Typical bunches of multiple vector solitons formed in the fiber laser. (a) and (b): Two states of the laser emission; (c) The details of the soliton bunch; (d) Polarization resolved optical spectra. Blue line: the total output; Green line: Output along the vertical axis; Red line: Output along the horizontal axis. (e) Autocorrelation trace of the pulse.

Multiple solitons were always formed initially in the laser cavity when the mode locking was achieved, where the pump power was ~80 mW. A typical state of the multiple solitons immediately after the mode locking is shown in Figure 2.1(a). The solitons were initially randomly distributed in the cavity but they were not static. The solitons moved slowly in the cavity and eventually came together, forming a soliton bunch in the cavity, as shown in Figure 2.1(b). After the soliton bunch was formed, the laser then operated in a stable state, and

the same soliton bunch repeated with the cavity repetition rate on the oscilloscope trace. Figure 2.1(c) shows a zoom-in structure of the stable soliton bunch. In the particular case there were 11 solitons in the bunch. The separation between the solitons was not constant and the average distance was ~1 ns. Figure 2.1(d) shows the corresponding optical spectra of the laser emission. The central wavelength of the solitons was at 1563.6 nm, and the 3 dB bandwidth was ~2.3 nm. Two sets of spectral sidebands appeared on the spectra. The one indicated by arrows was the Kelly sidebands. It confirmed that the mode locked pulses were solitons [63,64]. Apart from the Kelly sidebands, there was another set of sidebands. The set of sidebands exhibits peak-dip alteration in the polarization resolved spectra, whose appearance was a result of the coherent energy exchange between the two polarization components of the vector solitons [65]. Therefore, based on the characteristic optical spectra (particularly the additional peak-dip spectral sidebands) one can easily determine if the vector solitons are formed. It is noted that these extra sidebands always appeared on the spectra of the mode locked pulses, suggesting that the as-formed solitons were always vector solitons. Except the spectral sidebands, the optical spectra profile was smooth. The state of vector soliton bunch was very stable. It could last several hours if no laser operation conditions were changed. Figure 2.1(e) shows the measured autocorrelation trace of the solitons. The measured pulse width was 1.8 ps. If a $sech^2$ pulse profile is assumed, the actual pulse width was about 1.17 ps. The time bandwidth product of the pulses is 0.335, indicating that the pulses are transform-limited. A state of single vector soliton in cavity was obtained through carefully reducing the pump power to ~30 mW. The energy of a single vector soliton of the laser is estimated to be ~8 pJ.

b. Random Static Distribution of Vector Solitons

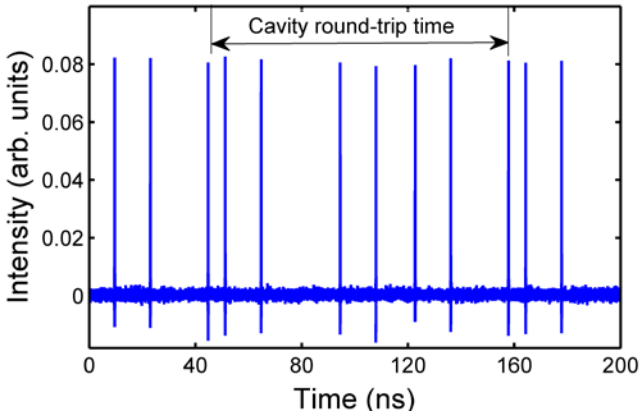

Figure 2.2 Random static vector soliton distribution at a low pump power.

By tuning the paddles of the PC but without introducing any unstable CW components, a vector soliton bunch could explode. Subsequently a state of steady random vector soliton distribution over the whole cavity could be obtained. Figure 2.2 shows a typical example. There were 7 solitons coexisting in the cavity and they were far apart from each other. The state shown was obtained under a pump power of ~50 mW. If the pump power was then increased, a CW spectral component appeared on the soliton spectrum, indicating that a CW background would be introduced into the cavity. In this

case the solitons started to move in the cavity due to the CW mediated soliton-soliton long distance interaction force. Once the CW component was suppressed through carefully reducing the pumping, another state of randomly distributed multiple vector soliton could be obtained. Similar phenomena were also observed previously on the multiple scalar soliton fiber lasers [16]. It shows that the unstable CW beam provides a global soliton interaction mechanism among the vector solitons formed in a laser.

c. Restless Vector Solitons

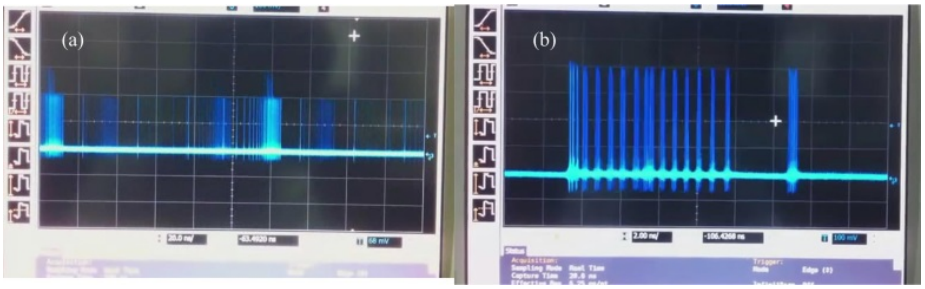

Figure 2.3 Bunch of restless vector soliton bunch (video). (a) Soliton bunch moving in the cavity (Media 1); (b) Solitons oscillating in the bunch (Media 2).

At a relatively stronger pump power (~130 mW), as a result of appearance of unstable CW component in the cavity an initially stable state of randomly distributed multiple solitons was destroyed and the solitons started to move in the cavity and eventually formed a soliton bunch. However, the vector solitons in the bunch were not static, but moved constantly with respect to each other, forming a so-called restless vector soliton bunch. A similar restless vector soliton bunch was also observed in a SESAM mode locked fiber laser by Zhao *et al.* [73]. As the saturable absorption properties of SESAM differ from those of the graphene only in that they have different recovery time and saturable absorption strength, it is not surprising why similar multiple vector soliton operation could be obtained in the graphene mode locked fiber lasers. In our experiments two different types of the restless vector soliton evolutions were observed. Figure 2.3 (see the Media 1 and Media 2 in the attachments) shows these two types of the restless vector soliton evolutions, respectively. Figure 2.3(a) shows a stroboscopic record of vector soliton bunch movement. The soliton bunch moved as a unit in the cavity, while some solitons within in the bunch moved at different velocities. Therefore, vector soliton collisions occurred as indicated by the appearance of the high intensity peaks in the pulse train. Despite of the collisions among the vector solitons within the bunch, the solitons could not escape from the bunch. The collision among the solitons became more frequent with the increase of the pump power. Figure 2.3(b) shows a stroboscopic record of another restless vector soliton evolution, where no soliton collisions occurred. However, the relative soliton positions within the bunch still varied.

d. Vector Soliton Rain

If the pump power was further increased, the number of solitons formed in the cavity continuously increased. At an appropriate PC setting, an interesting dynamic pattern as shown in Figure 2.4(a) could be obtained. In the scalar soliton lasers such a state was called “soliton rain” [79]. The state was called as “soliton rain” because when measured with a low speed detection system, the soliton pulse train in one cavity length could be phenomenally considered as composed of two parts: a soliton flow part (the left hand side of the screen) and a soliton condensed part (the right hand side of the screen), and the solitons are constantly moving from the soliton flow part to the soliton condensed part, which is analogous to the process of rain droplet formation (evaporation from the noisy background/falling to the condensed part) in the nature. As can be seen in Figure 2.4(b), when measured with our high-speed detection system the soliton condensed phase is actually a bunch of solitons close to each other. It was experimentally observed that stronger pump power could induce higher density of the solitons within the bunch. Figure 2.4(c) shows a soliton rain state obtained at the pump power of 200 mW. Not only more solitons were formed in the train but also a large pulse was formed at the end of the flow. The large pulse was a result of the soliton collision within the train. It is worth noting that all the solitons in the train are constantly moving. Figure 2.4(d) (see Media 3 in the attachments) shows a record of the state.

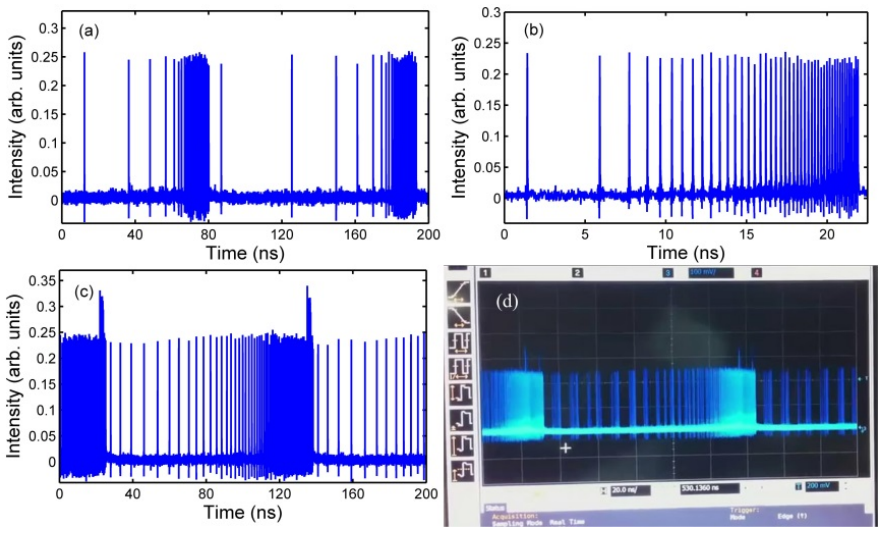

Figure 2.4 Polarization locked vector soliton pulse trains: (a) A typical soliton rain at a pump power of 140 mW; (b) zoom-in of the soliton condense phase; (c) Soliton rain at a pump power of 200 mW; (d) Snapshot of the vector soliton rain (Media 3).

The main difference between the vector solitons and scalar solitons is that a vector soliton has two coupled orthogonal polarization components. Depending on their coupling the polarization of the vector soliton could be either fixed or rotating [49,84]. Therefore, different from the scalar soliton rain, by using the polarization resolved measurement technique we are able to identify two different types of vector soliton rains, the polarization locked and rotation vector soliton rain. Figure 2.5(a) shows the case of the polarization locked vector soliton rain. It can be clearly seen that all the solitons in the flow are uniform both in the total output and the polarization resolved outputs, which is a feature of the polarization locked vector solitons. Figure 2.5(b) was obtained

by slightly changing the setting of the polarization controllers from that of a polarization locked vector soliton rain state. In this way a polarization rotation vector soliton rain state could be obtained. Comparing with Figure 2.5(a), it can be seen while all the solitons have the same pulse heights in the total output, the soliton pulse height varied periodically in the polarization resolved outputs, indicating that the solitons are polarization rotating vector solitons. In particular, the polarization of the vector solitons restore the original polarization every triple of the cavity round-trip time. Polarization rotation of the vector solitons could also be identified from their soliton spectra. Figure 2.5(c) shows the corresponding optical spectrum of the solitons shown in Figure 2.5(b). On the spectrum two extra sets of spectral sidebands could be observed, which were caused by the polarization rotation of the vector solitons in the laser cavity as mentioned in Section 1.

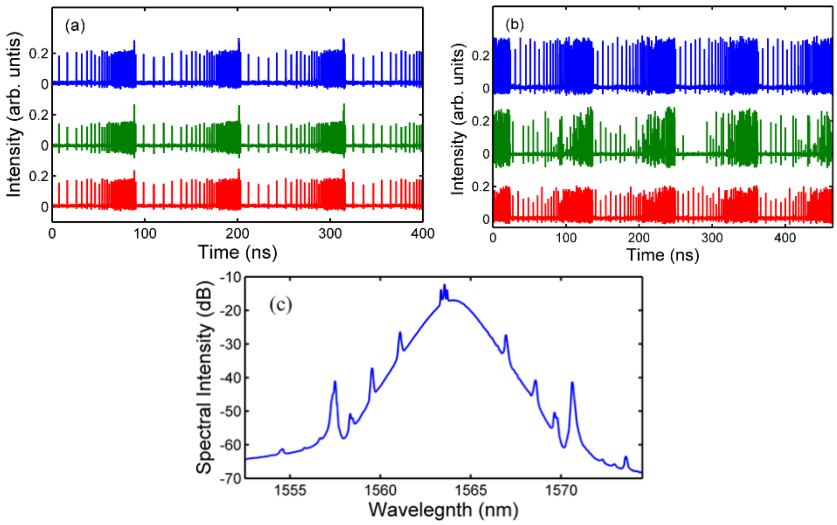

Figure 2.5 (a) Oscilloscope trace of the polarization locked vector soliton rain. Blue line: the total output; Green line: along the horizontal axis; Red line: along the vertical axis. (b) Oscilloscope trace of the polarization rotating vector soliton rain. Blue line: the total output; Green line: along the horizontal axis; Red line: along the vertical axis. (c) The optical spectrum of the polarization rotating vector soliton rain.

e. Giant Pulse State

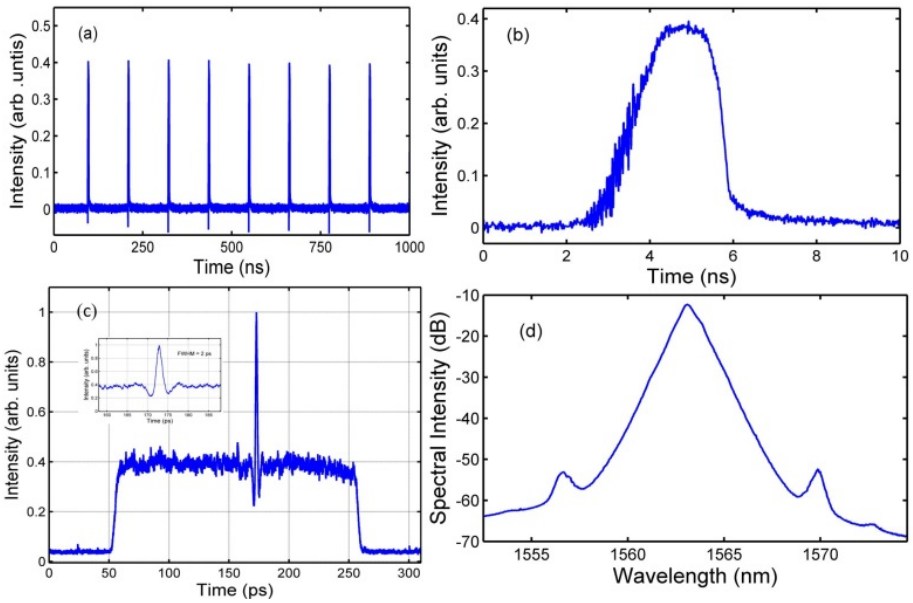

Figure 2.6 Giant pulse state when the soliton rain exploded at 200 mW pump power. (a) Oscilloscope trace; (b) 10 ns scale of the giant pulse; (c) Oscilloscope trace; (d) optical spectrum.

When the pump power is high enough (~200 mW), under an appropriate PC setting another multiple vector soliton operation state as shown in Figure 3.10 could be observed. Figure 3.10(a) shows a typical oscilloscope trace of the state. It displayed as a stable pulse train, and each pulse could have very large pulse energy. In our experiment pulse energy as large as 60 nJ had been obtained. Figure 3.10(b) shows the single pulse profile measured with our high-speed detection system. As the pump power increased the pulse width also increased, but the pulse peak power only increased slightly. Figure 3.10(c) shows the autocorrelation trace of the "giant pulses". It has an obvious pedestal. On top of the pedestal there is a pulse peak with pulse duration of about 1.29 ps, which is similar to that measured in the multiple vector soliton state. Figure 2.6(d) shows the optical spectrum of the giant pulses. It has a triangular shape with blurred spectral sidebands. Based on the measured autocorrelation trace and the pulse spectrum, we conclude that that giant pulses are made of many tightly packed solitons with random soliton separations.

2.1 Discussion

It is noted that similar multiple soliton patterns have also been observed in the scalar soliton fiber lasers, which shows that the formation of these multiple soliton patterns is a general feature of the soliton lasers, which is independent on whether they are scalar or vector solitons. In a previous work on the scalar soliton interaction in the passively mode locked fiber lasers, it have been shown that various modes of the multiple scalar soliton operation could be traced back to the specific features of the soliton interaction in the cavity [16]. Experimentally, we found that the same is valid for the vector solitons. Despite of the fact that a vector soliton consists of two orthogonally coupled polarization components, and therefore has more complicated dynamics than that of a scalar soliton, the interaction between the vector solitons in a fiber laser cavity is still mainly determined by the same types of interactions mechanisms: the unstable CW caused global type of soliton interaction, the

dispersive wave mediated long range soliton interaction, and the direct soliton interaction, in the fiber lasers that are mode locked by the saturable absorbers like the SESAM or graphene, there is also a absorber caused attraction force, whose strength and action range depends on the saturable absorption strength and the recovery time of the saturable absorbers. The various modes of the vector soliton operation are actually the combined consequence of the mutual actions of these soliton interaction mechanisms on the multiple solitons formed in the laser cavity, e.g. under the effects of a weak unstable CW in the cavity and the saturable absorber effect, the multiple solitons would always have the tendency of soliton bunching. Depending on the strength of the dispersive waves generated by the solitons, one would expect that the solitons in a bunch could be either static or moving restlessly. A soliton rain state could be considered as a special case of the soliton bunch formed under strong pumping, where a lot of solitons are formed in the cavity. In this case due to the fast saturable absorption of the absorber, the soliton distribution displays an increasing density with the time. A state of bunched solitons is formed due to the direct soliton interaction [16]. So far in our experiments no stable states of the closely bunched vector solitons have been observed. Nevertheless, we believe that the giant pulse emission states could be formed as a result of the direct soliton interaction in the laser. However, in the current case many solitons are bunched together with random soliton separations, leading to the observed features of the multiple vector soliton laser emission.

3. Bound Solitons in Graphene Mode-locked Fiber Lasers

Bound states of solitons, also known as soliton molecules, are referred to as the situation where two or more fundamental solitons bind tightly together in the temporal or spatial domain through the direct soliton interaction. The solitons in the state have not only fixed separations but also fixed phase differences, and the assembly of the solitons behaves like a new super-soliton. Theoretically, formation of bound states of solitons in the extended nonlinear Schrödinger equation (NLSE) systems was first predicted by B. Malomed [75, 85]. N. N. Akhmediev *et al.* had also studied the formation of bound states of solitons in the complex Ginzburg-Landau equation (CGLE) systems [86,87]. It was shown that dissipative property renders the solitons with unique new features of interaction that can result in the formation of stable bound states of dissipative solitons [88]. Experimentally, formation of bound states of solitons in fiber lasers has attracted considerable interest. Owing to the existence of gain and losses, solitons formed in a fiber laser are essentially dissipative solitons [89]. It is anticipated that the soliton fiber lasers could serve as an ideal testbed for the study on bound solitons. The bound states of solitons were first experimentally observed in a fiber laser mode locked with the nonlinear polarization rotation (NPR) technique [74]. Later, with the development of novel material based real saturable absorber (SA) mode locking techniques, such as the carbon nanotube mode locking, 2D-nano-materials mode locking, formation of bound states of solitons has also been observed in fiber lasers mode locked with the carbon nanotubes [89-93], graphene [94-96] and MoS_2 [97]. Unlike the NPR mode-locked fiber lasers where the formed solitons have a fixed polarization due to the insertion of a polarizer in cavity, the polarization insensitive saturable absorption of the carbon nanotube and graphene saturable absorbers allows the

formation of vector solitons in fiber lasers. Here a vector soliton is referred to as a soliton that has two coupled orthogonal polarization components [98]. Therefore, one would expect that bound states of dissipative vector solitons could also be formed in fiber lasers mode locked with these saturable absorbers. We note that the phase locked vector solitons were first experimentally observed in a SESAM mode locked fiber laser [99]. C. Mou *et al.* reported the existence of bound vector solitons in a carbon nanotube mode locked fiber laser [92]. However, so far the experimental studies have mainly focused on the formation of the bound solitons or bound vector solitons in fiber lasers. Although it is well-known that the formation of bound states of solitons is a result of the direct soliton interaction [16, 74, 75], how the bound solitons inetract or a soliton interacts with the bound solitons has not been addressed.

In this section we report on the experimental study of interaction between the vector solitons and bound vector solitons in a fiber laser passively mode locked with graphene. In our fiber laser we have obtained various types of solitons, including the vector solitons, bound states of vector solitons, and bound states of bound vector solitons. Coexistence of vector solitons and bound vector solitons in the same laser cavity is also first experimentally observed. Dispersive wave mediated vector soliton interaction and collision between the vector solitons are also experimentally visualized. Our experimental results confirm the stability and robustness of the bound vector solitons in fiber lasers.

The schematic of the graphene mode-locked fiber laser is similar to Figure 1.1. The fiber laser has a ring cavity of 15.6 m long. A piece of 3 m erbium doped fiber with a group velocity dispersion (GVD) parameter of -48 ps/nm/km was used as the gain fiber. Other fibers used are all the standard single mode fiber (SMF-28) with a GVD parameter of 18 ps/nm/km. Thus the cavity is dispersion-managed and has net anomalous dispersion. A polarization independent isolator is employed in the cavity to force the unidirectional operation of the ring cavity, and an intra-cavity polarization controller (PC) is used to fine-tune the linear cavity birefringence. The laser is reverse pumped by a high power fiber Raman Laser source (KPS-BT2-RFL-1480-60-FA) of wavelength 1480 nm. The pump laser can deliver a maximum pump power as high as 5 W. A 10% output coupler is used to output the laser emission. The graphene used is synthesized using the chemical vapor deposition (CVD) method, and it has multiple layers [20]. The graphene sheets are carefully deposited on the end facet of an optical fiber, which is inserted in a fiber connector. The laser emission is measured by an optical spectrum analyzer (OSA) and a 32 GHz real-time oscilloscope (RTO). The laser output is split into two paths: one is monitored by the OSA and the other by the RTO. Therefore, both the optical spectrum and the time evolution of the laser emission are measured simultaneously. To detect the vector soliton feature of the laser emission, a polarization beam splitter was used to separate the two orthogonal polarizations. In addition, a commercial autocorrelator (FR-103XL) is used to measure the pulse width and observe the details of the bound solitons.

3.1 Vector soliton mode-locking

Mode locking of the fiber laser can self-start at a pump power of ~100 mW. Figure 3.1 illustrates a typical soliton mode locked state of the laser. Figure

3.1(a) shows the oscilloscope traces of the polarization resolved laser emissions. Along the two orthogonal polarization directions of the laser cavity synchronized pulses are measured. Figure 3.1(b) shows the corresponding optical spectrum. The 3-dB spectral bandwidth of the laser emission is ~10.2 nm. As the fiber laser has a dispersion-managed cavity with a small net anomalous dispersion, the spectral profile displays a near Gaussian shape. Nevertheless, a weak asymmetrical Kelly spectral sideband can still be identified at ~1571 nm, which shows that the mode locked pulses have been shaped into dissipative solitons in the fiber laser [63]. It is noted that the number of the soliton pulses in the cavity can be increased or decreased by carefully changing the pump power. The vector nature of the solitons is also confirmed by the coexistence of two synchronized polarization components. Figure 3.1(c) shows the autocorrelation trace of the solitons. If a $sech^2$ profile is assumed, the solitons have a FWHM pulse width of 390 fs, given a time-bandwidth product of 0.492. Therefore, the formed solitons are slightly chirped.

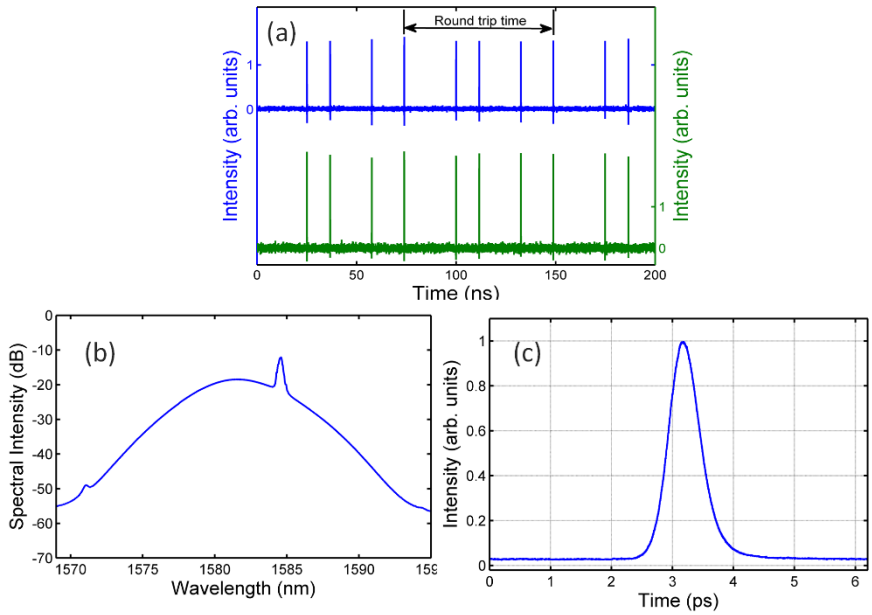

Figure 3.1. A typical state of vector soliton operation of the mode locked fiber laser. (a) Oscilloscope trace; (b) Optical spectrum; (c) Autocorrelation trace.

3.2 Bound states of vector solitons

Apart from the above multiple vector soliton operation, bound states of vector solitons could also be experimentally observed in the fiber laser. A typical bound state of two vector solitons is shown in Figure 3.2. One of the characteristics of the bound solitons is that its optical spectrum is strongly periodically modulated, which reflects the fixed soliton separation [74]. Figure 3.2(a) shows the total and the polarization resolved optical spectra of the laser emission. As can be seen in Figure 3.2(a), the optical spectra of the state are strongly modulated. The spectral modulation period is about 1 nm, which corresponds to a soliton separation of ~8 ps in the time domain. The 3-dB spectral bandwidth of the pulses is ~10.2 nm, which is the same as that of the fundamental soliton. We note that two CW components also exist in one of the two orthogonal polarization directions. Moreover, the spectral bandwidth of the

solitons along the two orthogonal polarization directions, as well as the spectral modulation period and the central wavelength are the same, indicating that the solitons along the two orthogonal polarizations have the same pulse duration and pulse separation. Hence, it is a bound state of vector solitons. The bound state of vector solitons is further confirmed by measuring the autocorrelation trace, as shown in Figure 3.2(b). There are three peaks in the trace with a height ratio of 1:2:1, which corresponds to the case where two pulses with identical intensity and duration are bound in the time domain. The measured soliton separation in the bound state is 8.1 ps, which coincides with the modulation period observed on the optical spectrum. The oscilloscope trace of the bound state of vector solitons is shown in Figure 3.2(c). The pulse trace is almost similar to those shown in Figure 3.1(b). Due to the limited bandwidth of the oscilloscope, it cannot be determined simply from the oscilloscope traces if the pulse is single soliton or bound solitons.

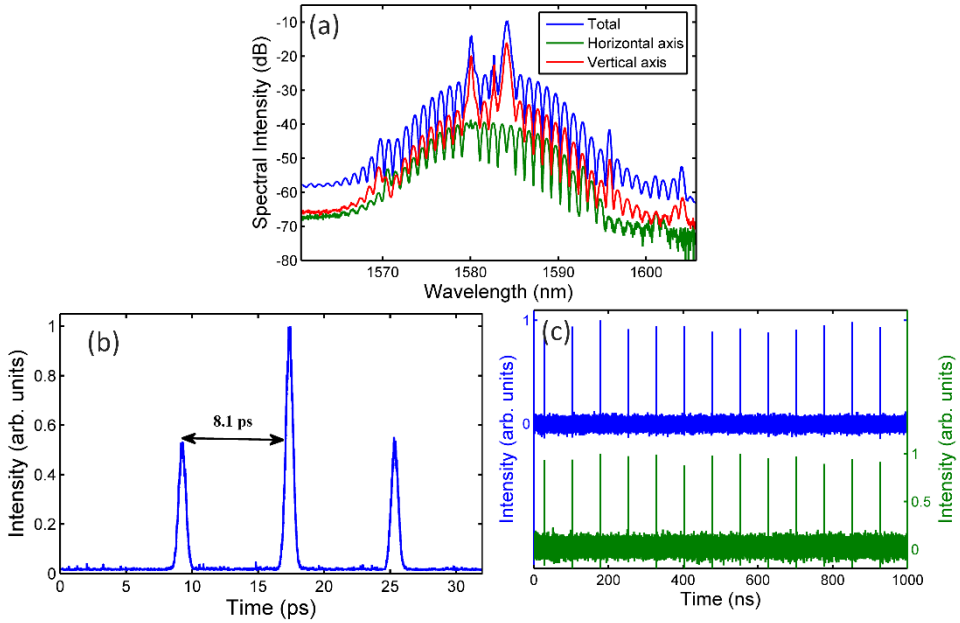

Figure 3.2 A state of bound vector solitons of the fiber laser. (a) Optical spectra. Blue line: the total output; Green line: output along the horizontal axis; Red line: output along the vertical axis. (b) Autocorrelation trace; (c) the polarization resolved oscilloscope traces.

3.3 Coexistence of vector solitons and bound-vector-solitons

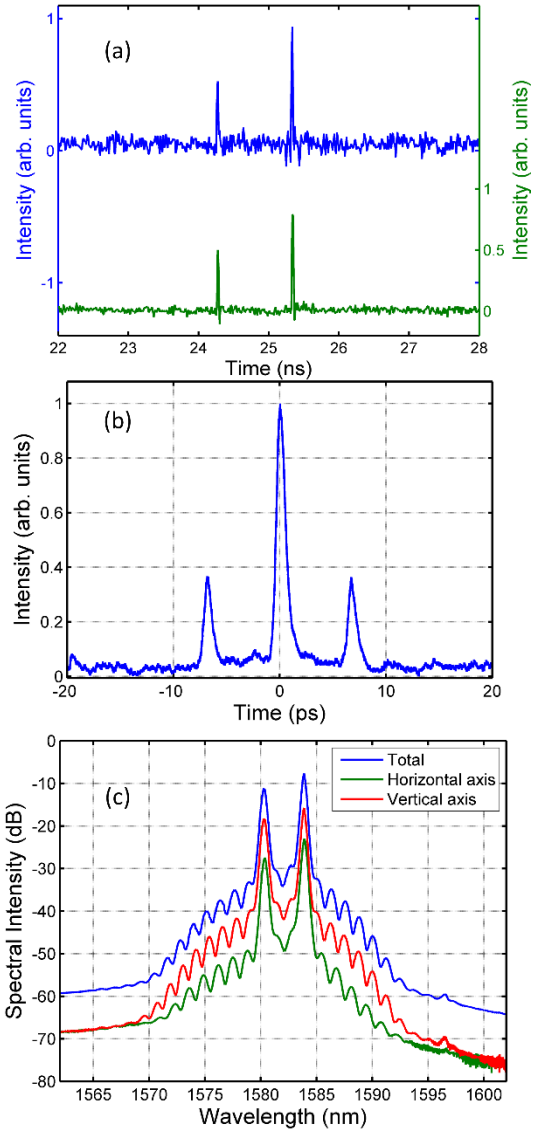

Figure 3.3 Coexistence of single soliton and bound solitons. (a) the polarization resolved oscilloscope trace; (b) Autocorrelation trace; (c) Optical spectra.

An interesting soliton operation state of the fiber laser is the coexistence of bound vector solitons and single vector soliton, as shown in Figure 3.3. To the best of our knowledge, such a state has never been reported before. The oscilloscope traces in Fig. 4(a) show that two soliton pulses with different pulse intensities coexist in the cavity. The one with higher intensity is a state of bound vector solitons, and the one with lower intensity is a vector soliton. To confirm that the higher intensity one is a bound state of vector solitons, we further measured the autocorrelation trace of the state, it is depicted in Figure 3.3(b). Obviously, a bound state of solitons is formed in the laser. However, unlike the autocorrelation trace of the bound solitons shown in Figure 3.3(b), where the central peak to the side-peak height ratio is 2:1, in the current case the central peak to the side-peak height ratio is ~2.5:1. The difference is caused due to the coexistence of the vector soliton in the cavity. The measured autocorrelation trace is actually an average of that of the vector soliton and the bound vector solitons. Considering that the autocorrelation trace of the vector soliton has only

one peak (see Figure 3.1), one will be able to understand why the intensity ratio of the central peak to side-peak measured in the autocorrelation trace is larger than 2:1. Figure 3.3(c) shows the corresponding polarization resolved optical spectra. The spectral modulation again confirms the existence of the bound state of vector solitons in the cavity. A spectral dip is at the centre of the spectra, indicating that the bound solitons could have π phase difference [101].

3.4 Interaction between vector soliton and bound vector solitons

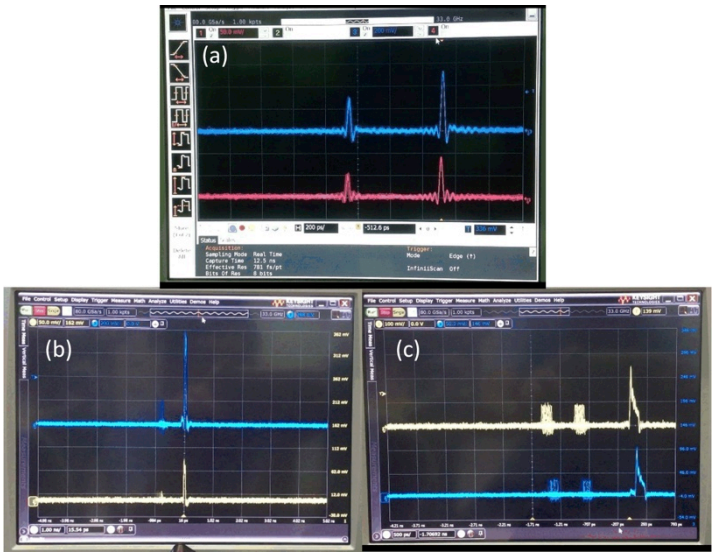

Figure 3.4. Interactions between vector soliton and bound vector solitons. (a) Snapshot of the moving solitons and the bound solitons (200 ps/div, see Media 4). (b) Snapshot of vector soliton move through a bound vector solitons (1 ns/div, see Media 5). (c) Snapshot of vector solitons moving into a soliton bunch (500 ps/div, see Media 6).

We have experimentally investigated the interaction between the single vector soliton and the bound vector solitons in the laser cavity. An interesting case is recorded in Media 4 of Figure 3.4(a). In the case a vector soliton and a bound state of two vector solitons coexist in the cavity. On the oscilloscope traces the pulse with higher intensity is the bound vector solitons while the one with lower intensity is the single vector soliton. As the bound vector solitons are used to trigger the oscilloscope, hence it is stationary in the oscilloscope trace. One can clearly see that the single soliton moves slowly with respect to the bound solitons. However, it is trapped in a certain range and moves repeatedly towards and then away from the bound solitons. The minimum distance that the singe soliton comes close to the bound solitons is ~150 ps. The soliton interaction is localized. We believe it could be caused by the dispersive waves mediated soliton interaction [16]. Media 4 not only provides a direct evidence of the coexistence of the single and the bound vector solitons, but also reveals that they can interact with each other in the laser cavity. By carefully changing the cavity condition, the single and the bound vector solitons can also collide in the cavity. Figure 3.4(b) (see Media 5) shows that a single vector soliton passes through bound vector solitons. It can be clearly seen that the speed of the soliton is significantly reduced after passing through the bound vector solitons, which indicates that the soliton and the bound solitons may strongly interact

with each other when they overlap in the space. Our experimental result clearly shows that the collision destroys neither the bound state of the vector solitons nor the single vector soliton. Figure 3.4(c) (Media 6) shows another situation experimentally observed. In the situation a soliton bunch is initially in the laser cavity. A soliton bunch is different from a bound state of solitons in that the adjacent solitons are far apart from each other and loosely bound. However, the bunch as a unit propagates in the cavity. A soliton bunch propagates with a very different group velocity in the cavity from that of the single soliton, therefore, they collide in the cavity. Different from that shown in Media 5 where the single soliton passes through the bound solitons, the soliton bunch shown in Media 6 behaves like a soliton sink, which simply absorbs the solitons coming to it.

3.5 A bound state of bound vector solitons

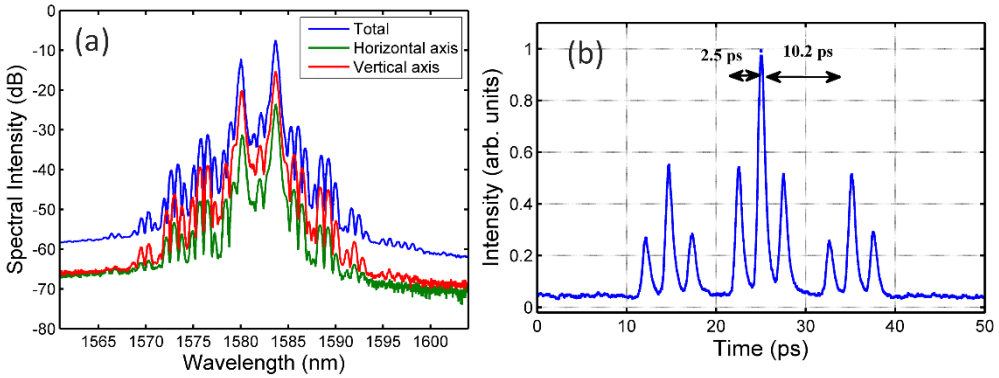

Figure 3.5. A bound state of bound vector solitons. (a) Optical spectra; (b) Autocorrelation trace.

Like first experimentally observed in a soliton fiber laser mode locked with the NPR technique [74], bound states of bound vector solitons are also experimentally observed in the graphene mode locked fiber laser. A typical example is shown in Figure 3.5. Here a bound state of bound vector solitons is referred to as the state where two sets of the bound vector solitons are very close to each other and bind together through the direct soliton interaction. Figure 3.5(a) is the polarization resolved optical spectra of the laser emission. The vector nature of the bound solitons is confirmed by the polarization resolved spectra. There are two sets of modulation in the spectra correspond to the vector soliton separations in primary bound solitons, which is about 2.5 ps, and the separation between the primary bound-solitons, which is about 10.2 ps. Figure 3.5(b) shows the measured autocorrelation trace. It clearly shows the pulse separations. The autocorrelation measured pulse separations are well in agreement with those calculated from the spectral modulation periods. We note that bound states of bound solitons were previously also observed in the carbon nanotube mode locked fiber lasers [90].

3.6 Discussion

The graphene mode locked fiber lasers have now been experimentally extensively investigated. Since polarization independent saturable absorption could be easily achieved with the graphene-based saturable absorbers, through exploiting the nonlinear light propagation in the vector cavity fiber lasers, one

could easily achieve the vector soliton operation in the graphene mode locked fiber laser. Due to the dissipative nature of the formed solitons in a fiber laser, under strong pumping multiple vector solitons could further be formed. Multiple solitons in a fiber laser can have complicated interaction. Previous experimental studies based on multiple scalar solitons have shown various types of interaction forces, the global interaction caused by the continuous wave in the cavity, the dispersive waves mediated interaction and the direct soliton interaction. Our experimental results suggest that even for the vector solitons, these types of interactions still remain. Obviously the vector nature of the solitons does not change their interaction features. Moreover, the various soliton interactions did not destroy the vector soliton either. This result shows that the polarization coupling strength is very strong. This could also be easily understood, as the polarization coupling could also be treated as a kind of direct solitons interaction. As a result of different types of soliton interactions, as well as under different conditions, different situations of the multiple vector soliton operation have been observed in our fiber laser. What we have shown here are just some of the special cases, it is anticipated that more interesting cases could be further obtained. We hope that our results could trigger further extended studies.

In conclusion, we have experimentally investigated the vector soliton operation of a graphene mode locked fiber laser. It has been shown that under strong pumping, multiple vector solitons could be formed in the fiber laser, and as a result of the various types of the soliton interactions, different forms of stable and dynamic multi-vector-soliton operation states could be formed. These include the bound states of vector solitons, and bound states of the bound vector solitons. Coexistence and interaction of vector soliton and bound vector solitons is obtained and experimentally investigated. In addition, collision between the vector solitons is experimentally visualized. Our experimental results demonstrated the richness of the vector soliton interactions and the formed phenomena.

4. Quasi-periodicity of Vector Solitons in Graphene Mode-locked Fiber Lasers

Passively mode-locked fiber lasers have been intensively investigated both due to their practical applications as a cost-effective ultrashort pulse source and rich dissipative soliton dynamics, which can be well described by the complex Ginzburg-Landau equation (CGLE) [38]. Theoretical studies on the dissipative solitons have revealed that apart from their stability against perturbations, they can also exhibit different types of complicate dynamics [38,102]. These include the soliton pulsations, soliton quasi-periodicity, soliton period-doubling bifurcations and route to chaos. Indeed, all of these features of the dissipative solitons have been experimentally confirmed, e. g. the soliton period doubling and tripling effect was first reported by K. Tamura *et al.* [103], the soliton period doubling and quasi periodicity was observed by G. Sucha *et al.* in an additive pulse mode locked laser [104], the quasi-periodic route to chaos was reported by F. Sanchez *et al.* in an erbium-doped fiber laser [105], and by S. Bolton and M. Acton in a Kerr-lens mode locked Ti:sapphire laser [106]. L. Zhao *et al.* obtained both experimentally and numerically soliton period-

doubling route to chaos in a fiber laser [107]. Moreover, detailed experimental studies have shown that associate with the occurrence of the soliton dynamics, extra spectral sidebands always appear on the soliton spectra, which was later turned out to be a result of the soliton modulation instability (MI) in the lasers [108]. The soliton MI leads to coherent wave coupling between the solitons and dispersive waves. Under strong coherent wave mixing a dissipative soliton could display various types of dynamic features.

However, the majority of the previous experimental studies on the dissipative soliton dynamics were focused on the mode locked solid state lasers with a polarization selective element in cavity, or fiber lasers mode locked with the nonlinear polarization rotation (NPR) technique, where in order to achieve the self-started passive mode locking a polarizer was inserted into the cavity. The polarization selective element or polarizer defines the polarization of light at the cavity position. Under the effect of cavity boundary condition it further fixes the polarization of light everywhere in the cavity. Solitons obtained in the lasers are essentially scalar solitons. In a mode locked fiber laser if there is no any polarization sensitive components in cavity, the vector nature of light needs to be considered, consequently the vector solitons, which are solitons with two coupled orthogonal polarization components, would be formed. Compared with the scalar solitons, a vector soliton could exhibit more complicated dynamics.

Several groups have experimentally demonstrated vector soliton operation in SESAM fiber lasers. Using a semiconductor saturable absorber mirror (SESAM) as the mode locker S. Cundiff *et al.* have first experimentally obtained the polarization locked and polarization rotation vector solitons in a linear cavity fiber laser [84]. L. Zhao *et al.* have experimentally investigated features of the vector solitons formed in a ring fiber laser, and observed period-doubling bifurcation of the vector solitons [109]. Nevertheless, experimental study on features of the vector solitons is still rare and there is still no study on this topic based on the graphene fiber laser, to the best of our knowledge. In this section, we present results of experimental studies on the vector soliton formation and dynamics in an erbium-doped fiber laser passively mode-locked with atomic-layer graphene. We show experimentally that apart from the periodic vector soliton evolution in the laser cavity, under certain conditions the vector solitons formed in the fiber laser can exhibit quasi-periodic evolution, where both the pulse energy and the polarization of the vector solitons vary quasi-periodically with the cavity roundtrips. Moreover, like the quasi-periodic evolution of the scalar solitons obtained in fiber lasers, associated with the occurrence of the quasi-periodic dynamics of the vector solitons, an extra set of spectral sidebands appeared on the optical spectrum of the solitons. The extra spectral sideband formation was found to be a threshold effect, which is a characteristic of the MI of the solitons formed in a laser. Hence, the experimental result suggests that it is the cavity induced MI that has caused the quasi-periodic dynamics of the vector solitons. Quasi-periodicity of multiple vector solitons was also observed, where the vector solitons exhibit uncorrelated quasi-periodic evolutions in the cavity. In the quasi-periodic state the vector solitons no longer possess the soliton energy quantization feature.

4.1 Experimental Results

The cavity configuration of the fiber laser is schematically same as Figure 1.1. The fiber laser was pumped by a Raman fiber laser of wavelength 1480 nm. The ring cavity has a length of 22.6 m. A piece of 0.7 m erbium doped fiber (EDF Er80-8/125 from Liekki) with GVD of -18 ps/nm/km was used as the gain medium. The rest fibers used in the cavity were all standard single mode fibers. A 10% fiber output coupler was employed to output the signal. A polarization independent isolator was used in the cavity to force the unidirectional operation of the ring cavity, and a polarization controller (PC) was inserted in the cavity to fine tune the linear cavity birefringence. A few-layer graphene film, grown with the CVD was used to mode lock the fiber laser. The graphene was transferred to an end of a fiber pigtail, which was then connected to another fiber through a fiber connector. It is noted that the graphene film we used is the same as that of Chapter 2 and the properties of the graphene will not be further discussed.

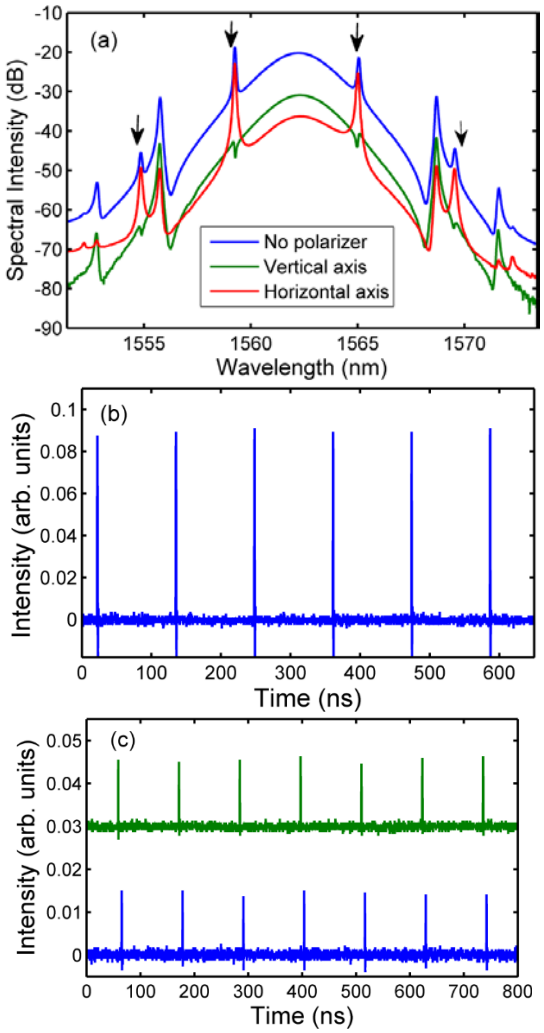

Figure 4.1 A state of the polarization locked vector soliton operation of the laser. (a) The total and the polarization resolved optical spectra of the vector soliton. The extra set of spectral sidebands is indicated by the arrows; (b) oscilloscope trace of the vector soliton pulse train. (c) The polarization resolved oscilloscope trace of the vector soliton pulse train.

Mode locking of the laser was achieved at a pump power of ~90 mW. Initially, multiple mode locked pulses were obtained. However, through carefully adjusting the pump power, a single pulse operation state was then achieved. Under the single pulse operation the pump power became as low as 39 mW. Figure 4.1 shows for example a state of the single soliton operation of the fiber laser. The optical spectra of the pulse are shown in Figure 4.1(a). The existence of the Kelly sidebands on the spectra confirms that the mode locked pulse is a soliton. To prove that the observed soliton is a vector soliton, we note that apart from the Kelly sidebands, there is another set of spectral sidebands (indicated by arrows) on the soliton spectra. The extra set of spectral sidebands differs from the Kelly sidebands because their positions vary sensitively with the change of the linear cavity birefringence. In addition, on the polarization resolved spectra the extra set of sidebands exhibits clear difference from the Kelly sidebands: the Kelly sidebands always display as spectral peaks, while the new set of sidebands show a dip-peak relation between the two orthogonal polarization components, indicating the existence of coherent energy exchange between them [65]. Figure 4.1(b) is the corresponding pulse train of the soliton. The time interval between the pulses is 113 ns, which coincides with the roundtrip time of the cavity. Based on the polarization resolved pulse trains shown in Figure 4.1(c), it is to conclude that the vector soliton is a polarization locked vector soliton as no polarization rotation exists. We note that despite of the existence of coherent energy exchange between the two polarization components, no linearly polarized soliton was obtained in our experiment. The observed vector soliton is elliptically polarized as no matter how the external cavity PC was adjusted, none of the two polarization resolved components could be turned to zero. In our experiments once the laser was mode locked, the obtained mode locked pulses were vector solitons, indicating that the average cavity birefringence of our laser was small. Depending on the pump strength, multiple phase locked vector solitons coexisting in cavity were also obtained, as shown in Figure 4.2(a) and (b). In the steady states all the vector solitons have exactly the same soliton parameters, indicating that under the polarization locked vector soliton operation the soliton energy is still quantized.

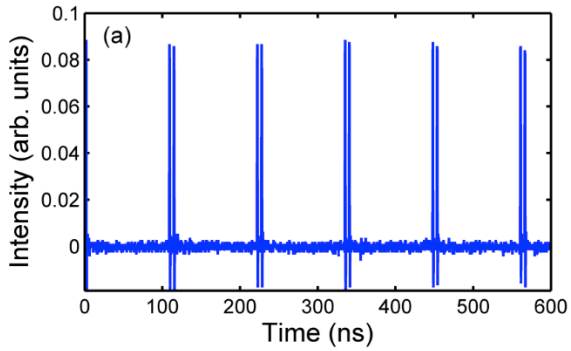

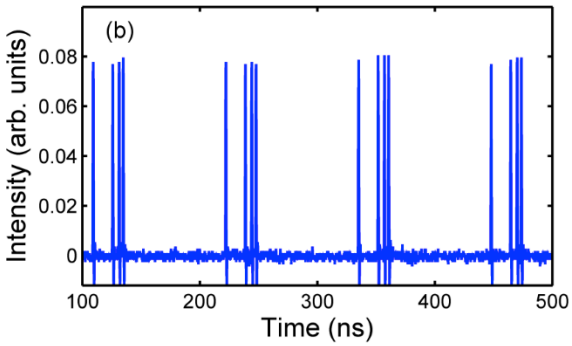

Figure 4.2 Polarization locked vector soliton pulse trains with (a) two solitons and (b) four solitons in the cavity.

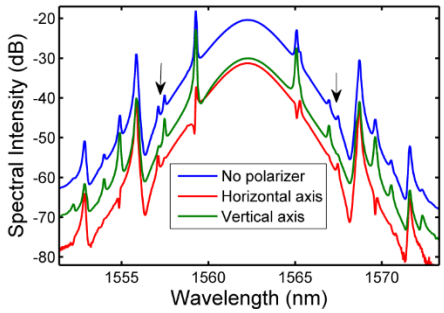

Figure 4.3 The total and the polarization resolved optical spectra of a polarization rotation vector soliton of the laser. The extra set of spectral sidebands is indicated by the arrows.

Starting from a polarization locked vector soliton state, when pump power of the laser or the orientation of the paddlers of the intra cavity PC was carefully changed, the polarization of the vector solitons then became unlocked. Consequently, the polarization of the vector solitons rotated in the cavity. Associated with the soliton polarization rotation, two extra sets of spectral sidebands were found to appear on the spectrum of the vector soliton, as shown in Figure 4.3 (indicated by arrows). A similar phenomenon was also reported by Cundiff *et al.*[84]. However, the appearance of the new spectral sidebands did not affect the pulse height of the vector solitons as on the oscilloscope trace the vector soliton pulses were still uniform. In the Chapter 2 we have already experimentally investigated the formation mechanism of the two sets of extra spectral sidebands. They were found to be the Kelly sidebands caused by the periodic polarization rotations of the vector solitons in the cavity. The periodic polarization rotation of the vector solitons introduces another periodicity in the laser, which causes extra constructive interference between the dispersive waves radiated by the solitons as they circulate in the cavity. As a polarization rotating vector soliton has two orthogonal polarization components with unlocked phases, each polarization component would form its own Kelly sidebands. Therefore, two extra sets of spectral sidebands appeared on the vector soliton spectrum, while on the polarization resolved spectra of the vector soliton, only one set of the extra Kelly sidebands would be observable, as also shown in Figure 4.3. We point out that in the case where multiple vector solitons coexist in the cavity, although each of the vector solitons rotated at the same speed of rotation, the polarization orientations of the vector solitons were different.

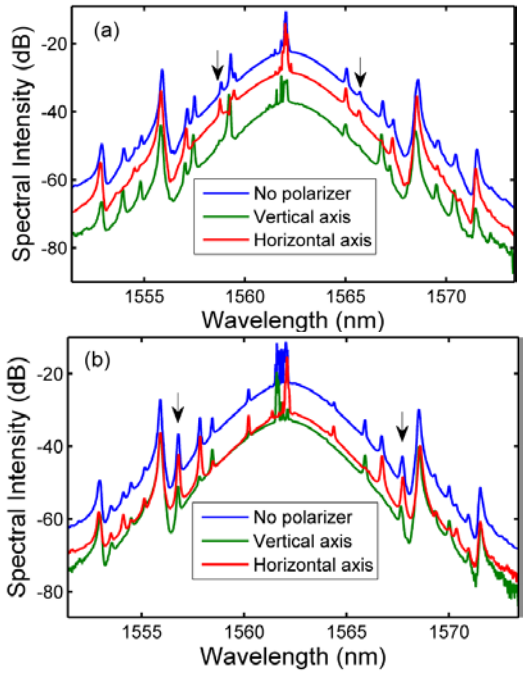

Figure 4.4 The total and the polarization resolved optical spectra of the vector solitons under quasi-periodic evolutions. The extra set of spectral sidebands is indicated by the arrows. (a) The case where the vector soliton has a large polarization ellipse; (b) The case where the strength of the two orthogonal polarization components of the vector soliton was comparable.

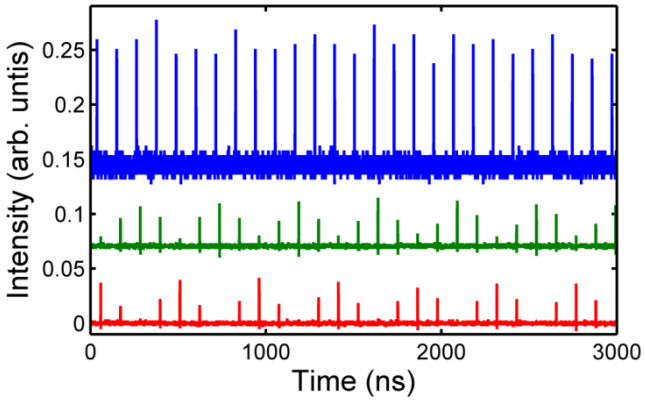

Figure 4.5 Oscilloscope traces of the vector soliton under quasi-periodic evolution. Blue line: the total vector soliton pulse train; Green line: the horizontal axis; Red line: the vertical axis.

Both the polarization locked and polarization rotation vector solitons could be easily obtained in our laser. Because the solitons are dissipative in nature, the energy of the vector solitons increases as the pump power increases. Experimentally we noticed that as the energy of the vector solitons increased to a certain level, an extra set of spectral sidebands further appeared on the vector soliton spectrum, as shown in Figure 4.4 (indicated by arrows). As the new extra set of spectral sidebands became clearly visible, the pulse height of the vector solitons on the oscilloscope trace also gradually became non-uniform, as shown in Figure 4.5. Based on the polarization resolved soliton pulse traces, it is easy to see that the polarization rotation of the vector soliton also became quasi-periodic with the cavity roundtrips.

Two different situations were revealed through the polarization resolved measurement. Figure 4.4(a) shows a case where the vector soliton has a large polarization ellipse. In this case the new extra spectral sidebands only appeared on the strong polarization component of the vector soliton. On the spectrum of the weak polarization component there is no sign of the new extra spectral sidebands. Figure 4.4(b) shows another case where the strength of the two orthogonal polarization components of the vector soliton was comparable. In this case the new extra spectral sidebands appeared at the same position on both polarization components. This experimental result suggests that the appearance of the new extra spectral sidebands is a threshold effect. Its appearance requires that the pulse intensity of the soliton is sufficiently strong. In addition, comparing with the results shown in Figure 4.4(a) and (b), which were taken under two different intracavity PC settings but the same pump power, the positions of the new extra spectral sidebands also depend on the laser cavity detuning.

In the past the formation mechanisms of various spectral sidebands of the scalar solitons formed in fiber lasers were both experimentally and numerically investigated and it was shown that coherent wave mixing between the solitons and dispersive waves could occur in a laser, which was previously named as the soliton modulation instability [108]. Under the effect of the soliton modulation instability the energy of the soliton and dispersive waves are coherently coupled. Under strong coherent energy coupling the energy of the soliton could become varying as it propagates in the cavity. A soliton circulating in a laser cavity also has to satisfy the cavity boundary condition, which modifies the phase matching condition of the coherent wave mixing. As shown by Haelterman *et al.*, the cavity feedback effect is reflected as that the resonant frequency now depends on the cavity detuning as well [68]. The features of the observed new extra spectral sidebands well match those formed due to the soliton MI reported for the scalar solitons.

The soliton MI is a threshold effect. Like the case of scalar solitons, in our experiment once the intensity of the vector solitons became beyond the MI threshold, a new set of spectral sidebands appeared at the positions where the phase matching condition between the soliton and dispersive waves is fulfilled. However, different from the scalar solitons, a vector soliton has two coupled orthogonal polarization components. Further depending on the strength of them, either both of the two polarization components or one of them could become unstable. Nevertheless, in either case the evolution of the vector soliton would become quasi-periodic. Here it is worth noting that because the coherent wave mixing is between the soliton and dispersive waves, no spectral dip-peak but only the spectral peaks were observed on the polarization resolved spectra. Furthermore, changing the cavity detuning also shifted the positions of the spectral sidebands on the soliton spectrum. From a quasi-periodic vector soliton evolution state, if the pump power was further increased, instead of that the laser emission evolved to the chaotic state, a new soliton would be generated, eventually the vector soliton evolution became periodic or quasi-periodic with less soliton energy variation. Further increasing the pump power, the same process as described above repeated.

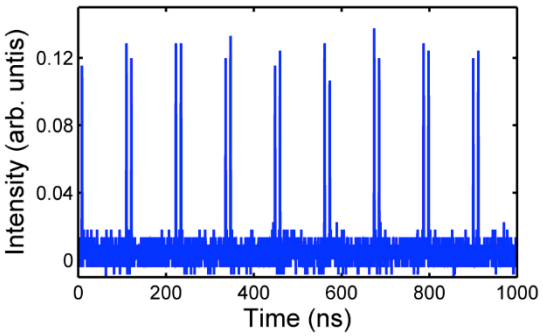

Figure 4.6 The quasi-periodic evolution of two vector solitons coexisting in cavity.

Quasi-periodic vector soliton intensity variations of multiple vector soliton in cavity were also observed. Figure 4.6 shows for example a case of two vector solitons coexisting in the cavity. Each of the vector solitons exhibits the quasi-periodic energy variation, as clearly shown by their oscilloscope traces. In the state the solitons in the cavity have uncorrelated soliton intensity variations. No soliton energy quantization exists in the case. With too many vector solitons in cavity, the interaction among the solitons could become very complicated.

4.2 Conclusions

In conclusion, we have experimentally studied the vector soliton operation of an erbium-doped fiber laser passively mode locked with atomic layer graphene. It was found that under certain operation conditions the vector solitons of the laser could exhibit quasi-periodic evolution. Similar to the case of quasi-periodic evolution of the scalar solitons observed in a fiber laser, in the state a new set of spectral sidebands appeared on the spectra of the vector solitons, and the appearance of the new spectral sidebands was a threshold effect. Based on the features of the vector solitons, we pointed out that the appearance of the extra spectral sidebands is due to the cavity induced soliton modulation instability, and the quasi-periodic vector soliton evolution is a result of the strong resonant energy coupling between the vector soliton and the dispersive waves. However, in comparison with the MI of the scalar solitons, our experimental results show that depending on the strength of each of the two orthogonal polarization components of the vector soliton, the MI could occur on one of the polarization components or both of them. Quasi-periodicity and quasi-periodic route to chaos are intrinsic features of the nonlinear dynamic systems. Our experimental results further confirm that the passively mode locked soliton fiber laser is a nonlinear dynamic system. No matter if scalar or vector solitons are formed in the laser, its dynamics follows the universal rules of the nonlinear dynamics.

5. Noise-like Pulses in Graphene Mode-locked Fiber lasers

In a passively mode locked fiber laser, soliton pulse formation in the cavity is a complicated dissipative process, in which except the impact of the saturable absorber, the balanced interaction among the laser gain, loss, cavity dispersion and the nonlinear Kerr effect also plays an important role, and directly affects the formed soliton pulse parameters. If the cavity parameters are not suitably controlled, the soliton fiber laser may operate in the regime of some distinct pulses such as noise like pulses, extreme pulses. Noise like pulses have been a well-documented phenomenon which has been investigated in the scalar soliton fiber lasers [110-112]. However, both of them have not been observed in the vector soliton fiber lasers. It is interesting and meaningful to investigate the formation and properties of the noise like pulses and rogue waves in a vector soliton fiber laser mode locked with graphene. In this section, we report on the experimental observation of noise-like (NL) pulses in a fiber laser passively mode locked by atomic layer graphene. Based on the experimental and numerical studies, we found that the formation of the NL pulses is a combined consequence of the pulse breaking induced by the excessive nonlinearity of the cavity and the mutual attraction of the soliton pulses caused by the ultra-fast saturable absorption of the graphene. The large energy and broadband spectrum of the NL pulses may find applications in super-continuum generation and metrology where low coherence is required. The experiment also suggests a new research direction for the graphene-based ultrafast laser photonics.

The noise-like pulse formation in fiber lasers passively mode locked by the nonlinear polarization rotation (NPR) technique has been widely studied and its properties and formation mechanism are already clear. It might be of importance to study the features of the NL pulses formed in other fiber lasers that are mode locked by different methods. In this paper, we experimentally and numerically show that the noise like pulses can also be formed in a graphene mode locked fiber laser. Moreover, extensive experimental and numerical studies have further shown that the pulse-to-pulse attraction, which physically correlates with the ultrafast recovery feature of the graphene saturable absorber, could have played a role on the formation of the NL pulses in the fiber laser. Based on the observed experimental results we point out that the graphene mode locked NL pulse emission fiber lasers could be a promising large energy pulse source with the advantages of compactness, small size, all-fiber-format and low cost.

5.1 Experimental Results

The experimental setup of the graphene mode locked fiber laser is similar to those shown in Fig 1.1. The laser was pumped by the high power fiber Raman Laser source with a central wavelength of 1480 nm, and a maximum pump power up to 5 W. The total cavity length was about ~70 m, comprising of 3 m erbium doped fiber (EDF)

with group velocity dispersion (GVD) of -48 (ps/nm)/km and ~67 m standard single mode fiber (SMF) with GVD of 18 (ps/nm)/km. The laser cavity was dispersion managed. It had a total cavity dispersion of about -8.50 ps^2. A 10% output coupler was used in the cavity to output the signal. A polarization independent isolator was employed to force the unidirectional operation of the ring cavity. An intra-cavity polarization controller (PC) was used to fine tune the linear cavity birefringence. All the passive components were made of the SMF. The graphene was fabricated by the chemical vapor deposition method. Optical Raman spectroscopy technique (Witec Alpha 300R) was used to identify the layer number of the graphene, and it was found that the graphene used had 3~4 layers.

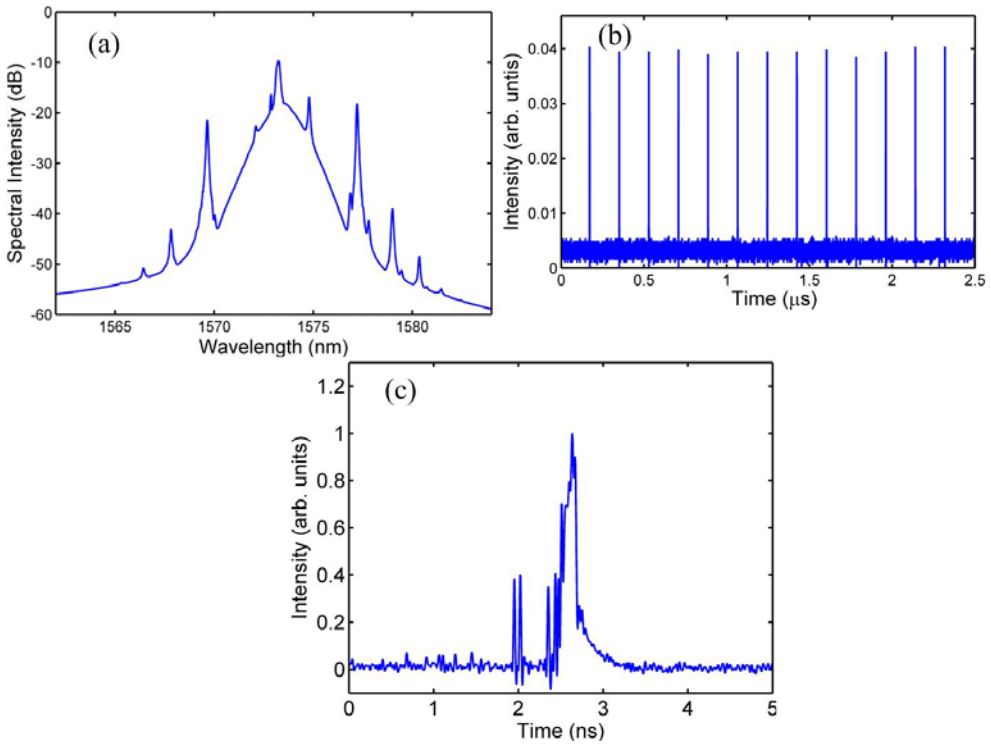

Figure 5.1 Soliton operation of the fiber laser. (a) Optical spectrum measured. (b) The mode locked pulse train. (c) One "single pulse" of (b) detected by a high-speed oscilloscope.

The ring cavity fiber laser has a self-starting mode-locking threshold of about 200 mW due to intra-cavity loss. Figure 5.1(a) shows a typical optical spectrum of the mode locked laser. Clear Kelly sidebands are visible on the spectrum, which is a characteristic of the soliton formation in the anomalous dispersion cavity fiber lasers. In addition, a continuous wave spectral component is also on the spectrum, indicating that an unstable CW coexists with the soliton pulses in the cavity. The central wavelength of the solitons is located at 1573.5 nm and the 3-dB bandwidth is ~1.7 nm. Figure 5.1(b) shows an oscilloscope trace of the state measured with a low speed (500 MHz) detection system. The roundtrip time of the pulses is about 350 ns, which matches with the total cavity length of 70 m. Under the low speed detection where the

internal structures of the mode locked pulses cannot be clearly resolved, the pulses on the oscilloscope trace look like a single pulse. However, measured with a 20 GHz high-speed oscilloscope (Agilent 86100A), the “single pulse” is visualized as shown in Figure 5.1(c). The “single pulse” in Figure 5.1(b) turns out to be a soliton bunch. Within the soliton bunch the relative positions of the solitons are unstable. The solitons are moving restlessly. By increasing the pump power while keeping all the other laser parameters unchanged, more soliton pulses emerged. In other words, the increase of pump power does not boost the energy of each individual solitons but increase the soliton number.

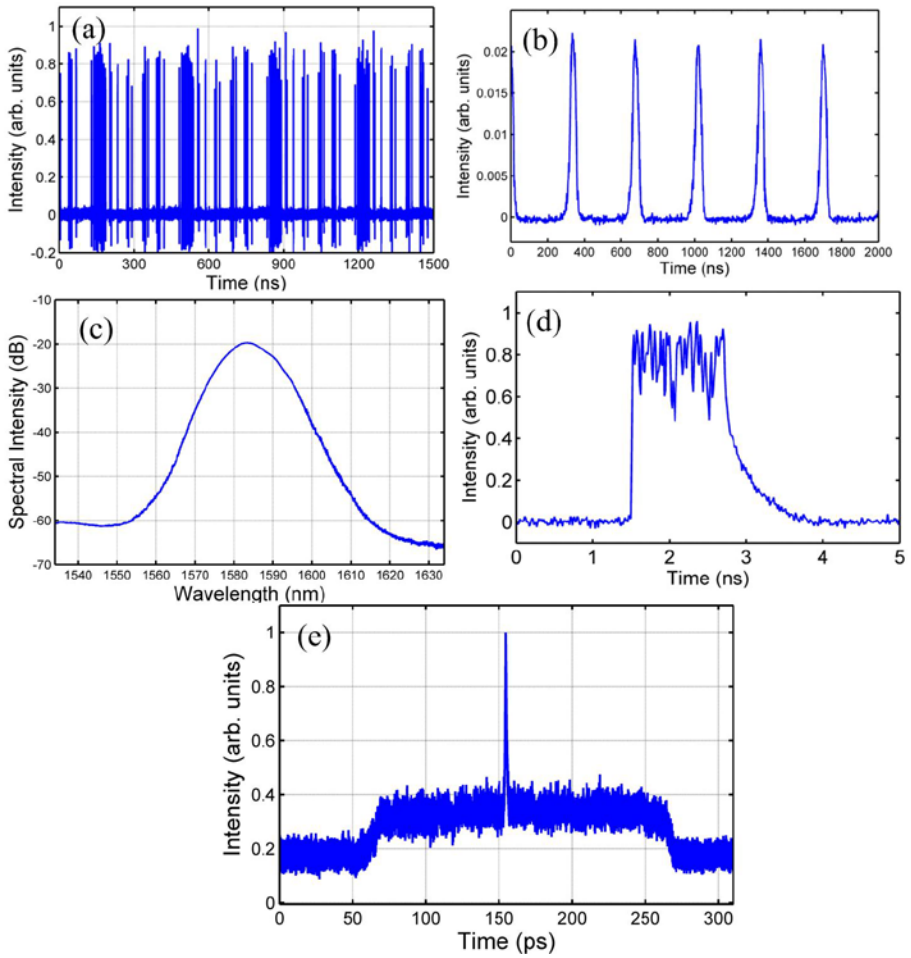

Figure 5.2 (a) Multiple solitons state. (b) NL pulse operation of the fiber laser. (c) Optical spectrum. (d) Pulse profile measured with a high-speed oscilloscope. (e) Autocorrelation trace (pulse width corresponds to the sharp peak is about 1.2 ps).

By adjusting the orientation of the intra-cavity PC, NL pulses could be generated from a multi-soliton state. A state thus obtained is shown in Figure 5.2. Figure 5.2(a) shows the multi-soliton state of the laser just before the NL pulse was formed. After changing the orientation of the intra-cavity PC, a NL pulse state as shown in Figure 5.2(b) was formed. The optical spectrum of the Figure 5.2(a) is same as shown in Figure 5.1(a). Figure 5.2(c) shows the optical spectrum of Figure 5.2(b) state.

Different from the multi-soliton operation state where the optical spectrum of the laser exhibits clear Kelly sidebands (see Figure 5.1(a)), the optical spectrum of the NL pulse state shown in Figure 5.2(b) is blurred and has no spectral sidebands. Figure 5.2(d) shows the high resolution oscilloscope trace of Figure 5.2(b). It is easy to see that within the mode-locked pulse there are a large number of solitons inside. The solitons travel together as one entity in the cavity. The NL pulse state shown in Figure 5.2(b) is very stable, which can last several hours until deliberately destroyed. Figure 5.2(e) shows the autocorrelation trace of the NL pulses. It shows a narrow peak atop a broad pedestal, which is a typical characteristic of the NL pulse states. If a sech^2 pulse shape is assumed, the average soliton pulse width in a NL pulse is estimated to be 1.2 ps.

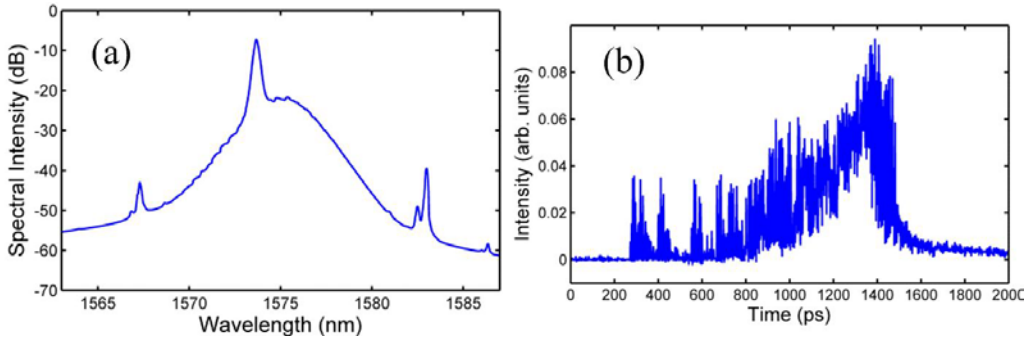

Figure 5.3 Multiple soliton pulses operation in a 30 m long cavity. (a) Optical spectrum measured. (b) Solitons within a bunch measured by a high-speed oscilloscope.

To understand the formation mechanism of the NL pulses, we used another laser that has a shorter cavity length of 30 m. The mode locking operation can still be achieved but with a higher threshold (250 mW). The optical spectrum of the multi-soliton state of the laser is shown in Figure 5.3(a), in which the Kelly sidebands are observable, indicating that the total cavity dispersion is still anomalous. The central wavelength is now shifted to 1575 nm and the 3-dB bandwidth is ~3.5 nm. As shown in Figure 5.3(b), the multiple solitons tend to form a bunch in a shorter laser cavity. If the pump power is decreased, the number of solitons in the bunch reduces until the mode locking state is lost. It is noted that in this process no single soliton could be obtained. We attribute the phenomenon as due to the relative high loss of the cavity induced by the graphene. When the quality of the graphene used is not high, we found that the cavity losses could be large. In this case only multiple solitons or the noise like pulse could be easily obtained under strong pump. It also explains why the mode-locking threshold of the current laser is as high as 250 mW.

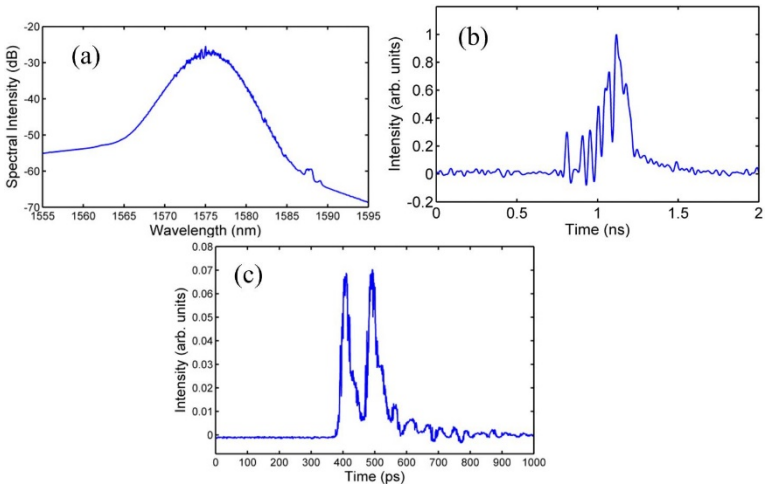

Figure 5.4 Multiple soliton pulses operation in a 20 m long cavity. (a) Optical spectrum measured. (b) Solitons within a bunch in the cavity at a high pump power. (c) A twin pulse state at a low pump power.

Further shortening the cavity length by reducing the SMF, the optical bandwidth of the soliton spectrum further broadens. For example, with a length of 13 m SMF (cavity length is 20 m), the 3-dB bandwidth increased to as large as ~ 4 nm, as shown in Figure 5.4(a). When the cavity length is reduced to 20 m, a stable soliton bunch is always obtained as shown in Figure 5.4(b). Compared with the state shown in Figure 5.3(b), no soliton can escape out of the bunch. When the pump power is decreased to the mode locking threshold value, a stable twin-pulse soliton state is generated, as shown in Figure 5.4(c). Interestingly, the twin-pulse soliton state cannot be obtained in a longer laser cavity.

Based on the above experimental results, we can conclude that in a long cavity the new solitons formed could move away from the others, eventually become freely moving solitons. While in a short cavity, the formed new solitons are trapped by those already existing in the cavity. Consequently they tend to form a soliton bunch. This phenomenon indicates that the pulse breaking takes place in the single mode fiber, and it can be deduced that more individual soliton pulses can be formed if the length of SMF is correspondingly increased. As the length of SMF in the cavity increases (see Figure 5.1), soliton bunch will become more unstable and finally all the solitons will come out of the bunch and move freely in the cavity.

5.2 Simulation Results

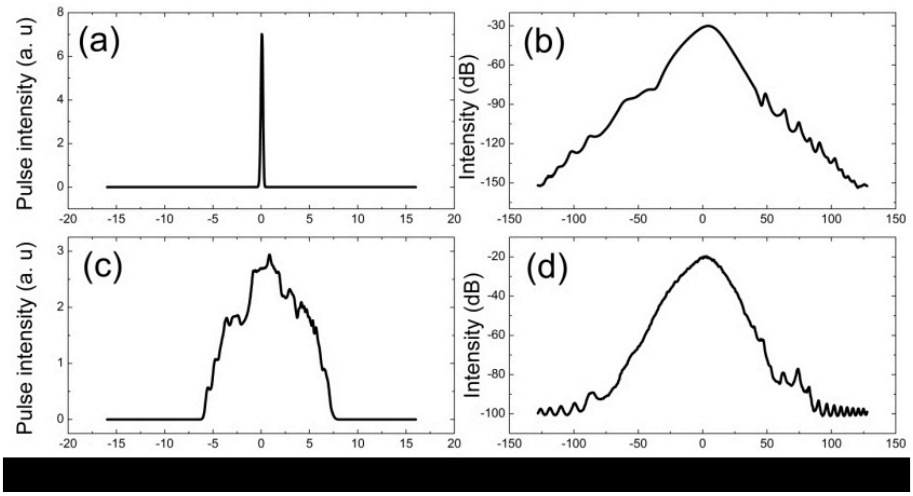

Figure 5.5 Numerically calculated pulse formation under different pumping strength. (a) The single pulse profile under gain= 100 and (b) the corresponding optical spectrum of (a). (c) The NL pulse profile under gain= 6000 and (d) the corresponding time-averaged optical spectrum of (c). Please note that the optical pulse and spectrum of the NL pulse had been averaged over 1000 round trips.

In order to gain an insight on the formation mechanism of the NL pulses, we performed numerical simulations with a model based on the coupled complex Ginzburg-Landau equations (GLEs) similar to that subscribed in reference [65], but the mode-locking component was replaced by the graphene saturable absorber. To make the simulation possibly close to the experimental results, the following simulation parameters were adopted: nonlinear fiber coefficient γ = 3 W^{-1} km^{-1}; erbium fiber gain bandwidth Ω_g = 16 nm; fiber dispersions D''_{EDF} = –32 (ps/nm) /km, D''_{SMF} = 18 (ps/nm) /km and D''' = 0.1 (ps^2/nm)/km; cavity length L = 3.0 m_{EDF} + 65 m_{SMF} = 68 m; cavity birefringence L/L_b = 100 and the nonlinear gain saturation energy P_{sat} = 50 pJ. The nonlinear response of the graphene saturable absorber is governed by the rate equation as follows:

$$\frac{\partial l_s}{\partial t} = -\frac{l_s - l_0}{T_{rec}} - \frac{|u|^2 + |v|^2}{E_{sat}} l_s \qquad (5.1.1)$$

Where T_{rec} is the absorption recovery time of graphene, l_0 is the initial absorption of the absorber, and E_{sat} is the absorber saturation energy. In view that graphene is an ultra-fast saturable absorber with a large modulation depth, we used the following saturable absorption parameters for simulation, E_{sat} = 1 nJ, l_0 = 0.3 and T_{rec} = 100 fs.

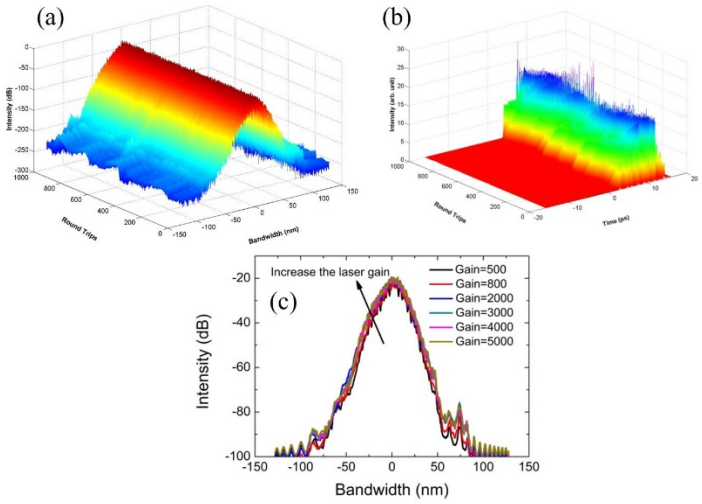

Figure 5.6 Evolution with respect to cavity roundtrips of (a) the optical spectrum and (b) the optical pulse profile of the NL pulse. (c) The change of time-averaged optical spectra of the NL pulse under different laser gain.

Once the laser gain coefficient G exceeds 60 km^{-1}, which corresponds to the threshold pump power required to balance the cavity loss, a stable single pulse could be numerically obtained. Figure 5.5(a) shows a typical state numerically calculated under the laser gain coefficient G = 100 km^{-1}. It is well-known that within a fiber laser mode locked by NPR with net cavity group velocity dispersion approaching zero, the combined actions of two types of soliton-shaping mechanisms: the balance between the fiber nonlinear Kerr effect and the linear cavity dispersion, and the other caused by the laser gain saturation and dispersion, results in the generation of asymmetric optical sideband. Herein, from the optical spectrum shown in Figure 5.5(b) where the Kelly spectral sidebands are asymmetric, one can conclude that the formation of asymmetric spectral sidebands is a feature of the soliton lasers with net near zero dispersion, which is independent on the concrete mode locking component. By further increasing the laser gain, the soliton pulse intensity continuously increases and its pulse width decreases. Eventually the pulse breakups at a pump power of G = 400 km^{-1}. The generation of multi-soliton pulses is correlated with the excessive nonlinearity of the optical pulse propagation along a long segment of the anomalous dispersion optical fiber. In the following, the multi-soliton pulses encounter the nonlinear shaping enabled by the nonlinear response of graphene. The transient nonlinear changes of transmission of graphene show two characteristic time constants: a fast component (100 fs) attributed mainly to the carrier-carrier intraband scattering and a slow component (1 ps) caused by the carrier-phonon intraband scattering and electron-hole inter-band recombination processes. The fast component of the saturable absorption of graphene exerts an attraction force among the multi-soliton pulses, making them unable to separate in time domain. Consequently, the multiple soliton pulses are tightly bound, resulting in the formation of the NL pulse state, as shown in Figure 5.5(c) and Figure 5.5(d). To further uncover the impact of the absorber

recovery time, we deliberately employed a slower recovery time (500 fs) for simulation whereas other parameters are kept unchanged. The state of multi-soliton propagation can be numerically obtained, but they are well separated. In the case the NL pulse state is hardly formed, indicating that a faster saturable absorber, which exhibits stronger mutual attraction force, helps the generation of the NL pulse state. To probe the internal structure, the roundtrip-to-roundtrip simulation is also carried out. Different from the single soliton where the optical spectra are almost identical and indistinguishable from one round to the other, the NL pulse state exhibits significant fluctuations in either the roundtrip-to-roundtrip optical spectra or pulse profiles, as shown in Figure 5.6. Each of the individual spectra or pulse profiles is highly structured and randomly varied with the evolution of the cavity roundtrips. Upon averaging for 1000 rounds a time-averaged optical spectral and pulse intensity profile as shown in Figure 5.5(c) and Figure 5.5(d) are obtained, which are comparable with the corresponding OSA and high speed oscilloscope trace measurements in experiments (see Figure 5.2). The change of optical spectra under different pump power is also summarized in Figure 5.6(c), from which the optical spectral sidebands are hardly observable. We find that the absence of spectral sidebands is a direct consequence of the NL pulse state. We know that the formation of the Kelly sidebands is resulted by the constructive interference between the intra-cavity dispersive wave and soliton wave, which co-circulate within the laser cavity. However, the restless movement and collision among the multi-soliton pulses in a NL pulse can make the dispersive wave and soliton wave unable to fulfil the mutual phase matching condition, which therefore suppresses the generation of optical spectral sidebands.

5.3 Discussions

Based on the experimental and numerical results discussed above, we can summarize the features of the current graphene mode locked and dispersion-managed cavity fiber lasers as the following. There exist two mode locking operation regimes, the multi-soliton regime and the NL pulse regime. In which regime is a laser operating can be easily distinguished from the optical spectrum of the laser emission. Usually, the multi-soliton (resp. NL pulse) has a smooth (resp. blurred) optical spectrum with (resp. without) optical spectral sidebands, and requires relatively lower (resp. higher) pump power. By controlling the intra-cavity birefringence (through the polarization controllers), the laser operation can be switched between the multi-soliton and NL pulse state. Moreover, the cavity length and net cavity dispersion also have an impact on the laser operation. In a short fiber laser cavity, the multi-soliton bunch state is readily obtained. With the increase of the SMF length, which enhances the accumulated optical nonlinearity and shifts the total cavity dispersion towards anomalous dispersion regime, more individual solitons will move out of the bunch, and finally the soliton bunch collapses.

The unique nonlinear optical property of graphene also contributes to the formation of

the NL pulse in the experiment. Unlike the soliton bunch observed in SESAM fiber laser [73], where all the solitons are almost uniform which can be considered as an effect caused by the bandwidth limitation of SESAM. Graphene has a wider operation wavelength. Therefore, no saturable bandwidth limiting effect exists. Like the NPR mode locking, the fast response of graphene saturable absorption imposes an extra soliton attraction force to the solitons. Under the effect the solitons tend to form a bunch in the cavity. Moreover, as the intensities of the pulses are unequal in the current laser cavity, the soliton bunch cannot be as stable as that in SESAM mode-locked fiber lasers. Once the pump power is sufficiently high, too many solitons will be formed and interact with each other simultaneously and NL pulses will be correspondingly obtained. The energy of the NL pulse could be large because all the solitons in the cavity are in a "bunch". A NL pulse usually looks like a "single pulse" in the cavity. However, once the length of SMF is increased, in which pulse breaking effect take places [115], where soliton bunches could collapse and finally the solitons move away from each other, a multiple soliton operation state would be formed in the cavity. Thus we can conclude that formation of both the multi-soliton and NL pulse state is an intrinsic feature of the graphene mode locked dispersion-managed fiber lasers.

6. Summary

In summary, we have both numerically and experimentally investigated the operation of quasi-vector cavity fiber lasers without any saturable absorber in the cavity. We have show experimentally that under strong pumping the CW emission of the laser is unstable, under certain conditions it could become a periodic pulse train. Moreover, the pulses in the pulse train could be further automatically shaped into dissipative solitons. Either periodic or randomly distributed dissipative solitons were experimentally observed. As the soliton formation is initiated by the destabilization of CW beam and no mode locking effect is involved in the process, which closely resembles that of the spatial cavity solitons, we have named the formed solitons the temporal cavity solitons. In addition of the temporal vector cavity formation, we have also experimentally obtained the induced cavity solitons. Formation of the induced dark solitons is also firstly observed in anomalous dispersion cavity fiber lasers. Under incoherent cross polarization coupling, polarization domains were also experimentally observed. We have shown experimentally that a bright soliton could induce a broad dark pulse on the orthogonal polarization direction. The broad dark pulse formation could be explained as a result of the polarization domain formation. All the experimental results could be well numerically reproduced based on a model of the coupled Ginzburg-Landau equations.

We have also experimentally investigated the vector soliton operation of fiber lasers mode locked with the atomic layer graphene. Similar to the case of SESAM mode locked fiber lasers, both the polarization locked and polarization rotation vector

solitons were experimentally obtained in the graphene mode locked fiber lasers. The cavity effect always induces resonant energy exchange between the two orthogonal polarizations components of the vector solitons, and for the polarization rotation vector solitons, two new sets of spectral sidebands appeared on the vector soliton spectrum. Under the multiple vector soliton operation of a fiber laser, various multiple vector soliton patterns were experimentally observed, including the vector soliton bunches, random static vector soliton distribution, restless vector soliton bunches, giant pulse emission, and vector soliton rains. In particular, the polarization-locked vector soliton rain and the polarization rotation vector soliton rain were experimentally identified. Based on results of the experimental studies, the appearance of the different modes of the multiple vector soliton operation could be well understood by the soliton interaction caused by the following four types of main mechanisms, the unstable CW related global type of soliton interaction, the dispersive wave mediated long range soliton interaction, the direct soliton interaction, and the saturable absorber induced soliton-soliton attraction. Furthermore, we have reported on the experimental observation of vector and bound vector solitons in a fiber laser passively mode locked by graphene. Localized interactions between vector solitons, vector soliton with bound vector solitons, and vector soliton with a bunch of vector solitons are experimentally investigated. We show that depending on the soliton interactions, various stable and dynamic multiple vector soliton states could be formed.

The nonlinear dynamics of the vector solitons in graphene fiber lasers was also investigated. Quasi-periodicity of the vector solitons was experimentally observed. The cavity induced soliton modulation instability was the origin of the quasi-periodicity. The vector solitons in the laser could be emitted with both quasi-periodic pulse energy variation and polarization rotation, which can be characterized by the respectively extra sidebands appearance in the optical spectrum. We have experimentally and numerically investigated the formation mechanism of the noise-like (NL) pulses in an erbium-doped dispersion- managed fiber laser passively mode locked by a few-layer graphene saturable absorber. The NL pulses can be regarded as another mode locking regime enabled by graphene saturable absorber, and characterized by sideband-free and broad optical spectrum and narrow peak atop a broad pedestal in its auto-correlation trace. Despite of its noise-like property, this state can lead to large energy operation, making graphene saturable absorber applicable for high power laser photonics. We have shown that the formation of the NL pulse is related to the ultrafast saturable absorption of the CVD graphene.

References

1. G. P. Agrawal, Nonlinear Fiber Optics, 3rd ed. (Academic, 2001).
2. Mollenauer L F, Stolen R H, Gordon J P. Experimental observation of picosecond pulse narrowing and solitons in optical fibers[J]. Physical Review Letters, 1980, 45(13): 1095.
3. J. M. Dudley, G. Genty, F. Dias, B. Kibler, and N. Akhmediev, "Modulation instability, Akhmediev Breathers and continuous wave supercontinuum generation," Opt. Express **17,** 21497-21508 (2009).
4. Henderson, K. L, Peregrine, D. H. & Dold, J. W. Unsteady water wave modulations: Fully nonlinear solutions and comparison with the nonlinear Schrödinger equation. Wave Motion29, 341–361 (1999).
5. B. Kibler, J. Fatome, C. Finot, G. Millot, F. Dias, G. Genty, N. Akhmediev, and J. M. Dudley, "The Peregrine soliton in nonlinear fibre optics," Nat. Phys. **6**, 790–795 (2010).
6. D. N. Christodoulides and R. I. Joseph, "Vector solitons in birefringent nonlinear dispersive media," Opt. Lett.13, 53-55 (1988).
7. D. N. Christodoulides, "Black and white vector solitons in weakly birefringent optical fibers," Phys. Lett. A **132**, 451–452 (1988).
8. M. Haelterman, "Modulational instability, periodic waves and black and white vector solitons in birefringent Kerr media," **111**, 86–92 (1994)..
9. H. A. Haus, J. G. Fujimoto, and E. P. Ippen, “Structures for additive pulse mode locking,” J. Opt. Soc. Am. B 8, 2068–2076 (1991).
10. S. Coen and M. Haelterman, "Modulational instability induced by cavity boundary conditions in a normally dispersive optical fiber," Phys. Rev. Lett. **79,** 4139–4142 (1997).
11. D. Y. Tang, J. Guo, Y. F. Song, L. Li, L. M. Zhao, and D. Y. Shen, "GHz pulse train generation in fiber lasers by cavity induced modulation instability," Opt. Fiber Technol. **20,** 610-614 (2014).
12. V. S. Grigoryan and T. S. Muradyan, “Evolution of light pulses into autosolitons in nonlinear amplifying media,” J. Opt. Soc. Am. B 8, 1757–1765 (1991).
13. G. P. Agrawal, Applications of Nonlinear Fiber Optics (Academic, 2001).
14. Y. V. Kartashov, V. A. Vysloukh, E. Marti-Panameno, D. Artigas, and L. Torner, “Dispersion-managed cnoidal pulse trains,” Phys. Rev. E 68, 026613 (2003).
15. L. M. Zhao, D. Y. Tang, T. H. Cheng, H. Y. Tam, and C. Lu, “Generation of multiple gain-guided solitons in a fiber laser,” Opt. Lett. 32, 1581–1583 (2007).
16. D. Y. Tang, B. Zhao, L. M. Zhao, and H. Y. Tam, “Soliton interaction in a fiber ring laser,” Phys. Rev. E 72, 016616 (2005).
17. P. Grelu, N. Akhmediev, "Dissipative solitons for mode locked lasers," Nat. Photonics **6,** 84-92 (2012).

18. S. M. J. Kelly, "Characteristic sideband instability of periodically amplified average soliton," Electron. Lett **28,** 806-807 (1992).
19. H. Zhang, D. Y. Tang, L. M. Zhao and N. Xiang, "Coherent energy exchange between components of a vector soliton in fiber lasers," Opt. Exp. **16,** 12618-12623 (2008).
20. H. Zhang, D. Y. Tang, L. M. Zhao, and H. Y. Tam, "Induced solitons formed by cross-polarization coupling in a birefringent cavity fiber laser," Opt. Lett. **33,** 2317-2319(2008).
21. D. Y. Tang, Y. F. Song, J. Guo, Y. J. Xiang, and D. Y. Shen, “Polarization domain formation and domain dynamics in a quasi-isotropic cavity fiber laser,” IEEE Journal of Selected Topics in Quantum Electronics, 20, 0901309(2014).
22. S. Wabnitz. "Modulational polarization instability of light in a nonlinear birefringent dispersive medium," Phys. Rev. A **38,** 2018 (1988).
23. S. Trillo and S. Wabnitz, “Ultrashort pulse train generation through induced modulational polarization instability in a birefringent Kerr-like medium,” J. Opt. Soc. Am. B, 6, 239-249(1989).
24. S. G. Murdoch, R. Leonhardt and J. D. Harvey, "Polarization modulation instability in weakly birefringent fibers," Opt. Lett. **20,** 866-868 (1995).
25. D. Amans, E. Brainis, M. Haelterman, and Ph. Emplit, "Vector modulation instability induced by vacuum fluctuations in highly birefringent fibers in the anomalous-dispersion regime," Opt. Lett. **30,** 1051-1053(2005).
26. A. Kudlinski, A. Bendahmane, D. Labat, S. Virally, R. T. Murray, E. J. R. Kelleher, and A. Mussot, "simultaneous scalar and cross-phase modulation instabilities in highly birefringent photonic crystal fiber, " Opt. Express **21,** 8437-8443(2013).
27. D. Amans, E. Brainis, M. Haelterman, and Ph. Emplit, "Vector modulation instability induced by vacuum fluctuations in highly birefringent fibers in the anomalous-dispersion regime," Opt. Lett. **30,** 1051-1053(2005).
28. D. Y. Tang, J. Guo, Y. F. Song, G. D. Shao, L. M. Zhao, and D. Y. Shen, "Temporal cavity soliton formation in an anomalous dispersion cavity fiber laser," J. Opt. Soc. Am. B **31,** 3050-3056 (2014).
29. L. M. Zhao, D. Y. Tang, H. Zhang, T. H. Cheng, H. Y. Tam, and C. Lu, "Dynamics of gain-guided solitons in an all-normal-dispersion fiber laser," *Opt. Lett.*, vol. 32, no. 13, pp. 1806-1808, Jul. 2007
30. M. Horowitz, Y. Barad, and Y. Silberberg, "Noise-like pulses with a broadband spectrum generated from an erbium-doped fiber laser," Opt. Lett., vol. 22, no. 11, pp. 799-801, Jun. 1997.
31. L. M. Zhao, D. Y. Tang, J. Wu, X. Q. Fu, and S. C. Wen, "Noise-like pulse in a gain-guided soliton fiber laser," Opt. Express, vol. 15, no. 5, pp. 2145-2150, Mar. 2007.
32. Y. F. Song, L. Li, H. Zhang, D. Y. Shen, D. Y. Tang, and K. P. Loh, "Vector

multi-soliton operation and interaction in a graphene mode-locked fiber laser," Opt. Express, vol. 21, no. 8, pp. 10010-10018, Apr. 2013.
33. S. Chouli and P. Grelu, “Soliton rains in a fiber laser: An experimental study,” Phys. Rev. A., vol. 81, no. 6, pp. 063829, Jun. 2010.
34. B. A. Malomed, “Domain wall between traveling waves,” Phys. Rev. E, 50(5), R3310–R3313 (1994).
35. B. A. Malomed, “Optical domain walls,” Phys. Rev. E, 50(2), 1565–1571 (1994).
36. A. Mecozzi, S. Trillo, S. Wabnitz, and B. Daino, “All-optical switching and intensity discrimination by polarization instability in periodically twisted fiber filters,” Opt. Lett., 12, 275-277 (1987).
37. S. T. Cundiff, B. C. Collings, N. N. Akhmediev, J. M. Soto-Crespo, K. Bergman, and W. H. Knox, “Observation of Polarization-Locked Vector Solitons in an Optical Fiber, ” Phys. Rev. Lett. 82, 3988-3991 (1999).
38. N. Akhmediev, J. M. Soto-Crespo, and G. Town, “Pulsating solitons, chaotic solitons, period doubling, and pulse coexistence in mode-locked lasers: Complex Ginzburg-Landau equation approach,” Phys. Rev. E 63, 056602 (2001).
39. Y. F. Song, L. Li, D. Y. Tang, and D. Y. Shen, “Quasi-periodicity of vector solitons in a graphene mode-locked fiber laser,” Laser Phys. Lett. 10(12), 125103 (2013).
40. Q. Y. Ning, S. K. Wang, A. P. Luo, Z. B. Lin, Z. C. Luo, and W. C. Xu, “Bright–dark pulse pair in a figure-eight dispersion-managed passively mode-locked fiber laser,” IEEE Photon. J. 4(5), 1647–1652 (2012).
41. M. Haelterman, “Modulational instability, periodic waves and black and white vector solitons in birefringent Kerr media,” Opt. Comm., 111(1), 86-92 (1994).
42. S.Chouli and P. Grelu, "Rains of solitons in a fiber laser," Opt. Express, 17, 11776-11781 (2009).
43. K. J. Blow, N. J. Doran, and David Wood, "Polarization instabilities for solitons in birefringent fibers," Opt. Lett. 12, 202-204 (1987).
44. G. D. Shao, Y. F. Song, L. M. Zhao, D. Y. Shen, and D. Y. Tang, "Soliton-dark pulse pair formation in birefringent cavity fiber lasers through cross phase coupling," Opt. Express 23, 26252-26258(2015)
45. C. Lecaplain, P. Grelu, and S. Wabnitz, “Polarization-domain-wall complexes in fiber lasers,” J. Opt. Soc. Am. B 30(1), 211–218 (2013).
46. Likarn Wang and C. C. Yang, "Existence of solitary waves in optical fibers owing to the mutual support between bright and dark pulses," Opt. Lett. 15, 474-476 (1990).
47. S. Trillo, E. M. Wright, G. I. Stegeman, and S. Wabnitz, "Optical solitary waves induced by cross-phase modulation," Opt. Lett. 13, 871-873 (1988).
48. C. R. Menyuk, "Stability of solitons in birefringent optical fibers .I. equal propagation amplitudes," Optics Letters 12 (8), 614 (1987).

49. V. V. Afanasjev, "Soliton Polarization Rotation in Fiber Lasers," Optics Letters 20 (3), 270 (1995).
50. D. N. Christodoulides and R. I. Joseph, "Vector Solitons in Birefringent Nonlinear Dispersive Media," Optics Letters 13 (1), 53 (1988).
51. N. Akhmediev, A. Buryak, and J. M. Sotocrespo, "Elliptically Polarized Solitons in Birefringent Optical Fibers," Optics Communications 112 (5-6), 278 (1994).
52. M. N. Islam, C. D. Poole, and J. P. Gordon, "Soliton trapping in birefringent optical fibers," Optics Letters 14 (18), 1011 (1989).
53. Q. L. Bao, H. Zhang, Y. Wang, Z. H. Ni, Y. L. Yan, Z. X. Shen, K. P. Loh, and D. Y. Tang, "Atomic-layer graphene as a saturable absorber for ultrafast pulsed lasers," Advanced Functional Materials 19 (19), 3077 (2009).
54. H. Zhang, D. Y. Tang, L. M. Zhao, Q. L. Bao, and K. P. Loh, "Vector dissipative solitons in graphene mode locked fiber lasers," Optics Communications 283 (17), 3334 (2010).
55. W. D. Tan, C. Y. Su, R. J. Knize, G. Q. Xie, L. J. Li, and D. Y. Tang, "Mode locking of ceramic Nd:yttrium aluminum garnet with graphene as a saturable absorber," Applied Physics Letters 96 (3), 031106 (2010).
56. M. N. Cizmeciyan, J. W. Kim, S. Bae, B. H. Hong, F. Rotermund, and A. Sennaroglu, "Graphene mode-locked femtosecond Cr:ZnSe laser at 2500 nm," Optics Letters 38 (3), 341 (2013).
57. J. Ma, G. Q. Xie, P. Lv, W. L. Gao, P. Yuan, L. J. Qian, H. H. Yu, H. J. Zhang, J. Y. Wang, and D. Y. Tang, "Graphene mode-locked femtosecond laser at 2 μm wavelength," Optics Letters 37 (11), 2085 (2012).
58. L. M. Zhao, D. Y. Tang, H. Zhang, and X. Wu, "Polarization rotation locking of vector solitons in a fiber ring laser," Optics Express 16 (14), 10053 (2008).
59. R. Gumenyuk, M. S. Gaponenko, K. V. Yumashev, A. A. Onushchenko, and O. G. Okhotnikov, "Vector soliton bunching in thulium-holmium fiber laser mode-locked with PbS quantum-dot-doped glass absorber," IEEE Journal of Quantum Electronics 48 (7), 903 (2012).
60. J. H. Wong, K. Wu, H. H. Liu, C. M. Ouyang, H. H. Wang, S. Aditya, P. Shum, S. N. Fu, E. J. R. Kelleher, A. Chernov, and E. D. Obraztsova, "Vector solitons in a laser passively mode-locked by single-wall carbon nanotubes," Optics Communications 284 (7), 2007 (2011).
61. L. M. Zhao, D. Y. Tang, X. Wu, H. Zhang, and H. Y. Tam, "Coexistence of polarization-locked and polarization-rotating vector solitons in a fiber laser with SESAM," Optics Letters 34 (20), 3059 (2009).
62. A. Martinez and S. Yamashita, "Multi-gigahertz repetition rate passively modelocked fiber lasers using carbon nanotubes," Optics Express 19 (7), 6155 (2011).
63. S. M. J. Kelly, "Characteristic side-band instability of periodically amplified average soliton," Electronics Letters 28 (8), 806 (1992).
64. B. A. Malomed, "Propagation of a soliton in a nonlinear wave-guide with

dissipation and pumping," Optics Communications 61 (3), 192 (1987).
65. H. Zhang, D. Y. Tang, L. M. Zhao, and N. Xiang, "Coherent energy exchange between components of a vector soliton in fiber lasers," Optics Express 16 (17), 12618 (2008).
66. S. Trillo, S. Wabnitz, R. H. Stolen, G. Assanto, C. T. Seaton, and G. I. Stegeman, "Experimental-observation of polarization instability in a birefringent optical fiber," Applied Physics Letters 49 (19), 1224 (1986).
67. K. J. Blow, N. J. Doran, and D. Wood, "Polarization instabilities for solitons in birefringent fibers," Optics Letters 12 (3), 202 (1987).
68. M. Haelterman, S. Trillo, and S. Wabnitz, "Dissipative modulation instability in a nonlinear dispersive ring cavity," Optics Communications 91 (5-6), 401 (1992).
69. P. Grelu and J. M. Soto-Crespo, "Multisoliton states and pulse fragmentation in a passively mode-locked fibre laser," Journal of Optics B-Quantum and Semiclassical Optics 6 (5), S271 (2004).
70. D. Y. Tang, L. M. Zhao, B. Zhao, and A. Q. Liu, "Mechanism of multisoliton formation and soliton energy quantization in passively mode-locked fiber lasers," Physical Review A 72 (4), 043816 (2005).
71. M. Olivier, V. Roy, M. Piche, and F. Babin, "Pulse collisions in the stretched-pulse fiber laser," Optics Letters 29 (13), 1461 (2004).
72. M. Grapinet and P. Grelu, "Vibrating soliton pairs in a mode-locked laser cavity," Optics Letters 31 (14), 2115 (2006).
73. L. M. Zhao, D. Y. Tang, H. Zhang, and X. Wu, "Bunch of restless vector solitons in a fiber laser with SESAM," Optics Express 17 (10), 8103 (2009).
74. D. Y. Tang, W. S. Man, H. Y. Tam, and P. D. Drummond, "Observation of bound states of solitons in a passively mode-locked fiber laser," Physical Review A 64 (3), 033814 (2001).
75. B. A. Malomed, "Bound Solitons in the Nonlinear Schrodinger-Ginzburg-Landau Equation," Physical Review A 44 (10), 6954 (1991).
76. B. A. Malomed, "Bound-States of Envelope Solitons," Physical Review E 47 (4), 2874 (1993).
77. V. V. Afanasjev, B. A. Malomed, and P. L. Chu, "Stability of bound states of pulses in the Ginzburg-Landau equations," Physical Review E 56 (5), 6020 (1997).
78. B. A. Malomed, A. Schwache, and F. Mitschke, "Soliton lattice and gas in passive fiber-ring resonators," Fiber and Integrated Optics 17 (4), 267 (1998).
79. S. Chouli and P. Grelu, "Soliton rains in a fiber laser: An experimental study," Physical Review A 81 (6), 063829 (2010).
80. S. Chouli and P. Grelu, "Rains of solitons in a fiber laser," Optics Express 17 (14), 11776 (2009).
81. R. Gumenyuk and O. G. Okhotnikov, "Temporal control of vector soliton bunching by slow/fast saturable absorption," Journal of the Optical Society of America B 29 (1), 1 (2012).

82. D. Popa, Z. Sun, F. Torrisi, T. Hasan, F. Wang, and A. C. Ferrari, "Sub 200 fs pulse generation from a graphene mode-locked fiber laser," Applied Physics Letters 97 (20), 203106 (2010).
83. L. M. Zhao, D. Y. Tang, H. Zhang, X. Wu, Q. L. Bao, and K. P. Loh, "Dissipative soliton operation of an ytterbium-doped fiber laser mode locked with atomic multilayer graphene," Optics Letters 35 (21), 3622 (2010).
84. S. Cundiff, B. Collings, and W. Knox, "Polarization locking in an isotropic, modelocked soliton Er/Yb fiber laser," Optics Express 1 (1), 12 (1997).
85. B. A. Malomed, “Bound solitons in coupled nonlinear Schrödinger equation,” Phys. Rev. A **45**, R8321-R8323 (1992).
86. N. N. Akhmediev, A. Ankiewicz, and J. Soto-Crespo, “Multisoliton solutions of the complex Ginzburg-Landau equation,” Phys. Rev. Lett. **79**(21), 4047–4051 (1997).
87. N. N. Akhmediev, A. Ankiewicz, and J. M. Soto-Crespo, “Stable soliton pairs in optical transmission lines and fiber lasers,” J. Opt. Soc. Am. B **15**(2), 515–523 (1998).
88. S. Latas and M. Ferreira, “Bound States of dissipative solitons in optical fiber systems,” in *Proceedings of the SPIE - The International Society for Optical Engineering*, 7582, p 75820P (9 pp.), 2010.
89. L. Gui, X. Xiao, C. Yang, “Observation of various bound solitons in a carbon-nanotube-based erbium fiber laser,” J. Opt. Soc. Am. B, 30(1), 158-164 (2013).
90. X. Wu, D. Tang, X. N. Luan, and Q. Zhang, “Bound states of solitons in a fiber laser mode locked with carbon nanotube saturable absorber,” Opt. Commun. 284(14), 3615–3618 (2011).
91. C. Zeng, Y. D. Cui, and J. Guo, “Observation of dual-wavelength solitons and bound states in a nanotube/microfiber mode-locking fiber laser,” Opt. Commun. 347, 44-49 (2015).
92. C. Mou, S. V. Sergeyev, A. G. Rozhin, and S. K. Turitsyn, “Bound state vector solitons with locked and precessing states of polarization,” Opt. Express 21(22), 26868-26875 (2013).
93. H. H. Liu and K. K. Chow, “High fundamental-repetition-rate bound solitons in carbon nanotube-based fiber lasers,” IEEE Photon. Tech. Lett. 27(8), 867-870 (2015).
94. H. R. Yang, G. W. Chen, Y. C. Kong, and W. L. Li, “Bound-state fiber laser mode-locked by a graphene-nanotube saturable absorber,” Laser Phys. 25(2), 025101 (2015).
95. X. Li, S. Zhang, Y. Meng, Y. Hao, H. Li, J. Du, and Z. Yang, “Observation of soliton bound states in a graphene mode locked erbium-doped fiber laser,” Laser Phys. 22(4), 774–777 (2012).
96. L. Gui, X. Li, X. Xiao, H. Zhu, and C. Yang, “Widely spaced bound states in a soliton fiber laser with graphene saturable absorber,” IEEE Photon. Tech. Lett. 25(12), 1184-1187 (2013).

97. Y. Wang, D. Mao, X. Gan, L. Han, C. Ma, T. Xi, Y. Zhang, W. Shang, S. Hua, and J. Zhao, “Harmonics mode locking of bound-state solitons fiber laser based on MoS2 saturable absorber,” Opt. Express 23(1), 205-210 (2015).
98. J. W. Haus, G. Shaulov, E. A. Kuzin, and J. Sanchez-Mondragon, “Vector soliton fiber lasers,” Opt. Lett. 24(6), 376-378 (1999).
99. B. C. Collings, S. T. Cundiff, N. N. Akhmediev, J. M. Soto-Crespo, K. Bergman, and W.H. Knox, “Polarization-locked temporal vector solitons in a fiber laser: experiment,” J. Opt. Soc. Am. B 17(3), 354-365 (2000).
100. A. Reina, X. T. Jia, J. Ho, D. Nezich, H. B. Son, V. Bulovic, M. S. Dresselhaus, and J. Kong, “Large area, few-layer graphene films on arbitrary substrates by chemical vapor deposition,” Nano Lett. **9**(1), 30-35 (2009).
101. P. Grelu, F. Belhache, F. Gutty, and J. M. Soto-Crespo, “Phase-locked soliton pairs in a stretched-pulse fiber laser,” Opt. Lett. **27**(11), 966-968 (2002).
102. J. M. Soto-Crespo, M. Grapinet, P. Grelu, and N. Akhmediev, "Bifurcations and multiple-period soliton pulsations in a passively mode-locked fiber laser," Physical Review E 70 (6), 066612 (2004).
103. K. Tamura, C. R. Doerr, H. A. Haus, and E. P. Ippen, "Soliton fiber ring laser stabilization and tuning with a broad intracavity Filter," IEEE Photonics Technology Letters 6 (6), 697 (1994).
104. G. Sucha, S. R. Bolton, S. Weiss, and D. S. Chemla, "Period-doubling and quasi-periodicity in additive-pulse mode-locked lasers," Optics Letters 20 (17), 1794 (1995).
105. F. Sanchez, M. Leflohic, G. M. Stephan, P. Leboudec, and P. L. Francois, "Quasi-periodic route to chaos in erbium-doped fiber laser," IEEE Journal of Quantum Electronics 31 (3), 481 (1995).
106. S. R. Bolton and M. R. Acton, "Quasiperiodic route to chaos in the Kerr-lens mode-locked Ti: sapphire laser," Physical Review A 62 (6), 063803 (2000).
107. L. M. Zhao, D. Y. Tang, F. Lin, and B. Zhao, "Observation of period-doubling bifurcations in a femtosecond fiber soliton laser with dispersion management cavity," Optics Express 12 (19), 4573 (2004).
108. D. Y. Tang, L. M. Zhao, X. Wu, and H. Zhang, "Soliton modulation instability in fiber lasers," Physical Review A 80 (2), 023806 (2009).
109. L. M. Zhao, D. Y. Tang, H. Zhang, X. Wu, C. Lu, and H. Y. Tam, "Period-doubling of vector solitons in a ring fiber laser," Optics Communications 281 (22), 5614 (2008).
110. L. M. Zhao, D. Y. Tang, J. Wu, X. Q. Fu, and S. C. Wen, "Noise-like pulse in a gain-guided soliton fiber laser," Optics Express 15 (5), 2145 (2007).
111. D. Y. Tang, L. M. Zhao, and B. Zhao, "Soliton collapse and bunched noise-like pulse generation in a passively mode-locked fiber ring laser," Optics Express 13 (7), 2289 (2005).
112. Y. Takushima, K. Yasunaka, Y. Ozeki, and K. Kikuchi, "87 nm bandwidth noise-like pulse generation from erbium-doped fibre laser," Electronics Letters 41 (7), 399 (2005).

113. D. Y. Tang, L. M. Zhao, G. Q. Xie, and L. J. Qian, "Coexistence and competition between different soliton-shaping mechanisms in a laser," Physical Review A 75 (6), 063810 (2007).
114. L. M. Zhao, D. Y. Tang, H. Y. Tam, and C. Lu, "Pulse breaking recovery in fiber lasers," Optics Express 16 (16), 12102 (2008).

List of publications

a) Papers published in peer-reviewed journals

1. D. Y. Tang, J. Guo, Y. F. Song, G. D. Shao, L. M. Zhao, and D. Y. Shen, "Temporal cavity soliton formation in an anomalous dispersion cavity fiber laser," J. Opt. Soc. Am. B 31, 3050-3056 (2014).
2. G. D. Shao, Y. F. Song, L. M. Zhao, D. Y. Shen, and D. Y. Tang, "Vector gain - guided dissipative solitons in a net normal dispersive fiber laser," IEEE Photonics Technology Letter, 28(9), 975-978(2016).
3. G. Shao, Y. Song, L. Zhao, D. Shen, and D. Tang, "Temporal vector cavity solitons in a net anomalous dispersion fiber laser," Laser Phys. Lett. 13, 025103 (2016).
4. G. Shao, Y. Song, J. Guo, L. Zhao, D. Shen, and D. Tang, "Induced dark solitary pulse in an anomalous dispersion cavity fiber laser," Opt. Express 23, 28430 (2015).
5. G. Shao, Y. Song, L. Zhao, D. Shen, and D. Tang, "Soliton-dark pulse pair formation in birefringent cavity fiber lasers through cross phase coupling," Opt. Express 23, 26252 (2015).
6. Y. F. Song, H. Zhang, D. Y. Tang, and D. Y. Shen, Optics Letters, “Coexistence and interaction of vector and bound vector solitons in a dispersion-managed fiber laser mode locked by graphene,” Optics Express, 24(2), 1814-1822 (2016).
7. D. Y. Tang, L. Li, Y. F. Song, L. M. Zhao, H. Zhang, and D. Y. Shen, “Evidence of dark solitons in all-normal-dispersion-fiber lasers,” Physical Review A, 88, 013849(2013).
8. D.Y. Tang, J. Guo, Y. F. Song, L. Li, L.M. Zhao, D. Y. Shen, “GHz pulse train generation in fiber lasers by cavity induced modulation instability,” Optical Fiber Technology, 20, 610-614(2014).
9. D. Y. Tang, J. Guo, Y. F. Song, H. Zhang, L. M. Zhao, and D. Y. Shen, “Dark soliton fiber lasers,” Optics Express, 22, 19831-19837(2014).
10. Y. F. Song, J. Guo, L. M. Zhao, D. Y. Shen, and D. Y. Tang, “280 GHz dark soliton fiber laser,” Optics Letters, 39, 3484-3487(2014).
11. D. Y. Tang, Y. F. Song, J. Guo, Y. J. Xiang, and D. Y. Shen, “Polarization Domain Formation and Domain Dynamics in a Quasi-Isotropic Cavity Fiber Laser, “IEEE journal of Selected Topics in Quantum Electronics, 20, 0901309 (2014).

b. Conference presentations without papers:

1. Y. F. Song, G. D. Shao and D. Y. Tang, “Cavity soliton fiber lasers,” Nonlinear Optics (NLO), July 26-31, 2015, Kauai, Hawaii, USA.
2. D. Y. Tang, J. Ma, and D. Y. Shen, “Dissipative soliton operation of mode locked solid state lasers,” Applied Optics and Photonics China- Advances in lasers technology and application, Beijing, May 5-7, 2015. Invited Talk.
3. D. Y. Tang, L. M. Zhao, and D. Y. Shen, “Novel nonlinear optical effects in quasi-vector cavity fiber lasers,” International conference on optoelectronic Technology and application, May 13-15, 2014, Beijing, China. Invited talk.
4. D. Y. Tang, Y. F. Song, L. M. Zhao, and D. Y. Shen, “Simultaneous black-white pulse emission of fiber lasers,” 23rd annual international laser physics workshop, July 14-18, 2014, Sofia, Bulgaria. Invited talk.
5. D. Y. Tang, Y. F. Song, L. M. Zhao, and D. Y. Shen, “Vector soliton dynamics of graphene mode locked fiber lasers,” The 6th international nanoelectronics conference 2014, July 28-31, 2014, Sapporo, Hokkaido, Japan. Invited talk.
6. D. Y. Tang, Y. F. Song, L. Li, L. M. Zhao, D. Y. Shen, “Vector cavity fiber lasers”, Optics 2013, December 5-7, 2013, Chungli, Taiwan. Invited talk.
7. D. Y. Tang, “Dark soliton fiber lasers,” 4th International Conference on Photonics 2013, October 28-30, 2013, Malacca, Malaysia. Invited talk.